Uncovering hidden seismic risks: Paleoseismic insights in Québec's intraplate seismic zones

Dévoiler les risques sismiques dissimulés : les premiers pas de la paléoséismologie dans les zones sismiques du Québec

Aube Gourdeau

Master of Science
August 2024

Earth and Planetary Sciences

McGill University
Montréal, Québec

A thesis submitted to McGill University in partial fulfillment of the requirements of the degree of Master of Science

Attends-moi je vais trouver la faille retrouver la faille
Attends-moi je vais retrouver retrouver

Lydia Képinski

Acknowledgments

I would first like to thank my two supervisors, Christie Rowe and Veronica Prush, who allowed me to catch every opportunity I was able to find even if it affected the time I could put into working on my thesis. Thank you both for having given me a chance and having pushed me very hard to make this master's happen. Thanks for having invested in our project and in my countless trips to the U.S. Thank you, Christie, for being such a supportive supervisor, attentive to our mental health, long-term objectives, and interests. Thank you for making sure that your research group was a safe and welcoming environment that held tightly. I think that the supervisors represent the central knot that can connect their community together, and you took this responsibility seriously. You represent a model for me that goes beyond science excellence. You are also an example of kindness, respect, open-mindedness, and generosity that will continue to inspire me during my professional journey. Thank you, V, for passing your passion for paleoseismology to me at the end of my bachelor's degree. You ignited a spark that held me from leaving academia (and we both know how close that was). Thank you for having carried me around during conferences in California, making me meet with the coolest geoscientists in town.

Merci à mes parents, mon amoureux et mes amis pour leur patience et leur support lors de cette épopée plutôt rock and roll, où je suis passée par toute une gamme d'émotions. Merci d'avoir tenu le fort quand toute mon énergie, pendant plusieurs semaines, était consacrée aux pages qui suivent. Merci aussi de m'avoir sortie de ma caverne quand j'en avais besoin sans le savoir, ou de m'avoir obligée à rester dans ma caverne les semaines où j'avais tendance à m'éparpiller parce que la motivation n'était pas au rendez-vous.

Finally, thank to my donors who financially contributed to my work through fellowships, conference support, or travel support. This help was greatly appreciated and helped me carry out the project without worrying as much about housing prices, inflation, and the more and more unaffordable cost of living for graduate students.

A big thanks to Maximilien Laly and Kaiyuan Wang, who were amazing partners in the making of this uniformized methodology during the completion of our bachelor theses. Thank you also for having remained in the loop way beyond the duration of the initial project, helping me a lot when trying to combine all the undergrad theses together. We really retrieved the best out of our three different backgrounds, notably regarding Kai's passion for glacial geomorphology and Max's expertise with GIS softwares.

Nous aimerions remercier tous les propriétaires nous ayant permis d'effectuer des recherches sur leur terrain, incluant André, Anthony, François, Jacques, Johanne, Marc, Mathieu, Mr. Gagnon, Philippe Desjardins, Sylvain et sa femme, ainsi que Yves. Merci aussi à Richard qui nous a laissées effectuer des levés sismiques sur sa propriété.

Un merci particulier à Mario Richer et sa fille, et Jannot qui nous ont permis de creuser une tranchée paléosismique au sein de leur ferme acéricole au nom de la science, et qui étaient toujours prêts à nous aider à l'aide de leurs VTTs et de leurs bonnes blagues. Finalement, merci à Israël/Isra Excavation qui a creusé la tranchée avec précaution et minutie.

We thank Félix Gervais at Montréal Polytechnique for introducing the geologists to the engineer which enabled this project to move forward.

Thanks to Kaiyuan Wang, Lan Xi Zhu, and Justin Chien for untying the knots during the refraction survey. Thanks to Maximilien Laly for helping with QGIS and ArcGIS. Thanks to Adil Takahashi for the help with the ambient noise survey. Merci à Miguel Saint-Denis pour avoir exploré l'escarpement avec nous. Thank you to Suzanne Owen at McGill Risk Management for making sure that everything we planned was legal. Thank you to Fiona Darbyshire for lending the Ground Penetrating Radar and to Yajing Liu for lending the geophones. Thanks to Bruce Harrison and Kyle Gallant at the New Mexico Institute of Mining and Technology who gave us very good feedback regarding the soil samples and descriptions.

The EKKO Project license was provided by the EarthScope Consortium through the PASSCAL Instrument Center at New Mexico Tech. The facilities of EarthScope Consortium are supported by the National Science Foundation's Seismological Facility for the Advancement of Geoscience (SAGE) Award under Cooperative Support Agreement EAR-1851048.

Thanks to my thesis reviewer, Magali Rizza, for her precise and helful comments, as well as John Adams and Jack Williams who reviewed my 1st chapter for its publication in Seismica.

Funding was provided by the National Science and Engineering Research Council, Canada (Discovery grant and Canada Research Chairs awards to Christie Rowe) and a Wares Faculty Scholarship to Rowe which supported Prush's postdoctoral fellowship. Aube Gourdeau was supported by a scholarship from Geotop (FRQNT), Helgi Soutar Masters Fellowship and the Eric Mountjoy Fellowship from McGill University.

Contents

List of Tables

List of Figures

3.4 Expression of the scarp in the field. Base of scarp is marked with white lines in a), b), and c). Thin white lines marking approximate local relief. a) Expression of the scarp in the forest, where the test pit was excavated (blue polygon shows extent of pit footprint; see blue star fig. 3.2 for location). The height is large (2 m), the scarp is sharp, and the bedrock is exposed on the upper surface. b) Expression of the scarp in cropland, in the southern branch of the suspected stepover near the center of the mapped scarp length (see pink dot fig. 3.2 for location). The scarp is subtle, but ~1 m of relief is still visible. The bedrock is exposed, compromising vegetable growth. c) View looking west along the scarp at the location of the paleoseismic trench, showing continuity and consistency of scarp height (see red star fig. 3.2 for location). d) Exposed bedrock on the scarp near (a). Planar laminated dolostones at the base are overlain by crossbedded calcite-cemented pebbly quartz sandstone. The top of the scarp displays ~30 cm soil development (covered with leaves)./ Apparence de l'escarpement sur le terrain. La base de l'escarpement est définie par des lignes blanches en a), b) et c). Les autres lignes blanches et fines indiquent la position approximative du relief de l'escarpement. a) Apparence de l'escarpement dans la forêt, là où l'excavation contrôle a été effectuée (le polygone bleu indique l'étendue de l'excavation à la surface) (voir étoile bleue fig. 3.2 pour connaître le positionnement). La hauteur est importante (2 m), l'escarpement est net et le socle rocheux est exposé en surface. b) Apparence de l'escarpement dans les champs cultivés, sur l'embranchement Sud du possible stepover près du centre de l'escarpement (voir point rose fig. 3.2 pour connaître le positionnement). L'escarpement y est plus subtil, mais ~1 m de relief est tout de même visible. Le socle rocheux est exposé dans le champs, rendant la culture de légumes impossible. c) Vue de l'escarpement en direction Ouest, près de la tranchée paléosismique (voir étoile rouge fig. 3.2 pour connaître le positionnement). La constance et la continuité dans le relief de l'escarpement y sont bien visibles. d) Socle rocheux exposé près de la photo (a). Des dolomies planaires et laminées à la base sont surmontées de grès cimentés par de la calcite et comportent des

Abstract

Intraplate seismic zones represent challenging environments to quantify earthquake risk. Many of the tools and methods used in plate boundary seismic hazard estimation are harder to apply in intraplate seismic zones, due to low strain rates, sparse records of source faults, and local climate/surface conditions. In southern Québec, significant historic earthquakes have occurred in regions which are now considered having a high earthquake risk due to urbanization and infrastructure development. Despite a high seismicity rate and known historically damaging earthquakes in several seismic zones (e.g. 1732 M5.8 Montréal, 1663 M7 Charlevoix, 1935 M6.2 Temiskaming), no surface-rupturing faults have been discovered in the province due to a combination of dense vegetation cover, recent glaciation, sparse earthquake records, and low regional strain rates. The lack of specific earthquake source scenarios impedes hazard estimation. Major ice sheets covered the region until only ~12 kya, leaving little time for the development of characteristic tectonic geomorphology, so locally-informed methods are required to identify potential fault traces.

I manually searched lidar-derived digital elevation models (DEMs) of the region to search for potential post-glacial surface-rupturing faults across southern Québec and identified a scarp ~50 km north of Montréal. Here I present an inventory of scarps identified in 1-m lidar

topography in three high-risk areas of southern Québec. I present a detailed locally-adapted criteria table for assessment of the scarps for the potential to represent surface-rupturing faults. These criteria are appropriate for application across boreal/mixed North America including seismic zones of the Arctic, Maritimes and New England. This scarp inventory for southern Québec provides a basis for motivating the necessary paleoseismic studies needed to address seismic hazard in the region.

Based on the identification of a favorable geomorphic scarp close to Montréal as a candidate for the 1732 rupture trace, I performed three geophysical surveys (ground penetrating radar, depth estimates from ambient seismic noise, and refraction seismology) that revealed a buried scarp, confirmed with a <1 m-deep hand-dug test pit. These observations convinced us to excavate the first paleoseismic trench in Québec to test for the presence of a surface-rupturing fault in July 2023. We found a glacial diamict containing no signs of syn- or post-glacial deformation. I present the observations that led to the identification of a scarp and hypothesized faulting. I highlight the importance of trenching to confirm recent fault scarps in challenging environments, and present the workflow and necessary steps to advance a paleoseismic trench in Québec.

1

Résumé

Les zones sismiques intraplaques représentent des environments complexes pour quantifier le risque sismique. En effect, plusieurs outils utilisés pour estimer l'aléa sismique le long de limites de plaques tectoniques sont difficilement applicables dans des contextes intracratoniques, à cause des rythmes de déformation lents, des catalogues sismiques incomplets, et des conditions climatiques/geomorphologiques locales complexes. Dans le sud du Québec, plusieurs séismes historiques importants ont frappés des régions où l'on considère aujourd'hui le risque sismique comme étant élevé, dû à la densification récente de la population et des infrastructures. Malgré une activité sismique régulière et le dénombremment de multiples séismes dommageables dans plusieurs zones sismiques (e.g. 1732 M5.8 Montréal, 1663 M7 Charlevoix, 1935 M6.2 Temiskaming), l'identification de failles actives au Québec tarde, notamment dû à la végétation dense, à la déglaciation récente, au catalogue sismique incomplet et aux rythmes de déformation régionaux lents. Cette absence de failles actives identifiées compromet l'estimation de l'aléa sismique du Québec. La province, qui était couverte d'une calotte glaciaire majeure jusqu'à il y a 12kya, a permis le development d'une géomorphologie glaciaire unique nécessitant le development de méthodes paléosismiques adaptées au contexte régional et local pour permettre l'identification d'escarpements de failles.

Des données obtenues à l'aide de Modèles Numériques Topographiques (MNT) dérivés d'imagerie lidar ont été étudiées pour la région du sud du Québec afin d'identifer de potentielles failles post-glaciaires atteignant la surface, dont un escarpement intéressant identifié ~50 km au Nord de Montréal. Dans cette thèse, les escarpement inventoriés seront présentées pour trois régions à haut potentiel sismique du sud du Québec. Une table de critères détaillée et adaptée au contexte régional sera présentée. Cette table permettra d'évaluer des escarpements et leur potentiel d'être associés à des ruptures sismiques de surface récentes dans des environnements déglacés. Cette table pourra eventuellement être utilisée partout dans la forêt boréale/mixte du continent Nord-Américain, incluant des zones de l'Arctique, des Martimes et de la Nouvelle-Angleterre. Ce catalogue d'escarpements représente un premier pas nécessaire pour l'avancement des études paleoséismiques dans le sud du Québec qui pourra permettre de mieux évaluer l'aléa sismique régional.

À la suite de l'identification d'un escarpement prometteur qui aurait pu être associé au séisme de 1732 près de Montréal, trois méthodes géophysiques (géoradar, bruit ambiant sismique et réfraction sismique) ont été déployées sur le site. Ces levés révèlèrent un décalage du socle rocheux à faible profondeur, confirmé par une première excavation de l'ordre de 1 m de profondeur. Ces observations ont justifié l'excavation en juillet 2023 de la première tranchée paléosismique effectuée au Québec, afin de confirmer la présence d'une faille sismique récente atteignant la surface. Cette tranchée révèle la présence d'un diamicton ne contenant aucun signe de déformation syn- ou post-glaciaire. Cette thèse présente donc les observations ayant faussement mené à l'identification d'un escarpement érosif comme étant une faille sismique. L'importance de réaliser des tranchées paléosismiques lors de l'identification de failles actives est ainsi démontré, spécialement dans des environnements complexes. Cette étude permettra d'optimiser les recherches à venir dans le domaine de la paléosismologie au Québec et dans des environnements intracratoniques au passé glaciaire.

Contribution of authors

This document was written in full by Aube Gourdeau, and all analyses and interpretations in this thesis were completed by her with the exception of those contributions listed here:

Chapter 1 Completely written by Aube Gourdeau, with edits from Christie Rowe

Chapter 2 This chapter is in preparation for submission to *Canadian Journal of Earth Sciences* with several coauthors. With the exception of these specified contributions, all data acquisition and interpretation as well as writing, figure preparation and editing were completed by Aube Gourdeau.

The project was conceived by Veronica Prush and Christie Rowe. Veronica supervised the initial student work surveying the three target areas.

Kaiyuan Wang performed the initial survey of the Temiskaming region and wrote the first draft of the descriptive text for that area (Wang, 2022). He contributed to the first draft of the criteria table (Table 2.2). Aube Gourdeau subsequently revised these contributions and synthesized them into the final draft presented here. Kaiyuan's thesis formed the basis for the glacial history and possible drivers for seismicity section which was subsequently revised by Aube Gourdeau.

Maximilien Laly performed the initial survey of the Québec City region and wrote the first draft of the descriptive text for that area (Laly, 2021). He contributed to the first draft of the criteria table (Table 2.2). Aube Gourdeau subsequently revised these contributions and synthesized them into the final draft presented here. Max's thesis formed the basis for the lidar methods section which was subsequently revised by Aube Gourdeau.

Edits to text and figures were provided by Christie Rowe and Veronica Prush.

Chapter 3 This chapter has been submitted for publication in *Seismica* with several coauthors in its present form. With the exception of these specified contributions, all data acquisition and interpretation as well as writing, figure preparation and editing were completed by Aube Gourdeau.

This study was conceived by Aube Gourdeau and Veronica Prush, and the field plan was designed and led by Aube Gourdeau.

The seismic reflection data was collected by Aube Gourdeau and field assistants (see Acknowledgements) and processed by Hannah Mark, who produced Figure 3.8.

The ground-penetrating radar data was collected by Aube Gourdeau and Veronica Prush and processed by Isabel Morris, who provided the plots in Figure 3.6.

The ambient noise data was collected by Aube Gourdeau and field assistants and processed by Phillippe Rossett and Luc Chouinard, who provided the plots in Figure 3.7.

Claudine Nackers developed the site-specific safety plan which enabled the trench excavation and is included as a supplementary material in the submitted manuscript (included here as Section 3.7).

Matthew Tarling physically dug the test pit, stitched the photos of test pit and main trench using Agisoft Metashape to produce the images in Fig. 3.5A and 3.9 but did not participate in interpretation.

The field work was led by Aube Gourdeau with assistance in the trench from Christie Rowe, Veronica Prush, Claudine Nackers, and Michel Lamothe, with field assistants (see Acknowledgements).

Chapter 4 Completely written by Aube Gourdeau, with edits from Christie Rowe

CHAPTER 1

Introduction

In the field of paleoseismology, active faults record important information regarding past seismicity and represent critical sources of data when trying to forecast earthquakes. To this day, hazard estimation depends on developing realistic earthquake scenarios based on specific historical earthquakes and their attributes (location, depth, size, orientation of fault, propagation direction, etc.). These estimations are thus dependent on our capability to accurately identify and map paleoearthquakes, often at times when no reliable written testimonies are accessible. During the last century, most Quaternary faulting research developed in plate boundary settings, where the high seismicity and high magnitude (M7+) earthquakes represent significant hazards for the population and infrastructure. In plate boundary regions, studies revealed fast and relatively constant long term tectonic strain rates, and ruptures that recur in temporal patterns on the same fault systems (Kanamori, 2003).

In the last decades, more attention has been given to uncommon scenarios, such as intraplate seismicity including seismicity associated to deglaciation. These earthquakes often lead to moderate magnitude earthquakes (M5-M8), that can still be as deadly as their plate boundary counterparts (e.g. Stein, 2007; Soto-Cordero *et al.*, 2018). Indeed, the low tectonic strain rates and the chaotic recurrence intervals for intraplate seismicity lead to unpredictable behavior and unexpected earthquake locations that can hit unprepared regions harder. These settings are often harder to study since the slow strain rate and the recent resurfacing of deglaciated landscapes lead to the creation of subtle faults. The plate boundary settings, on the other hand, often develop in arid climates with slow geomorphologic changes relative to the rate of faulting which makes the features more apparent. Intraplate settings often represent challenging environments for remote and field mapping, but could be as rewarding as plate boundary settings in terms of seismic hazard predictability.

In this context, this thesis aims to develop a set of paleoseismology tools adapted for the province of Québec, which had never been closely monitored regarding neotectonics. This lack of investigations was probably associated with the challenges inherited from the glacial history of the area, such as the dense vegetation cover, the low tectonic strain rate associated to intraplate unloading, the dominant young glacial geomorphology, and the very sparse coverage for high-resolution lidar imagery prior to 2016. By developing these tools, the principal objective of this project was to identify potential fault scarps using remote sensing and confirm (or infirm) remote observations in the field. This set of observations may support the eventual optimization of earthquake hazard scenarios for the province of Quebec and for the Western Quebec Seismic Zone.

The second chapter of this thesis represents the draft of a paper that focuses on the general identification of potential fault scarps in Québec using remote sensing. The tectonic, glacial, and Quaternary history of Canada and Québec will be described, the historic and prehistoric earthquake record of eastern Canada will be revisited, and the possible drivers of the seismicity in the province of Québec will be presented. The orientation chosen for the project will be justified based on a literature review on an analog of Québec, Fennoscandia, where context-appropriate methods for paleoseismology and fault scarp identification have been more advanced than the nascent studies in eastern Canada. This background section will be followed by a detailed presentation of the method I developed, with coauthors, to identify potential fault scarps using remote sensing in deglaciated landscape, and the general map of potential active fault scarps we generated (see Author Contributions Section). This chapter forms the core of a manuscript in preparation for submission to *Canadian Journal of Earth Sciences*.

The third chapter is a submitted article, "Investigation of suspected Holocene fault scarp near Montréal, Québec: The first paleoseismic trench in eastern Canada" (submitted to the diamond open access journal *Seismica* in Jan. 2024, currently undergoing minor revisions). This chapter describes field investigations realized on on of the candidate scarp that was suspected to be a surface-rupturing fault identified in the second chapter. The scarp is located in St. Liguori, 50km away from Montréal. Three geophysical surveys (ground penetrating radar, depth estimates from ambient seismic noise, and refraction seismology) were realized on site, followed by the creation of a 1 m deep test pit. The investigations were completed by the creation of the first paleoseismic trench ever attempted in Québec, which will be described in detail.

The 4th chapter contains a few more details regarding the trench planning and work that was done to establish a legal frame for the practice of paleoseismology in Québec. Networking efforts made amongst the scientific community to build a solid group of scientists having varied backgrounds that could collaborate on future paleoseismology projects in the Province will also be presented.

CHAPTER 2

Geomorphic identification of possible fault scarps in southern Québec, Canada

---

2.1 Introduction

Although far from any active plate boundary, Eastern Canada is susceptible to damaging earthquakes. Historical records from the last 300+ years record several M>6 events and geologic evidence suggests the prehistoric occurrence of even larger earthquakes (Lajeunesse *et al.*, 2017). Several regions of Québec and Ontario have been distinguished by different seismic behavior, in particular the Charlevoix-Kamouraska (CSZ), the Western Quebec (WQSZ), and the Lower St. Lawrence Seismic Zone (LSZ) (Brooks & Adams, 2020). All these seismic zones sit in southern Québec/Western Ontario, and together comprise the cities of Montréal, Québec, and Ottawa-Gatineau. Montréal itself, represents the city having the second highest seismic risk in Canada, even though it is positioned in the middle of a stable craton in the North American Plate, far away from any plate boundary (Yu *et al.*, 2016b; Canada, 2023).

The moderate to large seismicity in the province of Québec is known to have caused numerous M6+ earthquakes (e.g. 1732 M5.8 Montréal, 1663 M7+ Charlevoix, 1935 M6.2 Timiskaming), damaging masonry and infrastructure, and triggering landslides and liquefaction (Lamontagne, 2002). Despite the evidence for recent and ongoing seismicity only a single surface-rupturing fault scarp has been identified in Québec, in the Ungava area (Figure 2.4; Adams *et al.*, 1991; Adams & Basham, 1991; Brooks & Adams, 2020; Mérindol *et al.*, 2022). The geologic records and historical accounts of shaking suggest that recent earthquakes may have been large enough to produce surface ruptures, but identification of scarps has been delayed by challenging mapping conditions, such as the dense vegetation, recent resurfacing that took place during the Quaternary, low strain rates, and the large potential search area (Brooks & Adams, 2020). The use of this very sparse to absent paleo-earthquake record combined with the very brief instrumental record thus limits our understanding of the seismicity and poses a potential threat to the densely populated cities of Montréal, Ottawa, and Québec, which are plagued by significant uncertainties in defining seismic hazard (Swafford & Stein, 2007; Kolaj *et al.*, 2023). Identification of recent earthquake rupture traces has the potential to provide specific earthquake scenarios for hazard modeling, support the understanding of fault activity rates and the spatiotemporal patterns of paleoearthquake activity (e.g. Morell *et al.*, 2020; Vallage & Bollinger, 2020; Scott *et al.*, 2023).The present sporadic earthquake data for ruptures in intraplate regions and poor constraints on recurrence holds the community from determining if individual faults represent strain accommodators, or if volumes of crust containing many faults are responsible for post-glacial strain release, information that could be crucial for the creation of hazard maps. Recent scarps, if dated, can also clarify the driving forces of continental seismicity by comparison to models of tectonic stressing and post-glacial rebound (Stewart *et al.*, 2000).

The recent release of high-resolution lidar imagery for southern Québec by the Gouvernement du Québec (Ministère des Forêts, 2016) offers a new opportunity to examine the landscape of the seismic zones to look for evidence of surface-rupturing faults. We investigated three subregions near population centres in Québec which had experienced significant seismic shaking in historic times. Survey areas were chosen either for proximity to historical earthquakes or for significant societal hazard.

The surface expression of faults in an intracontinental, recently de-glaciated boreal environment is different from more tectonically active regions where geomorphic indicators of faulting are better established (McCalpin, 2009; Vallage & Bollinger, 2020). Usually, erosion rates exceed fault slip rates in stable continental interiors, resulting landscapes with few characteristics clearly linked to seismicity (McCalpin, 2009). Young landscapes in the recently deglaciated areas also have short times to develop fault-related features. Therefore, we incorporate and adapt criteria for scarp description and interpretation developed in related environments, in particular, cratonic Fennoscandia. There, the motivation for safe nuclear waste repository management has led to significant advances in intracratonic paleoseismology (Sutinen *et al.*, 2014).

In this contribution, we report an inventory of topographic lineaments we identified in lidar DEMs and assessed relative to our adapted criteria to estimate the likelihood of surface rupturing earthquake as the origin of the lineation. We conclude with a synthesis of recommendations for future investigations and report the most favorable potential scarp locations for further paleoseismic studies.

2.1.1 Geological setting and glacial history of Québec

Québec is part of the northern part of the North American tectonic plate. The vast majority of the province is made of the Precambrian rocks of the Canadian shield (2.85-0.97 Ga; Shilts *et al.*, 1987). The Canadian Shield is a large area, which stabilized during the Archean and Proterozoic and now outcrop as low relief peneplains carved by the last glaciation (Shilts *et al.*, 1987; Dyke *et al.*, 1989; Comeau *et al.*, 2017). The late Archean-aged Superior province, composed of crystalline rocks, dominates the landscape in Northern Quebec, while the Grenville geological Province, made of metamorphosed volcano-sedimentary rocks of Archean

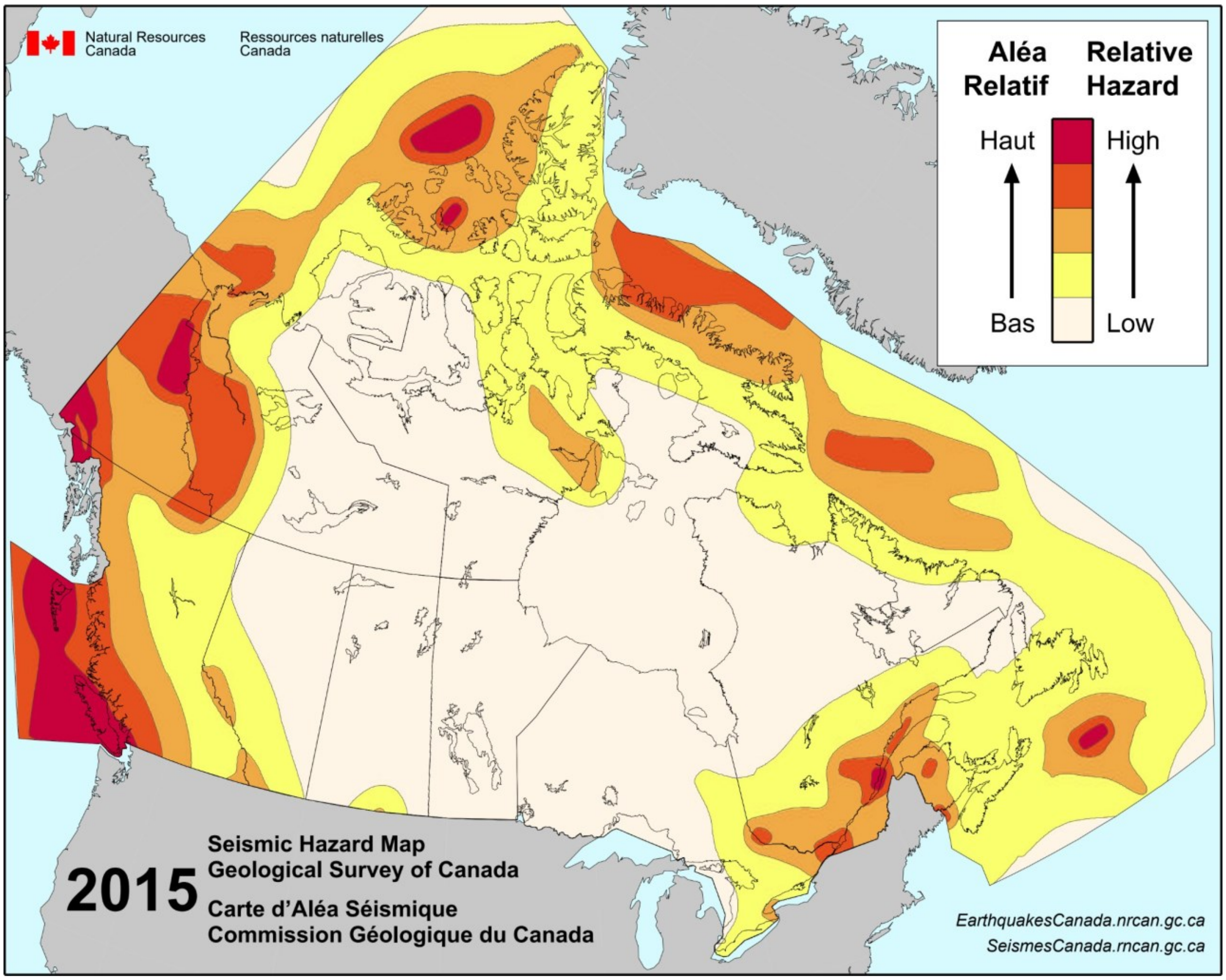

Figure 2.1 Simplified seismic hazard map for Canada created by the geological survey of CanadaHalchuk *et al.* (2014)

to Mesoproterozoic age, dominates in Southern Québec (Comeau *et al.*, 2017; Lambert *et al.*, 2018). These rocks were metamorphosed during the Grenville orogeny, which started during the Mesoproterozoic (around ~1.3-1 Ga ago) along the margin of the Laurentia continent, and was related to the formation of the supercontinent Rodinia (Lambert *et al.*, 2018; Robert *et al.*, 2021). When the supercontinent rifted apart three oceans formed: the West Iapetus, the East Iapetus, and the Tornquist Ocean (representing a triple junction), which separated the continents of Laurentia, Amazonia, and Baltica (Rimando, 1994; Robert *et al.*, 2021). The West Iapetus ocean opened up between 750-700 Ma ago, while the East Iapetus ocean opened up at ~590 Ma ago, creating the Saint-Lawrence rift system, which encompasses the Ottawa Bonnechère Graben, the Temiskaming graben and the Saguenay Graben (fig. 2.2) (Lambert *et al.*, 2018; Brooks & Pugin, 2020). The rifting and the graben development stopped ~450 Ma ago, when the Paleozoic Appalachian orogenies reworked the cratonic margin and accreted supra-crustal belts, supra-subduction zone rocks, and arc terranes to the edge of Laurentia, closing the Iapetus Ocean and causing continental shortening (Rimando, 1994; Brown *et al.*, 2011; Lambert *et al.*, 2018). The Ottawa Bonnechère Graben and Saguenay Graben are now referred to as aulocogens, or failed rift arms (fig. 2.2) (Kumarapeli & Saull, 1966; Lowe, 2024; Tremblay *et al.*, 2003; Rimando & Peace, 2021). Today, the grabens are striking NW-SE, While the main rift along the St-Lawrence trends NE-SW (Rimando, 1994). Mid-Paleozoic and Mesozoic reactivation of these extensional faults contributed to the graben geometry (Tremblay & Lemieux, 2001; Lemieux *et al.*, 2003; Sasseville *et al.*, 2012) offsetting the Devonian Charlevoix impact structure creating the throw on the bounding faults that was enhanced by differential erosion to create the present day topography (Rocher *et al.*, 2003; Tremblay *et al.*, 2013). These ancient tectonic events set the stage for late Cenozoic uplift and denudation to create today's landscape.

Québec has experienced cyclic continental ice sheet advances and retreats since the onset of northern hemisphere ice ages in the early Pleistocene about 2.7 Mya (Willeit *et al.*, 2019). However, the glacial sedimentary record in Québec is thin or absent before the late

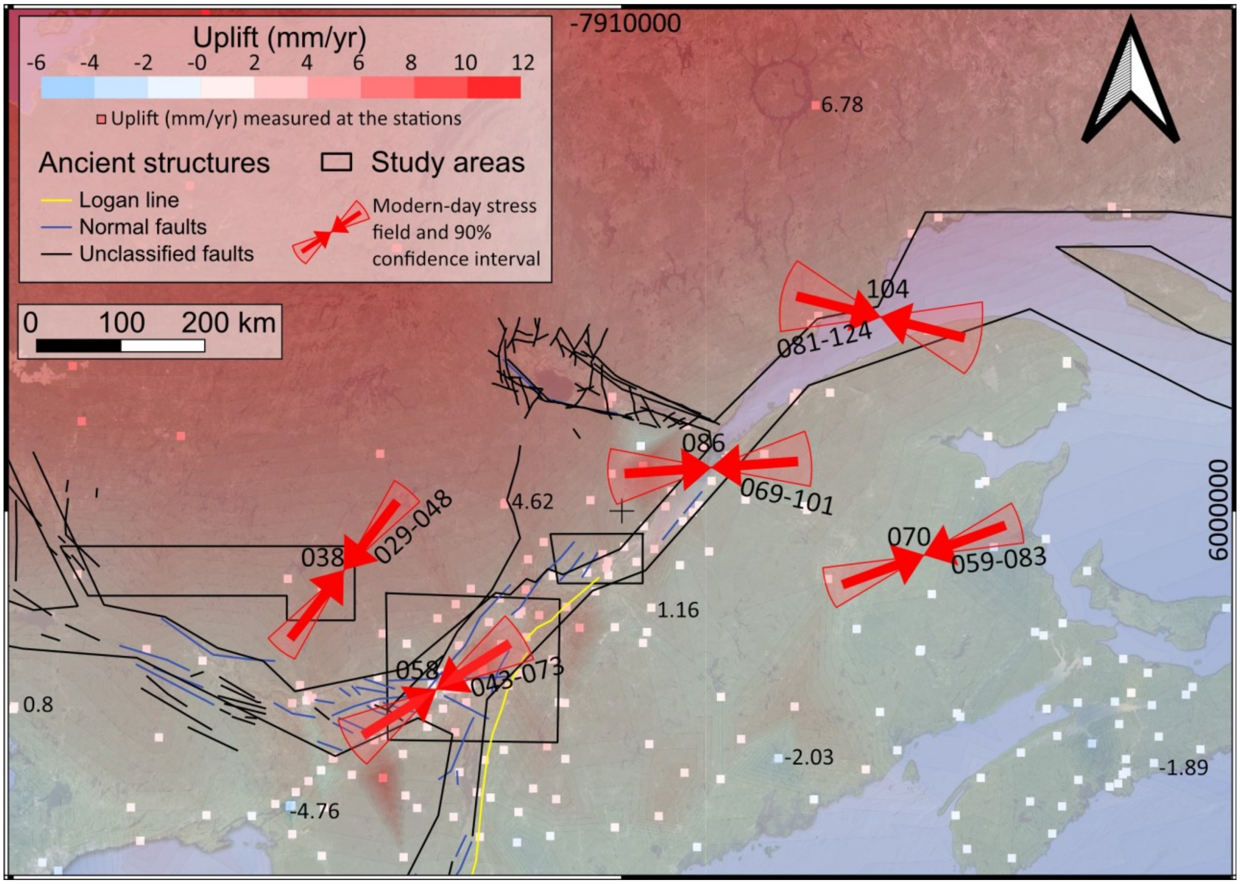

Figure 2.2 Contours of the current regional vertical component of the velocity field of Canada in mm/yr, retrieved from Robin *et al.* (2020). Blue contours represent subsidence while red contours represent uplift. Colored squares represent velocity values measured at the stations where the data was collected. The red arrows in the map represent the median of the modern-day maximum horizontal compressive stress from focal mechanisms modified from Mazzotti & Townend (2010). The red polygons represent the 90% confidence interval azimuth for the maximum horizontal compressive stress, again from Mazzotti & Townend (2010). The black boxes represent the research areas. The major inherited structures and faults are presented as black, blue, and yellow lines in the figure. They represent a compilation of different reports, the Saguenay Graben area mostly mapped using Lowe (2024), and the Ottawa-Bonnechère Graben using Kumarapeli & Saull (1966).

Pleistocene, probably due to erosion of previous deposits by subsequent advances (Shilts *et al.*, 1987; Occhietti *et al.*, 2011). The Wisconsinian ice sheets probably started accumulating mass around the Marine Isotope Substage 5d (~109 ka Occhietti *et al.*, 2011). The last glacial maximum (LGM) occurred during the late Wisconsonian at about 21 kya, when the Laurentide Ice Sheet (LIS) covered much of modern-day central and eastern Canada and US (Fulton & Prest, 1987; Dyke, 2004). The LIS was up to 3 km thick at that time, and the formation of ice was responsible for the drop of the sea levels by 120 m (Peltier, 2004).

After the LGM, the climate began warming (Clark *et al.*, 2012), and the Labrador sector of the LIS started to melt, causing a rise of 80 m in the mean sea level height between 19 - 11 ka (Clark *et al.*, 2012). The thinning led to the exposition of various landforms (such as end moraines, ice flow lineaments, and eskers) formed during the glacial advance that could be mistaken for post-glacial fault scarps, and initiated the glacial adjustment of the region (Occhietti *et al.*, 2011). These glacial features help reconstruct the history of glacial advances and retreats and flow direction of the ice sheet (Clark *et al.*, 2000). At ~12 ka, since the isostatic rebound had not yet compensated for the ice unloading and the sea level rise, holding the crust under sea level, the Saint-Lawrence Lowlands were inundated by saline waters from the Atlantic Ocean, forming a shallow marine environment: the Champlain Sea (Hocq *et al.*, 1994; Occhietti *et al.*, 2001). The ice sheet slowly continued its retreat northward, resulting in the formation of the Laflamme Sea in the Saguenay-Lac-Saint-Jean region and the Goldthwait Sea along the North Shore of the St. Lawrence Estuary (Hocq *et al.*, 1994; Occhietti *et al.*, 2001). The Champlain Sea fully retreated ~9.75 ka ago, leaving behind the freshwater of the Lake Lampsilis (Occhietti *et al.*, 2001). While Lake Lampsilis was at its full extent, the Tyrrell Sea, which runs along the edges of Hudson Bay, and the Iberville Sea, which runs along the edge of Ungava Bay, finally appeared (Hocq *et al.*, 1994). The Lake Lampsilis fully retreated 7.5 ka ago (Hocq *et al.*, 1994). It wasn't until 6 cal. kya that all of present-day Québec was fully free of ice (Occhietti *et al.*, 2011).

The Laurentide ice sheet that covered Québec left behind sediments thinly veiling bedrock (red areas in Figure 2.3; Brouard *et al.*, 2020). About half of Québec is covered by till (apple green areas in Figure 2.3), one quarter represents <1 m thick sediments or exposed bedrock, and the remaining area is covered by a mix of marine, lacustrine, fluvioglacial, and fluvial deposits (Brouard *et al.*, 2020). The surface of the Grenville province is dominated by outcropping bedrock, thin sediments, and undifferentiated tills. The surface of the Saint Lawrence Lowlands province, on the other hand, is dominated by glacio-lacustrine and glacio-marine sediments associated with the Champlain Sea (Brouard *et al.*, 2020). Mixed alluvial deposits are concentrated along the Saint-Lawrence River, but disappear away from the modern channel. Some undifferentiated till is also present in the Saint-Lawrence Lowlands, especially in the periphery of the province. Exposed bedrock is rarely observed in the Saint-Lawrence Province. The emergence of exposed bedrock south of the Saint-Lawrence Lowlands marks the edge of the Appalachian Province, which is dominated by Paleozoic metasedimentary bedrock and till (Brouard *et al.*, 2020).

2.1.2 Post-glacial earthquake history and the paleoseismic record

The Saint-Lawrence Lowlands clays were deposited in the Champlain Sea; some of these deposits are sensitive clays, which are prone to landsliding (Quinn, 2009; Bégin & Filion, 2010). The landslides can be triggered on land or in water by liquefaction during seismic shaking (Mérindol *et al.*, 2022). The presence of these clays is hazardous for the Québec population, especially near coastal areas, where they present a risk of tsunami, coastal erosion, and landsliding (Mérindol *et al.*, 2022). The increased vulnerability of the population from the sensitive clays justifies the urge to better understand the seismic record. Ironically, these clays become allies when trying to identify and date large paleoearthquakes which caused enough ground motion to generate paleolandslides or mass transport deposits in lake bottoms or in the St. Lawrence estuary, by creating a relatively precise and undisturbed record of past earthquakes correlated to sedimentary records of liquefaction and induced slope failures (Quinn, 2009; Tuttle & Atkinson, 2010; Brooks, 2014; Lajeunesse *et al.*, 2017; Trottier *et al.*,

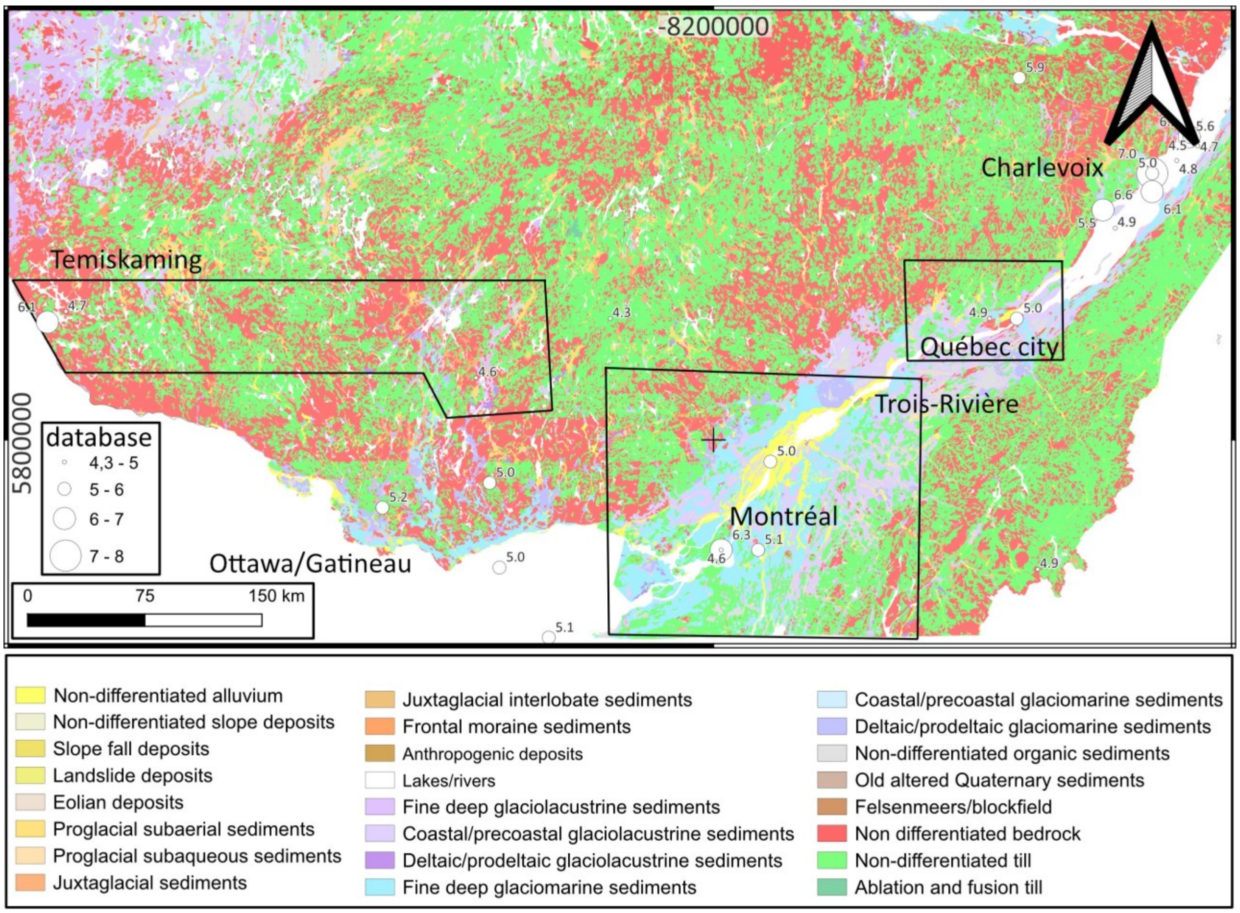

Figure 2.3 Distribution of bedrock exposure and glacial/postglacial sediments in southern Québec (Brouard *et al.*, 2020). The green areas represent undifferentiated tills and the red areas represent outcropping bedrock or <1 m thick sediments. Temiskaming area is mostly underlain by exposed bedrock and till, Montréal and Québec city areas have similar terrane in the north and the southern parts of the areas are on Paleozoic carbonate bedrock overlain by thicker glaciogenic and glaciomarine sediments, with minor recent fluvial deposits.

2019; Brooks & Pugin, 2020; Mérindol *et al.*, 2022).

Paleolandslides, mass transport deposits or post-glacial fault scarps also represent keys for the seismic history of Québec since it is almost unknown prior to the European settlement ~450 yrs ago (Trottier *et al.*, 2019). Even in the last 450 years, the earthquake record is highly sparse and dependent on the European settlements' position (Trottier *et al.*, 2019). Oral histories and place names may recount earlier earthquakes, such as the naming of Mont-Tremblant for a Weskarini traditional story about the danger of a large mountain which would shake and tremble if the spirit beneath was displeased by human activities (Graham, 2005). Moreover, the recurrence interval for earthquakes of M6+ in Eastern Canada has been estimated to be of thousands of years (Craig *et al.*, 2016) (or even absent Calais *et al.*, 2016), highlighting the importance of knowing the position and magnitude of pre-settlement earthquakes.

Numerous surveys were conducted in lacustrine basins, since their poor consolidation makes them sensitive to ground shaking, without encountering major anthropogenic disturbance (Trottier *et al.*, 2019). The vast majority of potentially triggered slope failure deposits found were associated with the Charlevoix seismic zone (Ouellet, 1997; Doig, 1998). The 1663 M7 Charlevoix earthquake was recorded in multiple lake bottoms and at multiple sites along the Saint-Lawrence Estuary using mass transport deposits, highlighting the intensity of this seismic event (Filion *et al.*, 1991; Trottier *et al.*, 2019; Mérindol *et al.*, 2022). The 1935 M6.2 Temiskaming earthquake also apparently triggered slumping of postglacial sediments in lake bottoms over an area of 600 km^2 (Shilts & Clague, 1992; Doughty *et al.*, 2010). Other evidence found in sediments at the Lac-aux-Sables in Southern Québec are suspected to be associated with the 1944 M5.8 Cornwall earthquake and the 1732 M5.8 Montréal earthquake (Lamontagne *et al.*, 2008; Trottier *et al.*, 2019).

In Québec, sparse evidence has led previous workers to suggest possible cycles of enhanced activity from the paleoseismic record, on the basis that a peak of frequent and intense activity might be common to multiple lake and river sediments across the province (Trottier *et al.*, 2019). Peaks in seismic activity have been proposed at ~13 - 10.5 ka cal BP for data collected to the north and west of Trois-Rivière (Trottier *et al.*, 2019), ~9.4 -8.95 ka cal year BP for the Abitibi-Temiskaming area (Brooks, 2018, 2020), and 10 – 9.5 kya close to Charlevoix (Tuttle & Atkinson, 2010). A second period of elevated seismicity might have taken place around ~980 to 1180 AD based on a few studies that revealed evidence for paleolandslides in river bottoms NW of Ottawa and in lake sediments West of Trois-Rivière (Brooks, 2013; Trottier *et al.*, 2019). The estimations for the peak seismicity following the deglaciation in Fennoscandia are better constrained than in Québec, peaking ~11.5 and 8.2 ka, with evidence of clustered ruptures from ~11-9 ka (Craig *et al.*, 2016; Lukk & Sidorin, 2019; Bungum & Eldholm, 2022), but differences in ice sheet sizes, deglaciation speed, and the number of paleoearthquakes might suggest that both regions have distinctive behaviors (Craig *et al.*, 2016; Bungum & Eldholm, 2022). However, without having a complete paleoseismic record, it is impossible to establish the patterns or peaks of seismicity in the recent past to statistically significant levels.

The sparse studies mentioned above, coupled with oral and written testimonies, helped to identify and estimate the magnitude and position of >25 damaging earthquakes affecting southern Québec between 1600 and 2024, of estimated M4.3-6.6 (Figure 2.4)(Lamontagne *et al.*, 2000). The earthquakes occurred mostly in the St Lawrence valley and the secondary aulocogens of Ottawa-Bonchère and Saguenay, except for the Ungava M6.3 and the Grand Banks earthquakes (Figure 2.4). In urban areas, the precise source location of these paleoearthquakes can only be determined once actual recent fault locations are identified in the field.

2.1.3 Possible drivers of seismicity

Because of the limited record and the complexity of intracratonic deformation, the drivers of the seismicity are still poorly understood (Lamontagne, 2002). The glacial history of Québec and the lithospheric strain accumulation in response to ice sheet loading may help explain its

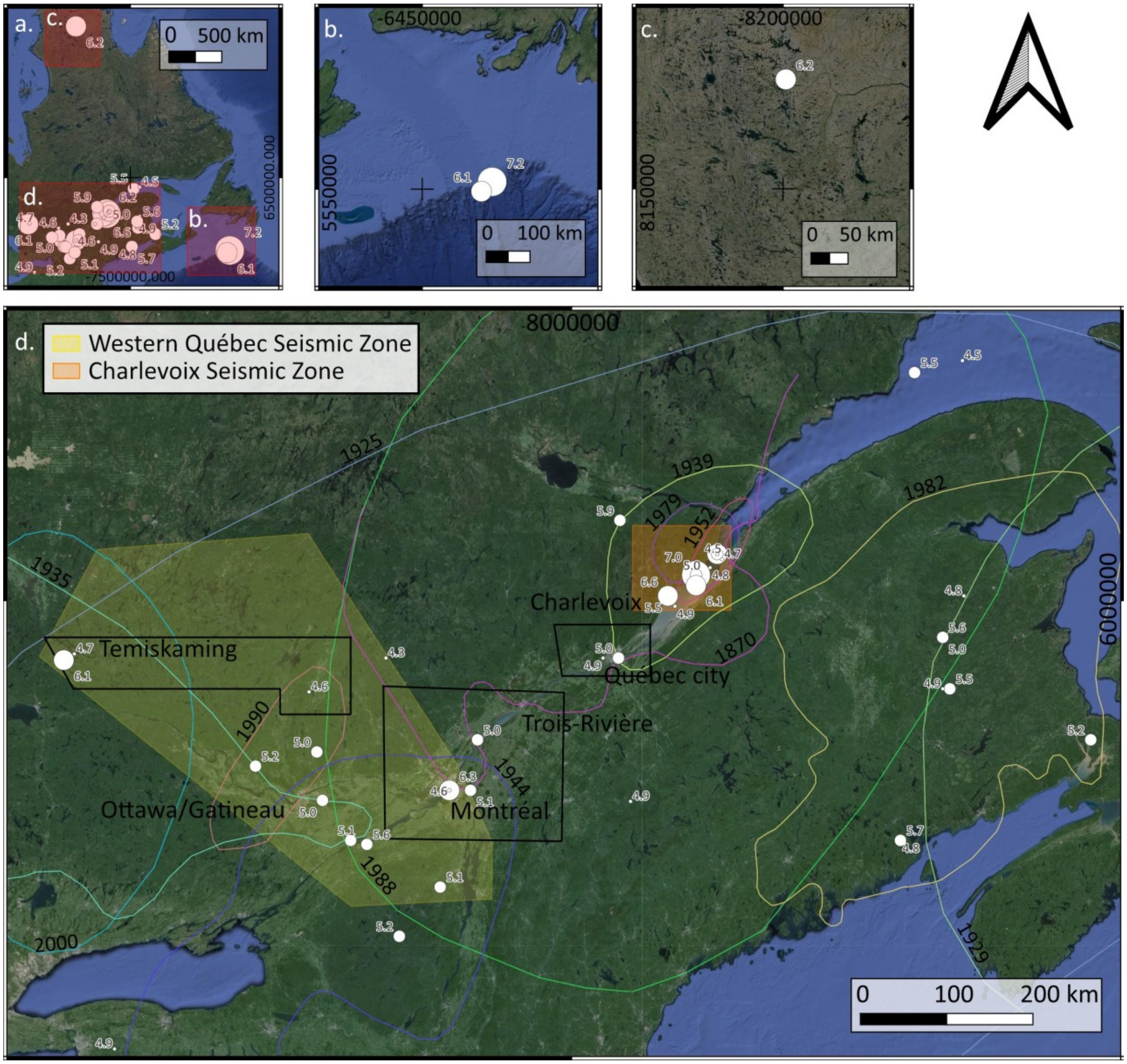

Figure 2.4 Map of the known historical earthquakes, generally of M5+, that struck Québec between 1600 and 2017 by Lamontagne *et al.* (2018). The available isoseismal lines for M5 (Mercalli) earthquakes were added to the map, with the events' year (Lamontagne *et al.* (2018)). The WQSZ and the Charlevoix Seismic Zones are highlighted in the figure. The modern-day stress field orientation measured from focal mechanisms and the 90% confidence interval azimuth of the axis of maximum horizontal compressive stress, retrieved from Mazzotti & Townend (2010), are indicated using red arrows and red polygons.

unusually high modern seismicity, which stands out compared to other regions located in a tectonically stable continental interior, away from plate boundaries(Craig *et al.*, 2016; Wu & Johnston, 2000). On timescales similar/longer to glacial cycles, the viscoelastic compressional strain accumulated due to glacial loading in the Canadian lithosphere (Craig *et al.*, 2016), which depressing the crust beneath the thickest ice during the LGM by up to half a kilometer (Jones *et al.*, 2019; Bungum & Eldholm, 2022). This load imposes a downward flexure of the crust which is partially accommodated by sub-crustal material migration, imposing up to ~60 m of uplift to the land in the periphery of the ice sheets and creating a forebuldge (Jones *et al.*, 2019; Bungum & Eldholm, 2022). This interaction between glaciations at the surface and the solid Earth not only induces varying vertical stress but also increases the horizontal stress within the covered regions (Bungum & Eldholm, 2022).

When the ice sheet melts, the accumulated strain can be released as extensional strain due to rapid and local transient stress changes, such as surface mass redistribution, fluid migration, surficial erosion, or glacial isostatic rebound (Steffen *et al.*, 2014a; Calais *et al.*, 2016; Craig *et al.*, 2016). In Québec, the mechanism that decreased the magnitude of the vertical minimum principal stress was the ice unloading, which resulted in a higher differential stress in the crust (Adams, 1989). As the rebound stress became more important, the crust began to uplift and expand horizontally, generating horizontal compression along the previous ice margins (fig. 2.2)(Lund Snee & Zoback, 2020). Because of stress distribution, post-glacial faults are most likely to be found at the margin of the ice sheets, with small-displacement postglacial faulting still expected throughout the extent of the area covered by the ice sheet (Adams, 1989). Since the unloading is rapid, the elastic response of the lithosphere results in brittle deformation and a rolling locus of seismicity as the inflection point migrates to follow the unloading front (Adams, 1989; Muir-Wood, 2000; Stewart *et al.*, 2000).

The area surrounding the St. Lawrence River currently experiences an average uplift of 3.1 mm/yr (fig. 2.2) (Goudarzi, 2016). As a result, stress perturbations due to glacial isostatic adjustment could trigger fault instability in eastern Canada today, which is experiencing a compressional stress field (fig. 2.2); hence postglacial faulting tends to be thrust faults (Steffen *et al.*, 2014b; Lund Snee & Zoback, 2020). The possibility for ice loading/unloading to induce faulting is supported by numerical simulations (Steffen *et al.*, 2014b; Wu & Johnston, 2000) and comparisons to Fennoscandia (Wu *et al.*, 1999). It is clear that regionally, post-ice sheet rebound contributes to continental seismicity. However, the isostatic rebound cannot explain the clustered distribution of the earthquakes in eastern Canada, nor the higher activity rates than other regions experiencing ongoing GIA due to the recession of the LIS.

The existence of local zones of increased seismic activity could be explained by the presence of pre-existing geological regions of weakness that are prone to disturbance. The seismicity is highly correlated with the aulocogens formed during the rifting of Rodinia: the Timiskaming Graben, Ottawa-Bonnechere Graben, and Saguenay Graben, branches of the Saint Lawrence Rift System (fig. 2.2) (Rimando & Peace, 2021). The local concentrations of seismicity could be associated to the reactivation of inherited weak structures under the prevailing present-day NE-SW-striking regional maximum horizontal stress (fig. 2.2) (Rimando & Peace, 2021). Another source of heterogeneity in continental structure, which is invisible from the surface, is the modified lithospheric mantle caused by the Mesozoic activity of the Great Meteor hotspot (Rondenay *et al.*, 2000). The clustered and deeper hypocenters observed in the WQSZ compared to the background seismicity have been suggested to indicate that the track could play an important role in modern-day earthquakes (Ma & Eaton, 2007). Tomographic maps show that a low velocity corridor in the lithospheric mantle parallels the trend of hot spot volcanics but the location is offset (Villemaire *et al.*, 2012). Previous authors suggested that this anomaly was produced by the hot spot, and the displacement of the mantle feature from the volcanic centres on the surface reflects some post-Cretaceous modification of the continental root (Rondenay *et al.*, 2000; Villemaire *et al.*, 2012). All these factors could have contributed to strength heterogeneities that focus seismicity: the hot spot impinging on the lithospheric mantle could have caused thermal rejuvenation of rift faults of the area associated with the Grenville orogeny and the Iapetan ocean opening, and the anomalous thickness or rigidity of the crust or mantle along the Monteregions/New England/Great Meteor hot spot track could be concentrating strain (Rondenay *et al.*, 2000; Ma & Eaton, 2007; Lang & ten Brink, 2022).

Succinctly, multiple drivers could explain the strong seismicity in eastern Canada, but none of them can fully explain the earthquake distribution on their own, and the relative importance of each driver is yet to be determined. Moreover, the recurrence intervals on these earthquakes, as well as the significance of studying intervals in an intracratonic environment, is poorly understood because of the short and restricted earthquake record (Swafford & Stein, 2007; Calais *et al.*, 2016). Finally, the poor constraints on seismic activity don't allow us to determine if the seismicity in eastern Canada is migrating, nor whether all the structures in the St. Lawrence Rift System have the same potential for reactivation (Muir-Wood, 2000; Swafford & Stein, 2007; Rimando & Peace, 2021).

2.2 Study area

Three high-population study areas were selected based on the number of historical earthquakes, and the overall seismic risk. Our remote mapping efforts were focused on regions that had recorded or were adjacent to the approximate location of major historical earthquake epicenters, including the 1935 Timiskaming (M6.2), 1944 Cornwall (M6.2), 1990 Mont-Laurier (M5.0), 1732 Montréal (M5.8), 2000 Kipawa (M4.7), and the 1663 Charlevoix (M7.0) earthquakes (Figure 2.4)(Lamontagne *et al.*, 2008).

The first area chosen was the region around the island of Montréal, the biggest city in Québec and second largest in Canada, which encompasses roughly 20% of the province's population (Ministère de l'Économie, de l'Innovation et de l'Énergie, 2022). The Montréal zone extends ~100 km around the island of Montréal in all directions. It sits in the Saint-Lawrence Lowlands geological province, with the NW corner included in the southern edge of the Laurentians region of exposed Grenville Belt bedrock, and the SE corner included in the Appalachian

Orogeny. This area encompasses the possible position of the 1732 Montréal Earthquake's epicenter (M~5.8), which is thought to have been large enough to have potentially caused a surface rupture (Leblanc, 1981).

The second area around Timiskaming encompassed a wide band of forested and wild territory comprising a very sparse population but situated only 100 km away from Ottawa, the capital of Canada. This area extends from ~46°19'44.00"N to ~ 47°00'00.00"N latitude, on the Grenville Belt, which is only thinly sedimented and dominated outcropping bedrock and bedrock fractures (Fig. 2.3, 2.5). The area is also part of the Western Quebec Seismic Zone, and encompasses the likely source region of the 1935 M6.2 Temiskaming earthquake.

The third region is Québec, the capital city with a population of ~550,000, which has the most elevated seismic risk in Quebec due to its proximity to the Charlevoix seismic zone. The area is underlain by Grenville Belt bedrock in the north, the Saint-Lawrence Lowlands, and the Appalachian fold belt in the south, giving rise to a variety of landscapes and surface geomorphologic styles.

2.3 Identification Methods

2.3.1 Lidar Digital Elevation Models

Lidar elevation data are now considered indispensable tools for mapping geomorphic landforms for neotectonic study(Novoa, 2013; Palmu *et al.*, 2015; Öhrling *et al.*, 2018; Brooks & Adams, 2020). Lidar data collected from satellites or aircrafts can be processed to reveal a "bare-Earth" view of the land surface, removing vegetation or anthropogenic features (Mikko *et al.*, 2015). When available at high resolution, lidar is an exceptional tool for revealing 1-10s meters-scale landforms, such as fault scarps, river terraces or glacial lineations, which are too subtle to identify in the field or using topographic maps (Johnson *et al.*, 2015). Our approach relies on the interpretation of geomorphic features from LiDAR-derived topography products and is thus constrained by the availability, quality, and coverage of public datasets often made available by governments or public agencies. In 2006, the Government of Québec began collecting and releasing lidar-derived products and published them as 1:20,000-scale TIF tiles (Ministère des Forêts, 2016). In 2016, southern Quebec was fully mapped using high-resolution lidar imagery, opening the way for paleoseismic studies (Brooks & Adams, 2020).

In this study, 1 m digital elevation models made available by the Government of Québec were manipulated using geographical Information System software (ArcMap, version 10.7.1 & QGIS version 3.22.7). Three types of lidar-derived data products were used: 1) Digital Terrain Model (DTM), the triangular irregular network showing elevations and has a spatial resolution of 1 m for the imagery in Québec; 2) hillshade (or 'ombre'), a DTM-derived, three-dimensional visualization of the surface with a spatial resolution of 2 meters mimicking the shadow created by topographic variation using a simulated sun angle, and 3) a slope model, which identifies the inclination of the landscape by calculating the steepness at each cell of a raster surface (Ministère des Forêts, 2016). On the hillshade images, the default incident illumination azimuth was 315°at an altitude 45°, and the Z factor was varied from 1 to 2 to enhance low relief features. The default illumination azimuth was sometimes changed when interesting features looked to be obscured by the default parameters. To identify surficial features in low contrast areas, the darkness and brightness of the enlightened slopes were sometimes changed to exaggerate the appearance of landforms. Some of these settings were guided by the recommendations written in the handbook provided with the data (Leboeuf *et al.*, 2021).

2.3.2 Additional map sources

To facilitate the identification of potential post-glacial faults, multiple regional basemaps were used to add contextual information and complement the observations (Figure 2.5 (following McCalpin, 2009; Palmu *et al.*, 2015; Scott *et al.*, 2023). Although the existing publically available maps do not include identification of any known active fault traces, the

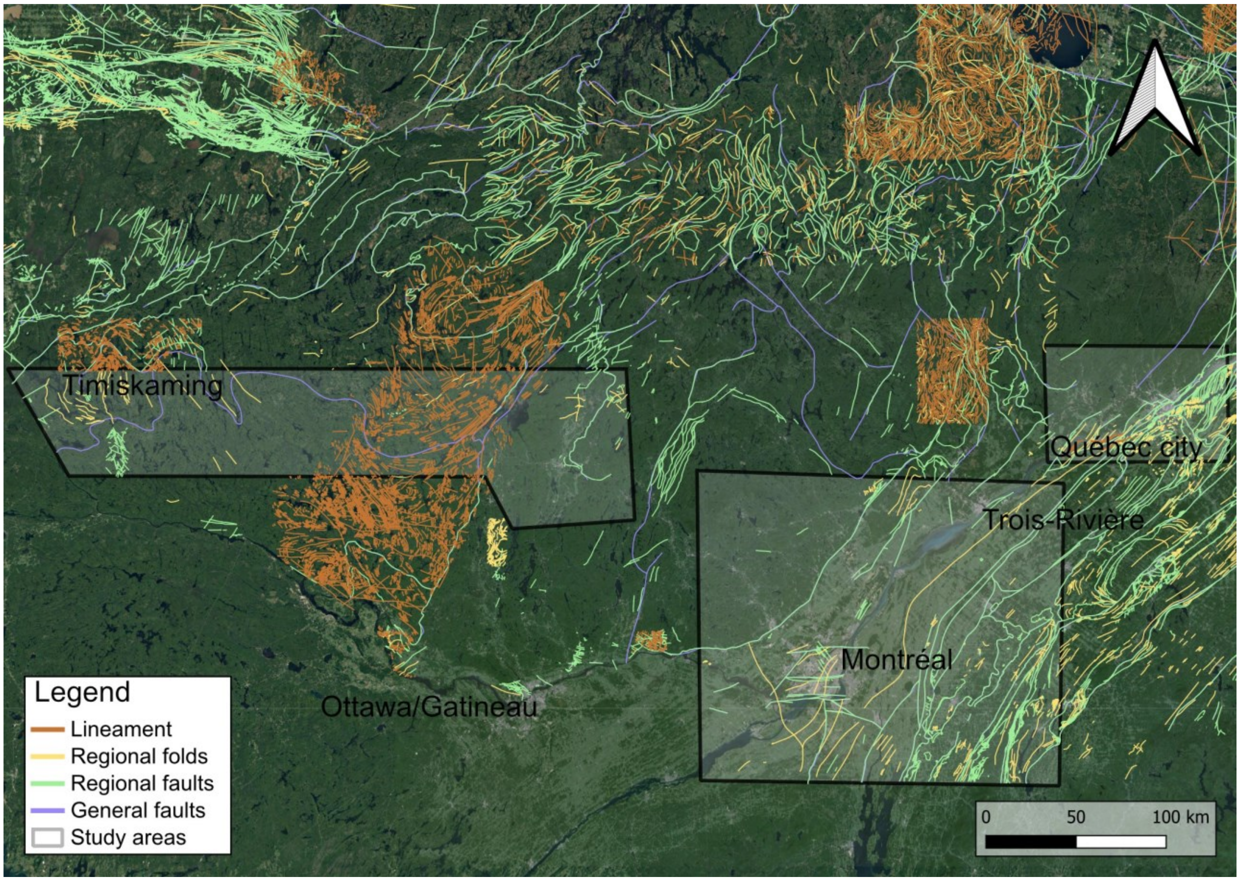

Figure 2.5 Google satellite basemap highlighting the 3 research areas in Southern Quebec (Montréal, Québec city, Timiskaming) and showing the uneven coverage of regional basemaps provided by the governmental agencies de l'Énergie et des Ressources naturelles (2021); des Ressources naturelles et des forêts (2024).

abundant field observations of geological contacts, fracture systems and other lineaments, mean that if active fault scarps or traces are discernable on the landscape they may have already been included in one of these more general databases, or may be associated with pre-existing structures such as fracture arrays or dikes (Firth & Stewart, 2000; Persaud & Pfiffner, 2004).

We considered the bedrock geology layers from the Système d'information géominière du Québec, the geomining information system of Québec (SIGÉOM), including regional faults and folds, geological contacts, and lineaments, and the layer of general morphological-sedimentological zones (Fenton, 1999; des Ressources naturelles et des forêts, 2024). Our study areas are either only partially covered or completely absent from these SIGÉOM layers, due to incomplete mapping coverage. Surface waterways were retrieved from the Quebec hydrographic network geobase (de l'Énergie et des Ressources naturelles, 2021). Finally, we considered the imagery base maps included in ArcMap that has a resolution of up to 1 meter in Canada (Esri *et al.*, 2021) and the Google satellite imagery basemap. These layers were used to separate anthropogenic landforms from natural geological features (Laly, 2021; Gourdeau, 2021; Wang, 2022).

To identify potential scarps, each study area was scanned at a scale between 1:10,000 and 1:20,000 for primary inspection and between 1:2,000 and 1:5,000 in areas of interest, following methods employed in similar studies in Fennoscandia (McCalpin, 2009; Palmu *et al.*, 2015). Potential scarps were defined using the criteria in Table 2.1 and were mapped as linear elements. These scarp traces were then color-coded based on the fault assessment criteria defined below (Table 2.2).

2.3.3 Development of scarp identification criteria table

To develop regionally appropriate scarp identification and assessment criteria, we began by adapting the criteria used in Fennoscandia paleoseismology studies (Smith *et al.*, 2014; Sutinen *et al.*, 2014; Mikko *et al.*, 2015; Palmu *et al.*, 2015), a region of similar bedrock, tectonic history, and recent ice sheet recession. Fennoscandia is an intracratonic setting currently experiencing strong isostatic rebound, following the Weichselian glaciation (correlative to the Wisconsinian glaciation in North America), between 22,000 and 9,000 years ago (Stroeven *et al.*, 2016). In Fennoscandia, post-glacial faulting is hazardous for the population, and also for nuclear disposal facilities (Smith *et al.*, 2014; Sutinen *et al.*, 2014; Mikko *et al.*, 2015; Palmu *et al.*, 2015). Sweden and Finland have a lidar coverage >80%, contributing to a higher density of neotectonic studies (Mikko *et al.*, 2015; Palmu *et al.*, 2015).

National repositories for the identified post-glacial faults now exist in Fennoscandia (Mikko *et al.*, 2015; Palmu *et al.*, 2015), although there is no published consensus criteria table for the identification of post-glacial faults. Similar to most other contexts, manual screening and case-by-case assessment in a variety of landscapes covered by confusing glacial landforms has contributed to the general maps (Mikko *et al.*, 2015). The regional variability inhibits the use of a common methodology since it has to be precise but applicable to a wide range of landscapes. From a survey of recent neotectonic studies in Fennoscandia, we compiled a set of commonly used criteria (Smith *et al.*, 2014; Sutinen *et al.*, 2014; Mikko *et al.*, 2015; Palmu *et al.*, 2015). We augmented this with selected criteria used in plate boundary settings and in post-glacial faulting areas (summarized by McCalpin, 2009).

Finally, Canadian studies made in Eastern Canada and western Ontario were also consulted and added to 2.1. They give information regarding mass transport deposits, modeled behavior of the crust with respect to isostatic rebound, and expected expression and distribution for potential surface rupturing faults (Adams, 1989; Adams *et al.*, 1991; Adams & Basham, 1991; Wu *et al.*, 1999; Wu & Johnston, 2000; Brooks, 2020; Bungum & Eldholm, 2022). Some of our criteria are informed by predictions, such as the expectation of typically low scarp heights, based on the short time periods of activity since glacial resurfacing (c.f. Sutinen *et al.*, 2014). In other cases, such as scarp aspect ratio, the Holocene history of deposition, rebound, and erosion means we don't expect the length and height of a fault scarp to necessarily reflect the expected ratios of formation during earthquakes (c.f. Bucknam & Anderson, 1979; Wesnousky, 2006).

Here we present the attributes prioritized by previous workers in Fennoscandia or North America, then describe the application of those attributes to our three study areas in southern Quebec (Table 2.1).

According to previous work summarized in Table 2.1, column 2, postglacial faults can often be continuous, in a single strand, and linear to angular. Many known postglacial earthquakes also produced discontinuous traces, but their ambiguous geomorphic signatures make them harder to identify (Berglund & Dahlström, 2015; Markovaara-Koivisto *et al.*, 2020). For this reason, we focused on continuous and single stranded traces, but did not strictly limit our search to perfect examples. The scarp height, length, and sense of faulting are highly variable, ranging from submeters to 10s of meters in height, 10 m to 100s of km in length(see 2.1), and the sense of motion is often reverse but also sometimes normal with sometimes small strike-slip components, depending on the position of the scarp with respect to the former ice sheet Fenton (1994); Hanson *et al.* (1999); McCalpin (2009). Since the crustal uplift follows the glacial unloading front, leading to a rolling locus of seismicity (Muir-Wood, 2000; Stewart *et al.*, 2000), the displacement on the observed scarps is expected to usually have occurred during a single or few events, resulting in very minimal flanking deformation (e.g. damage zone development, McCalpin, 2009). Note that a few criteria could not be tested since only remote sensing has been attempted in this study. With future field studies which could hypothetically constrain slip per event in the Quebec paleoseismic record, it may be reasonable to apply slip-to-length ratios as a fault assessment criteria. However the scarp height to length ratio does not function as a slip to length ratio proxy in Quebec due to recent erosion patterns.

The first version of the criteria table, highly influenced by the literature review and the authors presented in Table 2.1, was tested in different geological provinces in Québec and refined iteratively during scarp mapping. The objective was to keep the criteria table applicable to general deglaciated landscapes but in the most synthesized and precise way. Every lidar topography tile was scanned multiple times following updates in the criteria table to maintain uniformity in the dataset. Finally, we generated the first repository of potential post-glacial faults in Quebec Fig. 2.6, and the criteria table, which represents a set guidelines for use in recently deglaciated regions.

The scarps were then classified into 3 categories using Table 2.2 (Gourdeau, 2021). The use of categories was inspired by the the grading scales of (Muir Wood, 1993), that were adapted by Palmu *et al.* (2015); Steffen *et al.* (2021). The categories names and number were slightly changed for our criteria table. The 3 categories were "High", "medium" and "low" confidence scarps. A 4th category consisting of only one fault (Figure 2.6) includes scarps investigated in the field (Gourdeau *et al.*, submitted). That scarp, named the Saint-Liguori scarp, represented the highest-ranking and highest-priority scarp from the three maps, but was recognized as non-fault-related after trenching (Gourdeau *et al.*, submitted). This 4th category (which is not included in the table but included in the mapping) will hopefully represent more scarps in the future and will include confirmed active fault scarps. The use of the criteria table to divide the post-glacial faults into categories hopefully makes the categories as objective as possible, to overcome the inherent uncertainties in qualitative geomorphic analysis (e.g. Scott *et al.*, 2023). The criteria table used to make our decisions appears below.

Highly ranked (green on Fig. 2.6) potential post-glacial faults appeared on lidar imagery as surficial kilometer-long, sharp, curvilinear scarps that offset multiple landforms and/or cuts through sediments, with the scarp always facing the same direction, consistent with dip-slip faulting (McCalpin, 2009). The criterion considered the most important in selecting a high-ranking scarp is the observation of offset in Quaternary sedimentary features deposited after glacial retreat (Fenton, 1994; Olesen *et al.*, 2004; McCalpin, 2009). A recent fault scarp is expected to offset alluvial and glacial sediment and could potentially divert the flow of river channels if the erosion hasn't outpaced the slip rate. The scarp should also be traceable almost continuously in both bedrock and sediments, except where scarps aren't always made of a single strand (stepovers or splays) and have lower relief expression at some points along the trace. Highly-ranking fault scarps often appear as anomalous landforms compared to the rest of the surrounding geomorphology, due to their consistent azimuth and long and continuous strike (McCalpin, 2009). Most of the scarps we identified had a height of the order of a meter, with lengths of a few kilometers. However, the height and the length weren't considered the most important criteria because a high variability in scarp lengths and heights is observed in the Fennoscandian literature (Lindblom *et al.*, 2015; Munier *et al.*, 2020), and the detection of these size ranges could be associated with detection biases.

The scarps were classified as medium confidence when some but not all of the strong criteria were met. If the orientation of the scarp didn't match the strike of the surrounding features such as bedrock joints and fractures, the scarp was also classified as medium.

The low-confidence scarps represent lineaments with discontinuous or ambiguous expressions of the criteria. Some have higher sinuosity, unusually long trace or low relief, and/or by the observation of changes in their facing orientation, which is could only be consistent with strike-slip faulting. The scarps were also classified as low confidence when no sediments were present to confirm the crosscutting of Quaternary deposits. Scarps that appeared in landscapes with abundant bedrock fractures (such as parts of the Timiskaming area) without having sediments nearby were ranked low confidence since no conclusion on their age of activity or sense of offset could be drawn from the lidar topography. Gently sloped scarps were also classified as low-confidence, although erosion and time could have rounded the expression of the scarp (Wallace, 1977). We also classified as low-confidence scarps candidates that were sinuous and (sub)parallel to adjacent waterbodies, because they could represent terraces or shorelines. Scarps that couldn't even meet the low-confidence criteria were ignored and considered deglacial landforms.

2.4 Results

We discovered 193 geomorphic features classified as potential fault scarps in the three study areas; 20 high-confidence scarps, 114 low-confidence scarps, and 59 medium-confidence scarps. Amongst the 20 high-confidence scarps, a cluster of highly-ranking scarps appeared near the epicenter of the 1935 Temiskaming earthquake. Interestingly, the number of scarps found in each research area was relatively proportional, which suggests a relatively uniform methodology. The longest high-confidence scarp has a length of 10 km, while the shortest high-confidence scarp has a length of ~1 km. The majority of the high-confidence scarps have a length between 1 and 5 km, which makes them shorter than some of their Fennoscandia counterparts (Hanson *et al.*, 1999; Lindblom *et al.*, 2015; Munier *et al.*, 2020). All the high-ranking scarps have a cross-cutting relationship with a bedrock fracture, a glacial landform, or a fluvial channel, as required in the criteria table (Table 2.2). In each region, we identified

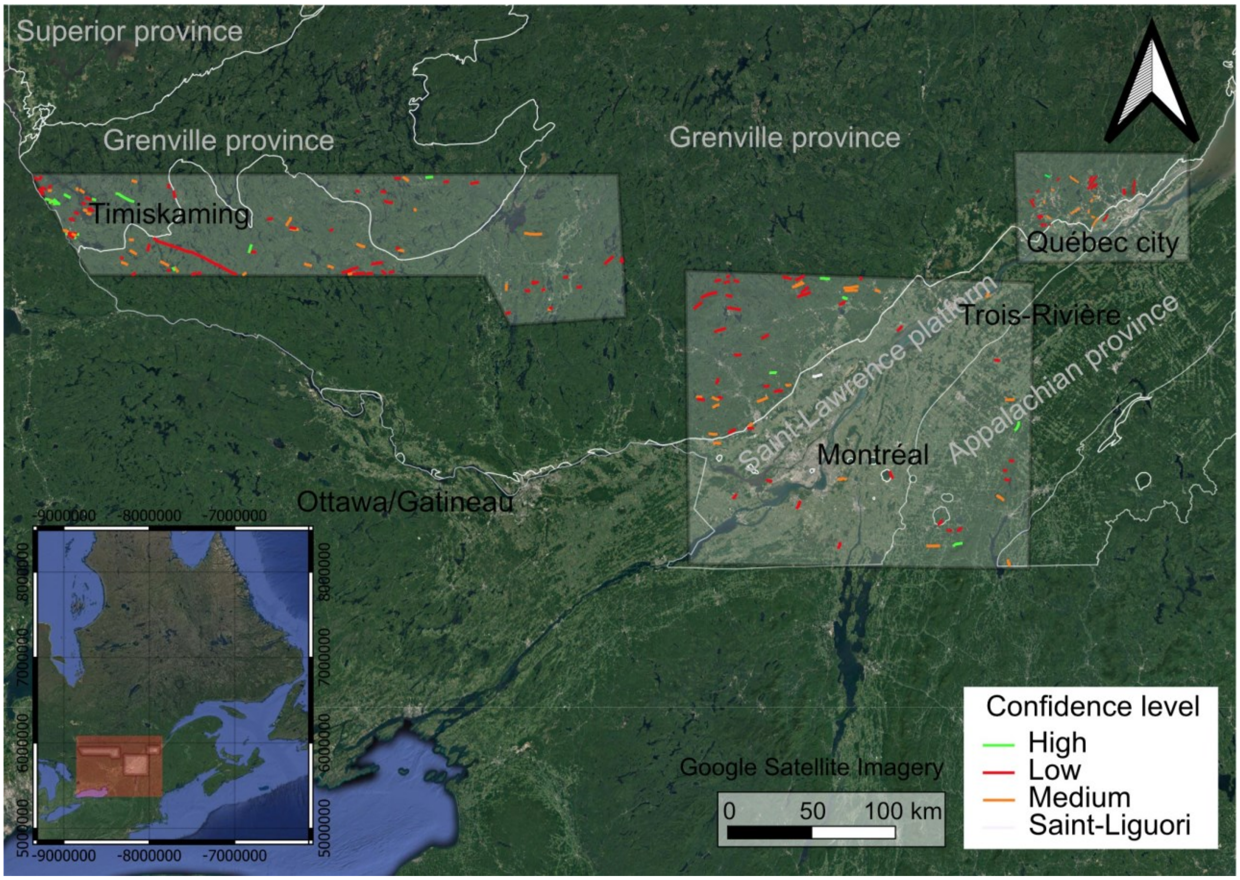

Figure 2.6 Google satellite basemap for highlighting the 3 research areas in Southern Quebec (Montréal, Québec city, Timiskaming) showing identified topographic scarps, confidence indicated by line color.

different landscapes of glaciogenic geomorphic features modified to different degrees by recent land use. All three study areas revealed numerous high-ranking linear features to be investigated for indications of recent offset. Priority should be given to these scarps for eventual field surveys.

In this section, one specific example of a high-confidence scarp for each study area will be presented in detail to demonstrate how the criteria table was used. The Québec City area was originally developed by Laly (2021), the Timiskaming area by Wang (2022), and the greater Montréal area by Gourdeau (2021), and later remapped (by Aube Gourdeau; this work) for consistent application of criteria in the preparation of this work. All results are presented for review here for the first time.

2.4.1 Timiskaming multi-stranded bedrock scarp

The Timiskaming region is dominated by exposed Proterozoic bedrock with thin or absent sedimentary cover. The Timiskaming area sits in the WQSZ and in the exhumed Grenville Province. The scarps are usually striking NW to W, while ice flow indicators, such as drumlins, grooved bedrock, and streamlined sediments, all indicate a predominant SW-NE movement of the ice sheet. Therefore, the ice flow direction often runs perpendicular to the strike of the scarps (although local discrepancies are possible). This contrast could be due to sampling biases if scarps parallel to sedimentary features are less apparent, or if the pattern is not biased, due to the fact that the scarp orientations are following the modern-day NE-SW maximum horizontal compressive stress. This area was characterized by a high density of bedrock fractures and relatively scarce sediments, reducing the confidence for the majority of potential scarps. A total of 94 potential fault scarps have been identified. We identified 53 low-confidence scarps, 27 medium-confidence scarps and 16 high-confidence scarps (Wang, 2022). There is a notably high density of potential post-glacial fault scarps in and around the Parc National d'Opémican, ~400 km NNW of Ottawa, and close to the epicentral region for the 1935 Timiskaming Earthquake and 2000 Kipawa Earthquake (Bent *et al.*, 2002; Bent, 1996; Wang, 2022).

The highest ranking scarp in the study area, which we called the Timiskaming scarp, is located in the Parc National d'Opémican (Fig. 2.7; Wang, 2022). Its surrounding physiography is typical of the Canadian Shield, with low relief, significantly exposed or very thinly buried bedrock, and mesoscale geomorphology dominated by glacial erosional features (Figure 2.7a). We mapped a network of branching faults with a zone of complexity and more numerous short traces connecting across a potential right stepover. This fault scarp has a generally WNW-ESE strike, and very low sinuosity Wang (2022). The northern block of this fault is upthrown relative to the southern block, and the scarp consistently faces south along its strike. With an approximate minimum length of 5 kilometers cutting sharply through Precambrian bedrock and Quaternary sediments, the scarp can be traced continuously, from bedrock to sediments (Wang, 2022). The trace of the scarp offsets multiple lineaments, such as drumlins and glacial grooves. This scarp meets all the mandatory and strong criteria for identification as a high-confidence fault scarp (Table 2.1). Figure 2.7 shows the Timiskaming scarp and its multiple strands, where we can see a maximum displacement of 10 meters across profile Wang (2022). In addition, the Timiskaming scarp is surrounded by several potential post-glacial faults of varied confidence levels (Figure 2.6), all of which are situated less than 15 km NW of the 1935 M6.2 Timiskaming Earthquake epicenter (2.4), although not striking parallel to the Temiskaming graben Doughty *et al.* (2010); Lamontagne *et al.* (2018).

2.4.2 Greater Montreal Area

Montréal is located within the WQSZ. The NW part of the Montréal study area sits in the Grenville geological province, the middle section in the Saint-Lawrence Lowlands geological province, and the SE part in the Appalachian geological province. I identified more abundant scarps in the Grenville and Appalachian provinces, possibly since they contain more bedrock fractures, resulting in more potential features of interest. Additionally, the Saint-Lawrence Lowlands have had significant deposition in the Holocene (Filion, 1987; Lamarche *et al.*, 2007), meaning an even younger land surface than the surrounding areas. A total of 62 scarps were found within a 200 km radius around Montreal, but only 5 were considered to be likely. The most likely candidate, the Saint-Liguori scarp, was investigated in the field and described in detail in Chapter 3 (Figure 2.8; Gourdeau *et al.*, submitted). The other most compelling possible fault scarp is presented here (Figure 2.9).

The Magog scarp is situated NW of the city of Magog, Québec, 120 km E of Montréal, next to Lake Stukely (Figure 2.9). The scarp appears as a feature striking 135°. The scarp is sharp and extends linearly for 3 km, almost continuously except for a small stepover (also adjacent to the green segments). The average height of the scarp is ~10 m, facing towards the SE. The Magog scarp meets most of the mandatory criteria of Table (Table 2.1), but does not match the high-confidence criteria as well as the favored scarps in Temiskaming and Québec, since

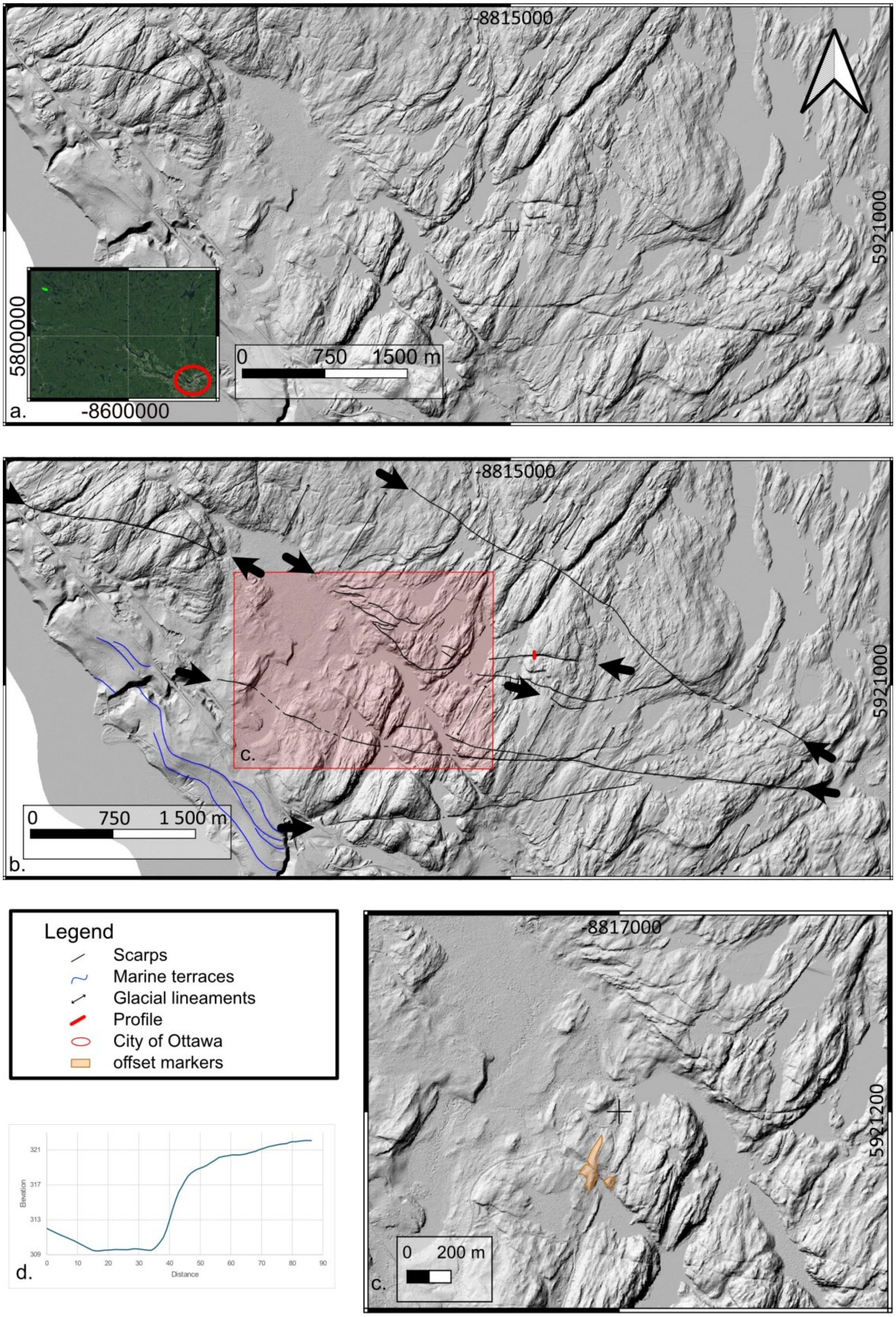

Figure 2.7 Highest confidence potential fault scarps found in Timiskaming area. Inset shows scarp location ~400 km away from Ottawa (red circle) on Google Earth imagery. The scarps appear between the black arrows, and is outlined on the second figure. Confidently located scarp trace indicated with solid lines, dashed traces are covered.

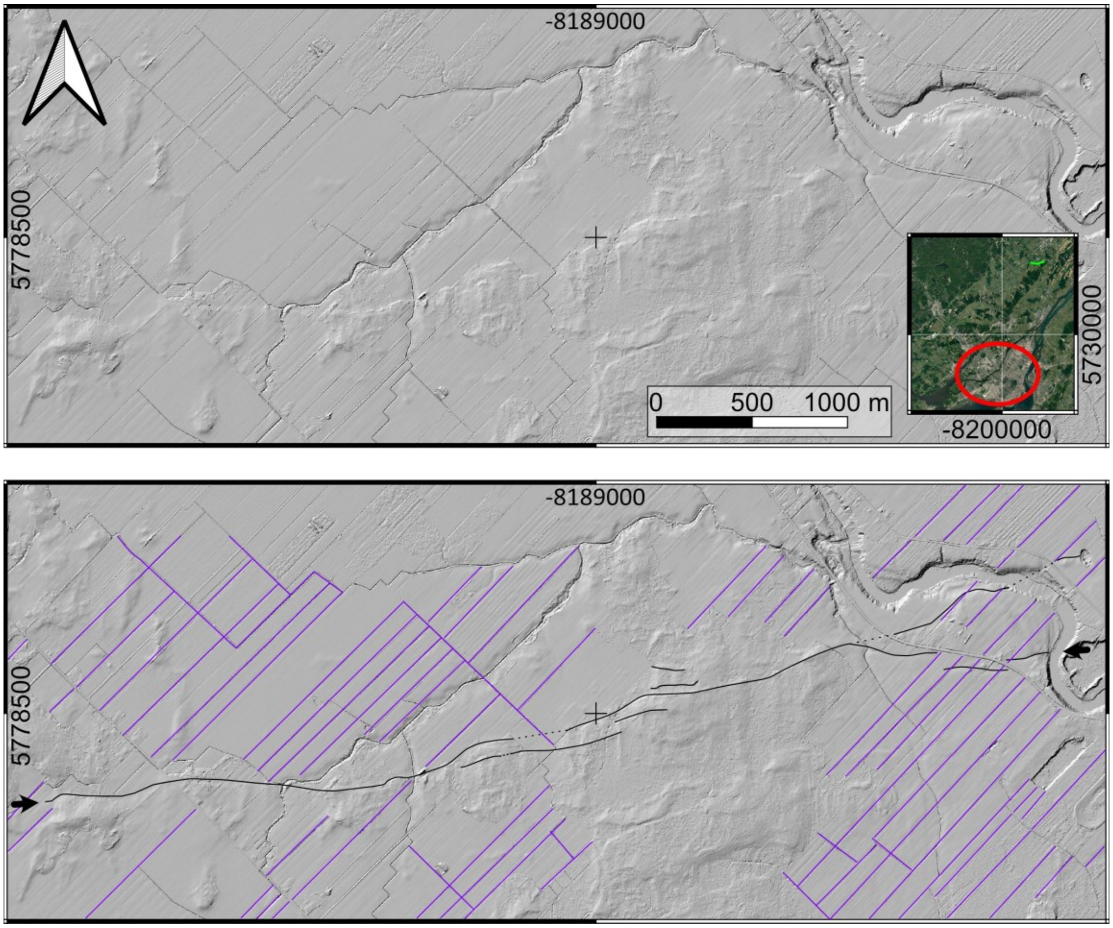

Figure 2.8 Saint-Liguori scarp, 50 km NE of Montréal (red circle). In b), The scarp appears between the black arrows, and is outlined. The purple lines represent crop fields visible on the lidar imagery. (Gourdeau *et al.*, submitted) performed a paleoseismic trench on this site, presented in Chapter 3.

the scarp is not as long and continuous, and doesn't as unequivocally penetrates Quaternary sediments. The scarp still subtly cuts through surficial sediments along the green segments, adjacent to a lake and next to a water channel (Figure 2.9). The bedrock surface cut by the scarp does not display any obvious glacial lineaments, but in the nearby area (within ~5 km) the glacial striations trend N-S.

2.4.3 Québec City Area

In the Québec city area, 35 potential post-glacial faults were identified (Laly, 2021). 1 of them was considered high confidence scarps, 10 medium confidence, and 24 low confidence (Laly, 2021). The area examined spans the boundary between the Grenville province and the

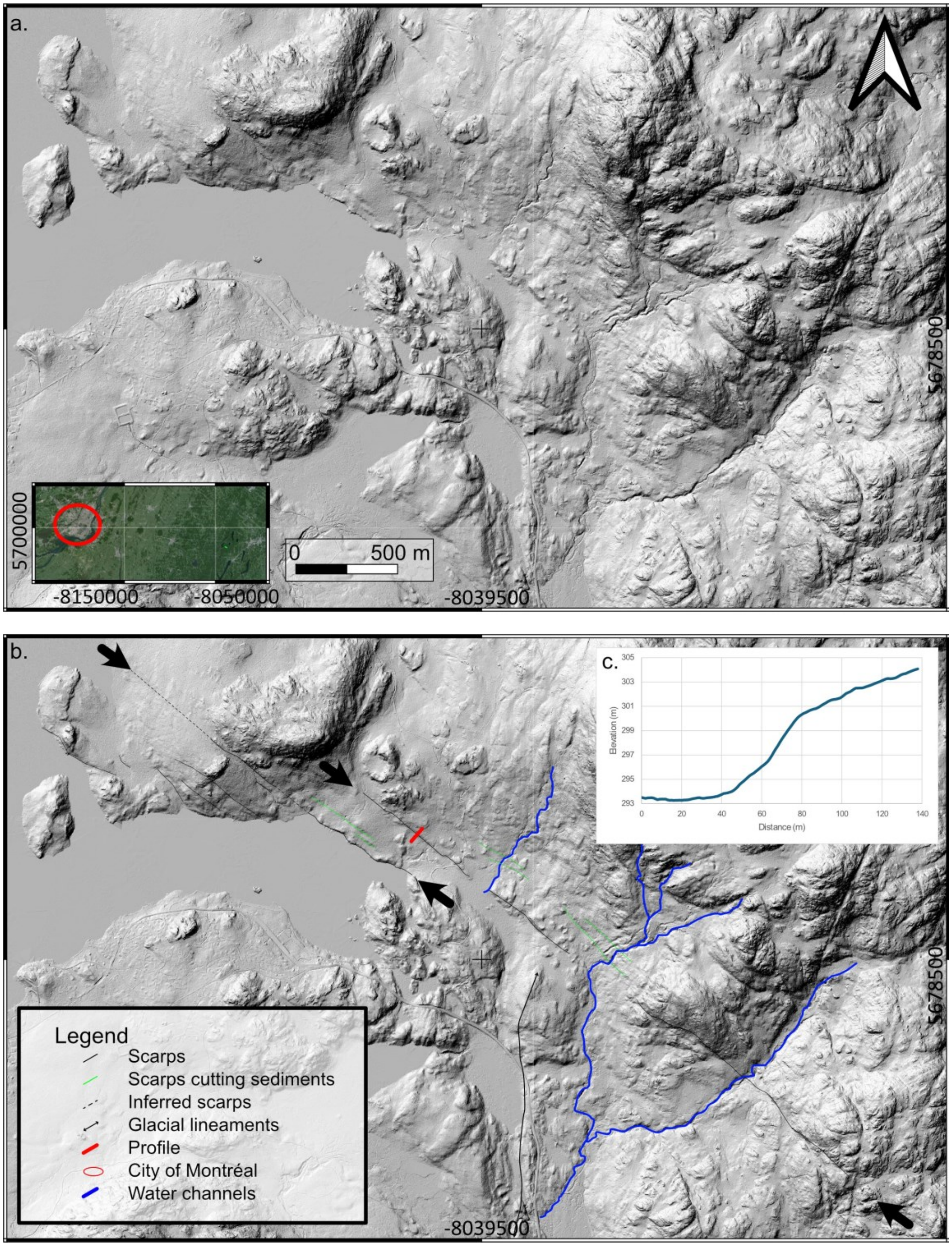

Figure 2.9 Strong candidate fault scarp found near Magog,120 km E of Montréal (red circle). a) Unannotated hillshade image. b) Annotated hillshade image. c) Across-scarp topographic profile shows average height of ~9 m.

Saint-Lawrence Lowlands, on the North shore of the Saint-Lawrence River. The potential post-glacial faults in Québec do not seem to have a preferential strike, in contrast to Timiskaming and Montreal. The length of identified scarps ranges from ~1-10 km.

The highest confidence potential fault scarp found around Québec city is the Saint-Raymond scarp NE of Québec City (Figure 2.10). The scarp is situated in the middle of a forest, on a semi-private property and a private property. The mapped extent of the scarp is 1.9 km long, SE-striking, singular, and linear. Evidence for displacement is revealed punctually by SW facing vertical offset in bedrock and Quaternary sediments. One of the segments also shows sharp lateral and vertical offsets on a moraine of a few meters (center of the Figure 2.10). This offset moraine represents one of the strongest evidence for faulting observed in southern Québec, and should be the next candidate to investigate in the field. . This scarp meets all the mandatory and strong criteria for identification as a high-confidence fault scarp. A field visit revealed a thin cataclasite on a smooth slickenside on the upthrown northern bedrock wall rock, confirming the lineament is a fault. Further investigation is warranted.

2.5 Discussion

To date, only one surface-rupturing post-glacial fault scarp has been confirmed in eastern Canada, related to the 1989 M6.3 Ungava Earthquake (Adams, 1989; Adams *et al.*, 1991). The release of high-resolution lidar imagery (Ministère des Forêts, 2016) created the opportunity for tectonic geomorphology studies which have only just begun; in fact, this is the first study we know of to utilize the lidar data for neotectonic investigations in eastern Canada. All the study areas selected for this first screening contained high-potential scarps inventoried using the methodology we adapted based on successful investigations in related regions (e.g. McCalpin, 2009; Sutinen *et al.*, 2014; Berglund & Dahlström, 2015; Mikko *et al.*, 2015). Although lineament maps have been an important resource in the search for active fault strands in the Western Québec Seismic Zone (Rimando & Peace, 2021; Rimando *et al.*, 2023), three-

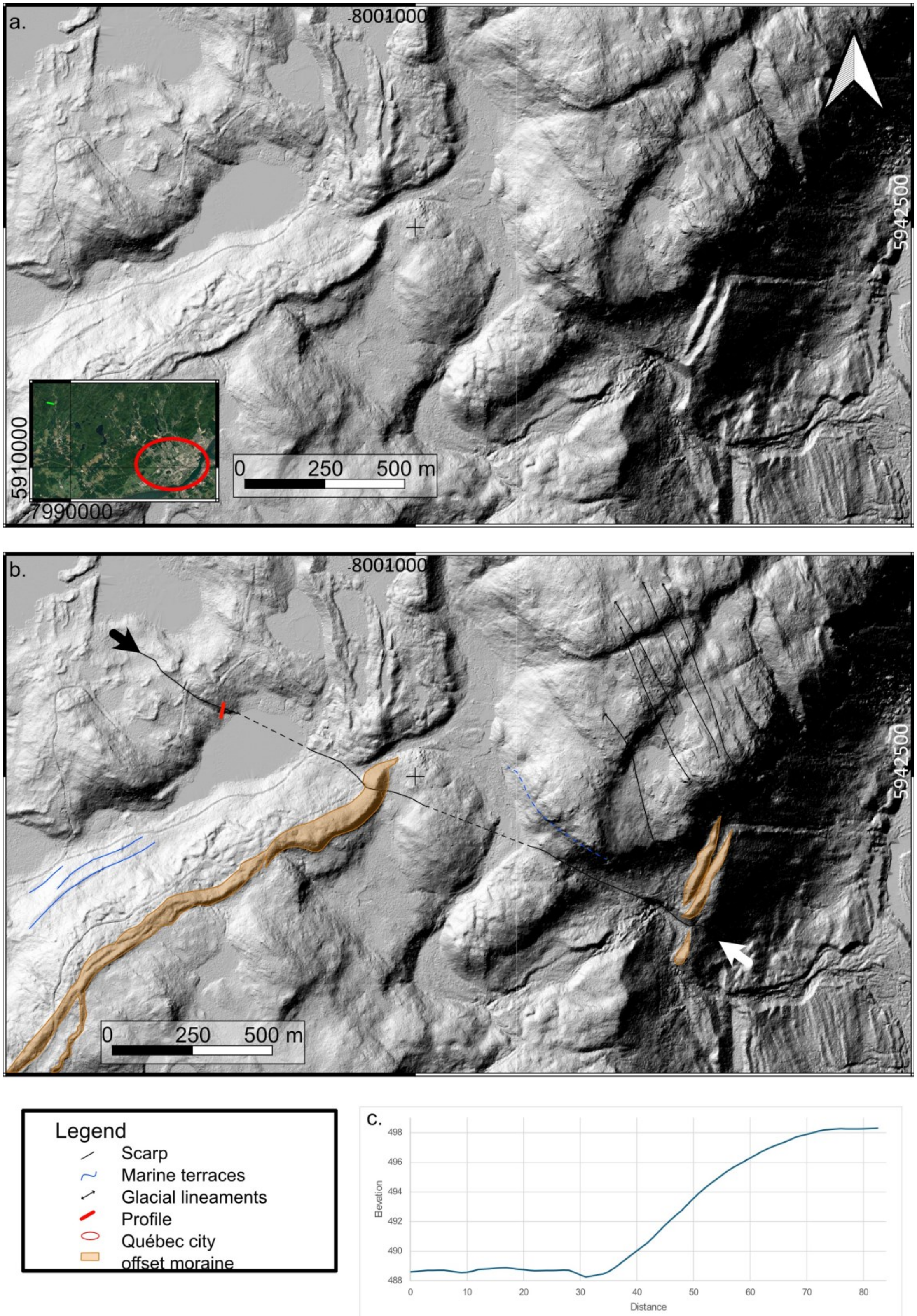

Figure 2.10 Best candidate found around Québec city, in sediment and bedrock, XXkm NO of Québec city (in the red circle). The scarp appears between the black arrows, and is outlined on the second figure. The inferred sections are traced with dotted lines and the apparent sections are traced with black lines.

dimensional bare earth models allow a much more robust assessment of crosscutting, throw, and orientation which are critical for prioritizing potential fault traces. Our investigation revealed many subtle scarps that are not included on publicly available lineament maps (des Ressources naturelles et des forêts, 2024; de l'Énergie et des Ressources naturelles, 2021). The number of high-confidence potential post-glacial faults we identified is somewhat consistent with the theoretical and extrapolated predictions by Brooks (2020). He suggested that between 28 and 160 surface rupturing scarps should exist in Eastern Canada based on global seismicity rates in stable cratons and the statistical calculations used by Fenton *et al.* (2006) in Ontario. Although their estimate wasn't very precise, our method at least highlights that it is selective enough to not overestimate the number of candidates beyond reasonable limits. Some of the identified candidate post-glacial faults also have the potential to be associated with known historical events, such as the old and poorly located 1935 M6.1 Temiskaming earthquake, the 1944 M6.2 Cornwall earthquake, the 1663 M7+ Charlevoix earthquake, the 1870 M6.6 Charlevoix-Kamouraska earthquake and the 1732 M5.8+ Montréal earthquake (see fig. 2.4)(Leblanc, 1981; Lamontagne, 2002; Lamontagne *et al.*, 2018). The identification of numerous potential scarps is also consistent with the moderate seismicity recorded in the province, and other evidence of shaking such as seismites in lakes and rivers, liquefaction, and triggered landslides and tsunami (Filion *et al.*, 1991; Poncet *et al.*, 2010; Trottier *et al.*, 2019; Brooks, 2020; Mérindol *et al.*, 2022). This would make the scarps particularly relevant to realize realistic earthquake scenarios, that are currently not based on fault-specific sources. Note that the current scarp selection is more likely to represent an overestimation since mapping uncertain features was favored, rather than making conservative estimates that could potentially disqualify true post-glacial faults.

2.5.1 Application of the fault scarp criteria table

Fault trace mapping criteria have been proposed for tectonicly active regions and have been successfully applied in a variety of global fault studies. Most recently, Scott *et al.* (2023)

tested the repeatability of fault trace mapping based on geomorphic indicators by researchers of diverse experience levels for several notable recent surface ruptures. The criteria used in this study rely on geomorphic features associated with fast strain rate (tectonic plate boundaries) and dynamic, often arid landscapes with characteristic depositional and erosional features. These were not directly applicable to our study areas due to the pause in landscape evolution following the glacial recession and the very low strain rates on these potential faults, which made the geomorphic features way more subtle than in plate boundary settings. We tentatively suggest that any development of fault geomorphic features is most likely linked to the transient maximum strain rates inferred to reflect the migration of the post-glacial flexural bulge. In Fennoscandia this post-dated the ice sheet recession by a few ky and similar events could have occurred in southern Québec.

When assessing and adapting the use of previously published criteria for landscape identification and analysis of post-glacial faults, we have relied only on observable geomorphic criteria (Table 2.2). Thus, the use of additional constraints on these criteria based on independent datasets shouldn't be excluded, especially if working in a different landscape, with a different resolution, or with different types of datasets. For example, McCalpin (2009) indicates that post-glacial faults most commonly have reverse shear sense. Our landscape observations do not independently confirm this, but decades-long seismicity catalogs (Adams, 1989; Hanson *et al.*, 1999; Lamontagne, 2002; McCalpin, 2009; Brooks & Adams, 2020; Chien & Liu, 2023) indicate that most earthquakes in southern Québec are reverse motion or oblique with a significant reverse component.

Due to greater expense, only a small subset of topographic lineaments can be examined in the field and with subsurface investigations (Palmu *et al.*, 2015). The certainty of the assessment thus varies considerably amongst the Fennoscandian repository and has to be used cautiously (Johnson *et al.*, 2015; Mikko *et al.*, 2015). A similar warning definitely applies to our first eastern Canadian database, for which a single trench has been attempted where shallow geophysics revealed a buried bedrock scarp, which revealed no signs of faulting

(Gourdeau *et al.*, submitted).

In the near future, if no shear displacement is identified during field surveys of these landforms, scarp candidates will be removed from the repository, a practice that is already in use in Fennoscandia (Mikko *et al.*, 2015).

2.5.2 Scarp geometry and scale

Past workers reported correlations between fault length-magnitude, displacement-magnitude, maximum displacement-length, or width-magnitude (Wells & Coppersmith, 1994; Pavlides & Caputo, 2004; Kim & Sanderson, 2005). Normal faults develop scarps that reflect their displacements, whose height and length scale in a predictable way (L = ~100D; Dawers & Anders, 1995), and should be the easiest to define in a terrane model. Normal faults commonly segment on scales of kms - 10s kms in actively extending regions. Strike-slip faults in stable continental regions display a consistent scaling of magnitude to surface rupture length (Leonard, 2014), in the range of ~1 - several km length. Thrust scarps show a different scaling factor but follow a similar relationship. Kim & Sanderson (2005) suggested that the aspect ratio of single slip events should generally be $<10^{-4}$, but the datasets were not specifically obtained in an intractonic setting. In other words, most of the work that aims to identify aspect ratios for fault scarps was not specifically realized for deglaciated continental interiors.

In practice, for Québec, with 1 m lidar DEMs, we are only likely to find detectable scarps for earthquakes >M5 and greater (≥30 cm slip on a ≤5 km long fault, for a shallow M5.5 earthquake; Leonard, 2014), as smaller or deeper earthquakes may not create enough surface displacement (Figueiredo *et al.*, 2022). Based on these constraints, and the DEM resolution, we could only detect scarps formed in earthquakes in the high M5 range or formed by several smaller repeated events increasing scarp height. Given that multi-km long earthquake ruptures are often segmented, we don't restrict our search to a precise scarp length range.

The largest known historic event for the province was the 1663 Charlevoix earthquake, estimated M7.3-7.9 (Ebel, 2011), with an inferred epicenter near La Malbaie. An earthquake like this would be likely to reach the ground surface and the surface rupture length would be similar to the true rupture length (Leonard, 2014). if true, we can expect that a surface scarp could be detectible only a few centuries later.

A few authors attempted to provide an aspect ratio for surface ruptures that occurred in Fennoscandia, providing hints on what to expect for Québec. In practice, these suggestions have never been tested in Québec due to a lack of identified ground-breaking scarps in the province (Muir Wood, 1993; Fenton, 1994; Hanson *et al.*, 1999; Olesen *et al.*, 2004). These authors suggest that the majority of postglacial faults should have higher displacement-to-length ratios than similar-sized tectonic faults, which should usually be $\leq 1:1{,}000$ (Fenton, 1994; Hanson *et al.*, 1999; Olesen *et al.*, 2004). Definitely, more data will have to be available and tested before applying this criterion to Southern Québec, to make sure that high-confidence scarps don't get discredited based on a poorly constrained criterion. For now, a high variability/uncertainty exists amongst papers describing aspect ratios. An even greater uncertainty probably exists when quantifying intracratonic deglaciated landscape aspect ratios, which probably behave differently than plate boundary settings or non-deglaciated intracratonic settings. intracratonic deglaciated landscapes often account for only a tiny portion of the datasets, if any (Wells & Coppersmith, 1994; Dawers & Anders, 1995; Pavlides & Caputo, 2004; Kim & Sanderson, 2005; Leonard, 2014).

2.5.3 Challenges arising from the landscape of the study areas

Obviously, the dense vegetation makes fieldwork way more challenging in Québec than in arid regions, but it also has an impact on the quality of the lidar imagery. Some isolated triangulation errors could appear in the lidar mesh, making the observations impossible for tiny portions of the imagery. The slow strain rates and the flat topography in the province can also make the scarps more subtle because erosion can rapidly attenuate the visible offset on surface-rupturing scarps and potentially make them short-lasting relative to the rate at which they grow. It is also reasonable to expect that the recent deglaciation of North America only gave a short period of time for the development of surficial offsets compared to longer-lived tectonic faults. According to models by Hampel *et al.* (2009), most of the slip on the thrust faults underlying the ice sheet should have occurred in the ~5 ka following the deglaciation, and in the ~2 ka following deglaciation for the normal faults. Therefore, we were still confident on our capacity to identify postglacial faults.

The impact of anthropogenic influence made the identification of scarps almost impossible on the Island of Montréal and in Québec city, but they represent the main metropolitan areas in the whole province. The rest of the province contains a sparse population and relatively low anthropogenic influence on the meters to kilometers-scale geomorphic features. The most important anthropogenic influence that has to be considered in this analysis is the presence of crop fields, which could have led to soil reworking and landform plowing. These croplands are at least easy to identify since they are constrained between sharp, repetitive, and rectangular sets of drainages built for water evacuation (as observed in Figure 2.8). These areas could have erased past evidence of post-glacial faulting and lowered our potential scarp detections in agriculture-dominated areas. On the other hand, these agricultural features could represent excellent offset markers for the most recent scarps, or the scarps that would result from an earthquake that hit during the agricultural era.

Especially for the high-confidence scarps, an overall preferential strike orientation East-West was observed in both the Timiskaming and the Montreal areas, while no preferred orientation was observed for the Québec area. The preferential scarp orientation could be associated with the (NE-SW-striking) modern-day stress field (fig. 2.2), as favorably oriented features are more likely to be recently reactivated (Heidbach *et al.*, 2018; Giona Bucci & Schoenbohm, 2022). No preferential orientation was retrieved from Québec city because only one high-confidence scarps was found, which was not enough to make a reasonably accurate analysis. The fact that a lot of glacial features run north-south might reduce our capability to find similarly striking scarps.

These criteria should allow the discrimination of potential fault scarps over glacial landforms. However, identification remains challenging, and deglaciation patterns vary across the Laurentide Ice Sheet (LIS), owing to differences in geomorphic and climatic settings, surface processes, fault geometry, displacement rates, rock type, sediment cover, as well as changes in sheet basal thermal conditions and terrestrial versus marine termination (McCalpin, 2009; Stokes *et al.*, 2016). Both the advancing and retreating phases of the LIS have left abundant glacial landforms in Québec. Some of the landforms and erosional features that had to be distinguished from faults included a) glacial striations, which had a preferential North-South orientation and generally appeared in groups, b) glacial plucking, which was generally quite short, non-continuous, more gradual along strike and wider perpendicular to strike, c) old shorelines/river terraces, which were concentric, d) post-glacial fluvial flows or meltwater channels, which were narrow, stranded and anastomosing e) drumlins, which are which are kilometer-scaled elongated humps, f) moraines and recessional moraines, which are thick and long, g) eskers, which are often undulating, and h) kettle and kame fields, i) buttress unconformities, j) ancient, pre-Quaternary faults (Shilts *et al.*, 1987; McCalpin, 2009; Johnson *et al.*, 2015). Eventually, a map of these landforms should be added to the datasets, to facilitate discrimination. Fluvial processes can also produce erosional features (e.g. river terraces, bedrock gorges) that could be mistaken for potential faults. On the other hand, a sharp riverbed deflection could suggest a lateral offset and provide visual evidence of a PGF, if coexisting with other strong criteria.

The primary pattern observed in Temiskaming is the high concentration of scarps identified near the inferred 1935 M6.2 Temiskaming earthquake epicenter (Lamontagne *et al.*, 2008). This outstanding concentration of scarps could be consistent with a higher rate of seismicity in the area. Slightly more abundant scarps were identified in the Montréal area within the Grenville province (NW section of the map). This clustering might highlight a sampling bias resulting from the particularly confusing and abundant bedrock fractures in these study areas. These bedrock fractures make it difficult to distinguish landscapes of glacial origin (e.g., enhanced bedrock fracture, glacially plucked scarps) from potential surface-rupturing fault scarps that were created during or after deglaciation. This sampling bias, if it exists, probably extends to the portion of the maps constrained within the Grenville province, which could suggest that a disproportionate number of scarps were identified in the Temiskaming area. Within all the field areas, there exists a possibility of misidentification of certain bedrock fractures and glacial plucking scarps as potential fault-related landforms.

Bedrock fractures are ubiquitous in areas of thin sedimentary cover. Overall, bedrock fractures often only showed some continuity without offsetting sediments or landforms or sharply disappeared at Quaternary sediments. Regular fractures also showed more waviness than the selected faults and often displayed a higher level of complexity by splitting up into multiple splays that were bisected by other fractures in many directions. When fractures appeared in environments lacking sediments, we were constrained from using the displacement of Quaternary sediments as a criterion. Sometimes, bedrock fractures were hard to classify since some fractures were glacially enhanced and thus long and penetrative in sediments. Because of their widely variable expression, bedrock fractures had to be classified using slightly stricter criteria to avoid mapping them all as possible fault scarps. A minimum along-strike length of 5 kilometers was chosen to consider the fractures as potentially fault-related scarps. The 5-km length threshold was a relatively arbitrary choice, although scarps in Fennoscandia rarely presented shorter lengths (Mikko *et al.*, 2015; Munier *et al.*, 2020). In retrospect, and now knowing that the average length of the high-ranking faults was between 2 and 5 km, this threshold could be brought down to 3 km. If a reasonable doubt had to be placed in the identification of a bedrock fracture, we think that more than any other features, investigation in the field will be required to distinguish them from active fault scarps. However, we still consider that structures that are not associated with bedrock fractures and thus less ambiguous should be prioritized for further investigations or even paleoseismic trenching.

2.5.4 Similarities between Fennoscandia and Québec

The work accomplished in Fennoscandia strongly influenced the creation of the first criteria table. However, the expression of scarps found in Québec sometimes differs from the Fennoscandian scarps, especially in terms of length. Fennoscandia identified longer scarps, which could be present due to larger magnitude earthquakes and more recurrent hazards (Wu *et al.*, 1999; Lindblom *et al.*, 2015; Mattila *et al.*, 2019; Ojala *et al.*, 2019). Some re-activation mechanisms identified in Fennoscandia and Québec are identical, such as the isostatic rebound and the reactivation of old fault networks (Rimando & Peace, 2021; Bungum & Eldholm, 2022). Québec, however, also has unique drivers, such as the great meteor hot-spot track that passed underneath the WQSZ, and the Charlevoix impact that could have weakened the crust around Charlevoix (Ma & Eaton, 2007; Osinski *et al.*, 2022). These uncommon drivers, as well as the potentially different recurrence intervals, might be responsible for the slightly different surface expressions (especially in length) that can be observed in Québec. The bedrock geology of Québec could also play a role in the length and expression of surface-rupturing faults.

2.5.5 Implications for earthquake hazard scenarios

Southern Québec has extremely high seismic risk due to the major historical earthquakes and infrastructure conditions, with Montréal having the highest seismic risk index of any Canadian city (Hobbs *et al.*, 2023) due to the abundance of unreinforced masonry (Nollet *et al.*, 2005; Bélec, 2016; Candela *et al.*, 2021).

Earthquake hazard estimation is challenging in intraplate seismic zones (Cramer, 2001; Stein, 2007; Li *et al.*, 2009; Stein *et al.*, 2017). The earthquake potential of a fault zone, even an inherited intraplate fault, is sensitive to far field deformation rates and also to local stress and earthquake history (Collettini *et al.*, 2005; Wang, 2007; Tarayoun *et al.*, 2018; Trugman & Ben-Zion, 2023), which are difficult to constrain in interplate seismic regions (Talwani, 1989; Cramer, 2001; Tarayoun *et al.*, 2019). The theoretical backing on which traditional earthquake hazard is based in plate boundary regions relies on determination of long term slip rate on persistent faults, revealed through determination of past earthquake size and timing, and through geodetic observations of strain accumulation on locked faults (Youngs & Coppersmith, 1985; Anderson *et al.*, 1996; Tapponnier *et al.*, 2001). In intraplate zones, there is no basis to assume that individual faults have quantifiable or consistent slip rates over geologic or human timescales (Weber *et al.*, 1998; Williams *et al.*, 2017), and the interseismic strain rates may be too low to measure (Mazzotti & Gueydan, 2018; Tarayoun *et al.*, 2018). Different approaches have been attempted for low slip rate faults, or those that don't appear to have constant slip rates. These utilize the concept of a characteristic event, implying that earthquakes could be magnitude-repeatable if not time-predictable on a particular fault segment (e.g. Schwartz & Coppersmith, 1984; Wesnousky, 1994; Estay *et al.*, 2016). An advantage of this approach is that it takes one or more specific earthquake scenarios and defines the probablistic seismic hazard, which may be one of the only ways to parameterize hazard in this setting (Convertito *et al.*, 2006). The definition of characteristic earthquakes may be highly sensitive to thorough interrogation of the geologic record, and therefore also to gaps in the record (e.g. Stein *et al.*, 2005).

Previous hazard estimates for Québec have called for better specific scenarios to improve shake maps and derived models, as synthetic and area earthquake sources are the only input for current efforts (Rosset & Chouinard, 2009; Ghofrani *et al.*, 2015; Yu *et al.*, 2016b; Kolaj *et al.*, 2020a). In the absence of confirmed paleoseismic faults, seismic hazard models for southern Québec are based on areas of historical earthquakes and areas with similar tectonic setting (e.g. continuations of the Iapetus rift structures; Kolaj *et al.*, 2020b,a). The need for more precise information on the historic and prehistoric large earthquakes to support hazard estimation has been motivated by researchers for decades (e.g. Adams, 1996; Brooks & Adams, 2020; Lamontagne & Flynn, 2016; Lamontagne & Bent, 2021). Paleoseismic trenching in western Canada has demonstrated the utility of this technique, even in recently deglaciated regions, for establishing timing and magnitude of prehistoric earthquakes (Morell *et al.*, 2018;

Harrichhausen *et al.*, 2021) which significantly influenced the subsequent seismic hazard estimate (Halchuk *et al.*, 2019; Kolaj *et al.*, 2020b). The addition of specific earthquake scenarios to seismic hazard models has increased the calculated risk for Montréal (Rosset *et al.*, 2023). Our hope is that this curated list of potential fault scarps can provide the basis for future paleoseismic investigations to better constrain earthquake sources (location and past magnitude) to improve seismic hazard estimation and risk assessment in southern Québec.

Ultimately, the results from remote sensing have to be coupled with fieldwork and dating in parallel to earthquake distribution models, to yield a satisfying conclusion and ensure the scientific rigor of this project (Gourdeau *et al.*, submitted). If no field data and no dates are obtained on scarps, it will make the cyclicity and predictability of hazard impossible to estimate using probabilistic scenarios.

2.5.6 Integration of other evidence of shaking and future work

In future studies, higher attention should be given to secondary indicators of fault activity and/or shaking such as paleolandslides, blowout pits, sagponds, mass transport deposits, etc. It is already the case in Fennoscandia, as mentioned by Mikko *et al.* (2015), Ojala *et al.* (2019), and Palmu *et al.* (2015) who used the abundance of paleolandslides in tills as evidence for post-glacial faulting in an area. Moreover, subaqueous mass transport deposits and paleolandslides in Québec have already been found, and these observations could relatively easily be added to our database to highlight zones of interest (Filion *et al.*, 1991; Quinn, 2009; Brooks, 2014; Lajeunesse *et al.*, 2017; Trottier *et al.*, 2019; Brooks & Adams, 2020; Mérindol *et al.*, 2022). However, it is suggested that not all post-glacial faults appear in regions containing an important number of paleolandslides (Sutinen *et al.*, 2014). It is the case for the Palojärvi area in Finland, which contains at least 3 post-glacial faults but no apparent paleolandslides, which could be possible if the earthquakes took place in frozen soil (Sutinen *et al.*, 2014). The presence or absence of paleolandslides thus doesn't guarantee the presence or absence of post-glacial faults.

Other tools used to assess the presence of post-glacial faults included borehole studies to observe signs of re-activation (Sutinen *et al.*, 2014), and the use of geophysical methods (McCalpin, 2009; Mikko *et al.*, 2015). These tools could be implemented in the field on highly-ranking candidates, which could help us to increase our confidence in the scarp before digging a paleoseismic trench. For instance, ground penetrating radar, H/V ambient seismic noise, and seismic refraction tomography surveys were conducted in Saint-Liguori before trenching (Gourdeau *et al.*, submitted).

Another tool that could be used in Québec is machine learning to help identify scarps. The idea has already been used in arid areas in California and proved its worth (Sare *et al.*, 2019), but isn't yet sharpened for areas as complex as intracratonic and deglaciated landscapes, where glacial landforms and vegetation cover add substantial complexity to the work. Cluster analysis has recently been applied to the WQSZ (Giona Bucci & Schoenbohm, 2022), but hasn't yet been ground-truthed. An extended version of Giona Bucci & Schoenbohm (2022)'s work could definitely be overlapped and compared to our regional database. If today's machine learning was used in Québec, it would most likely inventory all the bedrock fractures, which would subsequently result in the enforcement of manual screening. Machine learning approaches require a high-quality training datasets to mimic manual outcomes (van der Meij *et al.*, 2022), and our map could provide a training opportunity, although the quality would be much improved after field verification. Paleoseismology in deglaciated landscapes remains challenging and tricky, and will definitely benefit from the multiplication of tools and visual supports in the upcoming years to identify post-glacial faults.

Another pending question is if the lithospheric thickness has an impact on scarp distribution. So far, no tomographic models have been studied in this regard, which could represent an interesting avenue for future work (Lebedev *et al.*, 2023).

Eventually, the scarp catalog should be made available online as a vector layer that could be downloaded and updated following discoveries and field observations. Ideally, this dataset could be made available through public databases with the collaboration of public agencies. Over time, this repository should be extended and should be covering all of southern Quebec, to make the distribution of potential post-glacial faults more representative of the whole province. A complete repository would allow us to assess if the modern-day seismic zones are super-imposed over the same location of paleoearthquakes or not. The most pressing area to add to the survey right now is the Charlevoix area, which is experiencing the highest seismic hazard in the province, due to its unique setting associated with the Charlevoix impact. This assessment could lead to surprising discoveries regarding impact-related hazards, which could be applied to other impact structures around the world.

So far, no additional information could allow us to define and quantify the importance of each driver to earthquake hazard recorded in each of the seismic zones. There is still no consensus on whether intraplate faults display meaningful recurrence intervals (Calais *et al.*, 2016; Williams *et al.*, 2017). Assessment of recurrence intervals could only be possible once a PGF is identified in the field, using paleoseismic trenching and geochronological dating. Despite multiple scans of the assigned study area using progressively refined criteria, additional efforts will probably be required to establish a more robust and systematic framework for fault identification, especially once a decent number of scarps are assessed in the field.

2.6 Conclusion

A lot of work remains to be done to make this dataset usable for seismic hazard assessment and policy making. Once the repository is complete for all of Southern Québec and coupled with field assessment, we could better understand fault migration in the context of intracratonic landscapes experiencing isostatic rebound. Establishing an inventory of post-glacial faults will help us better evaluate and model the drivers and risks associated with potential earthquake hazards in Quebec and eastern Canada.

In addition to the immediate need for these investigations to be added to seismic hazard models, these results could potentially be useful in other regions and extrapolated to other intraplate and similar deglaciated terrains around the world. We strongly recommend the use of the criteria table for future paleoseismic studies conducted in eastern Canada/ north-eastern US, in the interest of reproducibility. The criteria table could eventually be updated based on observations made elsewhere, to make it more precise or applicable to a wider variety of intracratonic landscapes. This paper represents an initial milestone in the field of paleoseismology for Eastern Canada. The WQSZ stays a region of important earthquake risk, making this work highly significant and critical for city planning and population safety.

Descriptor	Other workers	Our preferred criteria for Québec
Scarp cuts...	postglacial sediments, water/meltwater channels, and geomorphic features (Fenton, 1994; Sutinen *et al.*, 2014; Mikko *et al.*, 2015)	Scarps cutting sediments are preferred. Offset of geomorphic features associated with glaciation or post-glacial fluvial settings, such as eskers, linear moraines, terraces. In areas without young sediments, we include offset of erosional bedrock features e.g. drumlins.
Plan pattern	linear and angular (Hanson *et al.*, 1999; McCalpin, 2009) up to smoothly curvilinear (Sutinen *et al.*, 2014)	linear and curvilinear, with constant facing direction. Distinct from fluvial scarps with meanders, we seek scarps with low amplitude curves
Continuity	generally continuous (Hanson *et al.*, 1999; McCalpin, 2009) or sometimes segmented on scale of a few km (Sutinen *et al.*, 2014; Mikko *et al.*, 2015; Bungum & Eldholm, 2022)	generally continuous with local 10s meter scale complexity and erosional gaps
Scarp strike orientation	Oriented normal to the contemporary and the flexural stresses (Adams, 1989); expected NNW-SSE to NW-SE strikes(Rimando & Peace, 2021)	The suggestions made by Rimando, 2021 and Adams,1989 are reasonable, but haven't been tested.
Scarp Height	mm-10s m, steeply dipping (Hanson *et al.*, 1999; McCalpin, 2009; Sutinen *et al.*, 2014)	Scarps identified down to detection limit of available dataset, in practice ≥30 cm at maximum height, often variable along strike, locally reaching several meters in bedrock scarps. Preferred scarps have maximum heights of 2-5 m.
Length of scarp	10s - 100s km (Hanson *et al.*, 1999; McCalpin, 2009); Usually ranging from 2 km to 100 km - longest PGF found = 155 km, Pärvie fault (Lindblom *et al.*, 2015; Munier *et al.*, 2020)	>5 km in bedrock, any detectable scarp in the post-glacial sediments (c. 1 km). The reasonable minimum to expect from surface-rupturing earthquake is 10s meters.
Scarp aspect ratio	1:1000 (Fenton, 1994). <1:1000 (Olesen *et al.*, 2004). Normally less than 1:1000, but sometimes 1:10 000 and aspect ratio is not always a necessary requirement (Steffen *et al.*, 2021). <1:11,000 (Hanson *et al.*, 1999)	Since scarp lengths may be limited by erosion or surface geology type, we did not apply an aspect ratio criterion.
Number of scarps	single (Fenton, 1999; Hanson *et al.*, 1999; McCalpin, 2009), but sometimes appearing in clusters on a larger regional scale (Bungum & Eldholm, 2022)	generally single but sometimes occur in nearby clusters.
Sense/style	predominantly reverse (Adams, 1989; Hanson *et al.*, 1999; McCalpin, 2009; Brooks & Adams, 2020), rarely normal, small component of strike-slip on small segments (Hanson *et al.*, 1999)	predominantly steep with apparent throw but sense is not always possible to constrain from landscape. Components of strike-slip and dominating reverse motion has been observed on focal mechanisms in the area (Chien & Liu, 2023).
Displacement history	single event (Hanson *et al.*, 1999; McCalpin, 2009; Craig *et al.*, 2016) with long recurrence intervals, or multiple events (Mattila *et al.*, 2019)	We did not use this criterion because it is not resolvable from geomorphology, introduces significant uncertainty (Bungum & Eldholm, 2022), and may be difficult even in trench studies to determine.
Secondary deformation	Minor faulting (McCalpin, 2009)	Not applied in our studies because cannot be resolved from lidar DEMs
Relationship to ice cover	Within former ice sheet area (Adams, 1989; McCalpin, 2009) and along preexisting faults (Hanson *et al.*, 1999)	Our study area is completely within former thick ice sheet region, but we acknowledge that syn-post glacial faulting may also occur outboard of the ice limit.
Proximity to stratigraphic evidence of shaking	Proximal mass transport deposits, landslides, or liquefaction features (Fenton, 1999; Mörner, 2004; Ojala *et al.*, 2019)	Québec's mapping is incomplete but this criteria could be applied to scarps discovered in proximity to lake coring or landslide mapping study areas (Ouellet, 1997; Doughty *et al.*, 2014; Brooks & Adams, 2020; Trottier *et al.*, 2019; Mérindol *et al.*, 2022).
Timing	Postglacial (McCalpin, 2009); shortly after ice sheet recession (Hanson *et al.*, 1999; Steffen *et al.*, 2014a; Craig *et al.*, 2016; Bungum & Eldholm, 2022; **?**)	Peak in flexural deformation rates in southern Québec may be a few ky after recession (Tuttle & Atkinson, 2010; Trottier *et al.*, 2019; Bungum & Eldholm, 2022); this could be reflected in potential crosscutting relations but due to high uncertainty we did not apply a criteria related to timing.

Table 2.1 Scarp identification and assessment criteria. First column indicates attributes, second column documents previous workers interpretation of these attributes, and third column indicates our preferred descriptions for Québec.

Criteria table			
	High	Medium	Low
Scarp cuts...	Surficial sediments or glacial and erosional landforms such as drumlins, eskers, linear moraines, terraces and/or causes horizontal offset (e.g. deflected channels)	Any intermediate scenarios	1. with sediment: vaguely cuts one feature or scarp disappears in young sediments 2. no sediment/only bedrock : no conclusion.
Plan pattern	linear to curvilinear	Any intermediate scenarios	Along-strike sinuosity is large
Continuity	Continuously traceable in both bedrock and sediment	Any intermediate scenarios	Abruptly terminating in bedrock, may reappear later – fractures
Scarp orientation	Strike different than the surrounding linear features (e.g. bedrock, joints and fractures, scarps from glacial plucking or frost heaving). Constant facing direction	Any intermediate scenarios	(Sub)parallel to adjacent waterbody – Terrace / shoreline. Changes in facing orientation
Scarp Height	≥30 cm at maximum height, have maximum heights of 2-5 m. Sharp break in slope; steep pronounced edges	Any intermediate scenarios	High erosion rate + time subdued the surface expression and flatten the scarp
Length of scarp	Any detectible scarp in the post-glacial sediments (c. 1 km), but >5 km in bedrock.		This criteria isn't considered, except in bedrock. Low confidence if scarp is <5 km in bedrock
Proximity to stratigraphic evidence of shaking	Proximal to paleolandslides, liquefaction evidence, tsunamis, mass transport deposits	Any intermediate scenarios	Distal to paleolandslides, liquefaction evidence, tsunamis, mass transport deposits

Table 2.2 Assessment criteria for determining whether a scarp is likely to be a fault scarp, modified from Gourdeau (2021); Laly (2021); Wang (2022).

CHAPTER 3

Investigation of suspected Holocene fault scarp near Montréal, Québec

Full title of submitted manuscript:

Investigation of suspected Holocene fault scarp near Montréal, Québec: The first paleoseismic trench in eastern Canada

Abstract

Québec has experienced historical damaging earthquakes in several seismic zones (e.g. 1732 M5.8 Montréal, 1663 M7 Charlevoix, 1935 M6.2 Temiskaming). Despite a high seismicity rate, no surface-rupturing faults have been discovered due to a combination of dense vegetation cover, recent glaciation, sparse earthquake records, and low regional strain rates. We manually searched lidar-derived digital elevation models (DEMs) of the region to search for potential post-glacial surface-rupturing faults across southern Québec and identified a scarp ~50km north of Montréal. We performed three geophysical surveys (ground penetrating radar, depth estimates from ambient seismic noise, and refraction seismology) that revealed a buried scarp, confirmed with a <1 m-deep hand-dug test pit. These observations convinced us to excavate the first paleoseismic trench in Québec to test for the presence of a surface-rupturing fault in July 2023. We found a glacial diamict containing no signs of syn- or post-glacial deformation. In this paper, we present the observations that led to the identification of a scarp and hypothesized faulting. We highlight the importance of trenching to confirm recent fault scarps in challenging environments. We hope our study can be used to optimize future paleoseismic research in the province of Québec and similar intracratonic glaciated landscapes.

Résumé

Le Québec se situe dans une région intraplaque sujette à de nombreux séismes ayant causés des dommages (e.g. 1732 M5.8 Montréal, 1663 M7 Charlevoix, 1935 M6.2 Temiskaming). Malgré une activité sismique régulière, la végétation dense, la déglaciation récente, les données sismiques sporadiques et le rythme de déformation lent ne concourent pas à l'identification de failles actives au Québec. Plusieurs modèles numériques topographiques (MNT) dérivés d'imagerie lidar (2016) du sud de la province ont été examinés afin d'identifier des candidats de failles sismiques post-glaciaires atteignant la surface, et montrent clairement un escarpement situé à ~50 km au Nord de Montréal. Trois méthodes géophysiques (géoradar, bruit ambiant sismique et réfraction sismique) ont été employées sur l'escarpement, qui montrent un décalage du socle rocheux à faible profondeur, confirmé par une première excavation de l'ordre de 1 m de profondeur. Ces observations ont justifié l'excavation en juillet 2023 de la première tranchée paléosismique effectuée au Québec, afin de confirmer la présence d'une faille sismique récente atteignant la surface. Cette tranchée révèle la présence d'un diamicton ne contenant aucun signe de déformation syn- ou post-glaciaire. Cet article présente les observations ayant faussement mené à l'identification d'un escarpement érosif comme étant une faille sismique. Il montre ainsi l'importance de réaliser des tranchées paléosismiques lors de l'identification de failles actives, spécialement dans des environnements complexes. Cette étude permettra

d'optimiser les recherches à venir dans le domaine de la paléosismologie au Québec et dans des environnements intracratoniques au passé glaciaire.

Non-technical summary

The cities of Montréal, Ottawa, and Ville-Marie lie within a zone of activity that has experienced historical damaging earthquakes (e.g. 1732 M5.8 Montréal, 1663 M7 Charlevoix, 1935 M6.2 Temiskaming), but no seismic faults have been identified in the region. Due to dense vegetation cover and recent glaciation that eroded the surface, faults are difficult to observe in this landscape. We used elevation maps from lidar data to search for topographic evidence of faulting and identified a scarp ~50 km north of Montréal. Three geophysical surveys revealed a buried bedrock offset that was confirmed with a <1 m-deep hand-dug test pit. These observations convinced us to excavate a trench across the scarp to test for evidence of sediment deformation and thus, faulting. We found glacial sediments containing no signs of deformation and concluded that the scarp was not formed by recent faulting. In this paper, we present the observations that led to the identification of a scarp and hypothesized faulting. We highlight the importance of trenching to confirm recent fault scarps in challenging environments. We hope our study can be used to optimize future research in paleoseismology in the province of Québec and similar recently deglaciated landscapes.

résumé non technique

Les villes de Montréal, Ottawa et Ville-Marie se situent dans une zone d'activité sismique sujette à de nombreux séismes destructeurs (e.g. 1732 M5.8 Montréal, 1663 M7 Charlevoix, 1935 M6.2 Temiskaming), mais aucune faille sismique n'a encore été identifié dans la région. La dernière glaciation, qui a érodé le territoire, et la végétation dense rendent la tâche ardue. Des cartes d'élévation lidar ont été utilisées afin d'identifier des changements abrupts et isolés de la topographie, potentiellement associés à des mouvements sismiques. Un escarpement bien individualisé a été observé à ~50km au nord de Montréal. Trois levés géophysiques et une excavation superficielle (1 m de profondeur) effectués sur le site ont permis de confirmer ce décalage du socle rocheux en profondeur. Ces observations ont poussé l'équipe à réaliser une tranchée plus importante contre le socle rocheux, l'objectif étant d'identifier si un déplacement des sédiments en profondeur est visible, ce qui prouverait l'activité d'une faille sismique. Les sédiments glaciaires dans la tranchée ne montrent aucun signe de déformation, ce qui invalide notre proposition de départ. Cet article présente les observations et mesures effectuées sur la faille identifiée en surface et souligne l'importance d'effectuer une tranchée lorsqu'une faille active est suspectée dans des environnements post-glaciaires et complexes. Cet article pourra aussi servir de guide afin d'optimiser les recherches en paléosismologie au Québec.

3.1 Introduction

Montréal lies within the western Québec Seismic Zone (WQSZ). The WQSZ is a region of elevated but poorly defined earthquake hazard which has experienced several historic, damaging earthquakes (Lamontagne, 2002; Ebel, 2011). In 1732, a M5.8 earthquake caused significant damage in the Montréal area, notably to chimneys, wells, and walls (Leblanc, 1981). Given the relatively large magnitude of this earthquake and other historic events in southern Québec (1935: M6.2, Temiskaming; 1663: M7.5, Charlevoix), it is possible that some of these events could have produced surface ruptures (Leblanc, 1981; Lamontagne, 2002; Brooks & Adams, 2020; Ebel, 2011; Mérindol *et al.*, 2022). However, despite these large earthquakes, no studies to date have identified active faults in the region (Brooks & Adams, 2020) and therefore observationally-constrained specific sources are not yet available to support ground motion models (e.g. Pagani *et al.*, 2014). The 1989 M_s6.3 Ungava earthquake and resultant Lac Turquoise fault scarp – the first known surface-rupturing earthquake on the eastern margin of North America and the only one in Québec (Adams *et al.*, 1991). Due to the lack of identified surface ruptures, a generalized region of elevated hazard appears in seismic hazard maps without any fault-specific sources or scenarios (Earthquakes Canada, 2020;

Thompson Jobe *et al.*, 2022). The complete instrumental record of historical M6+ seismicity for the whole country dates back only to 1950, and pre-instrumental earthquake history is reconstructed by estimating shaking magnitude from witness accounts (Lamontagne *et al.*, 2018; Tuttle & Atkinson, 2010), liquefaction records (e.g. Tuttle & Seeber, 1991) or landslides, and lake sediment records (Doig, 1990; St-Onge *et al.*, 2004; Brooks & Perret, 2023) rather than assessing hazard through paleoseismic techniques such as fault trenching or geomorphic slip rate analyses.

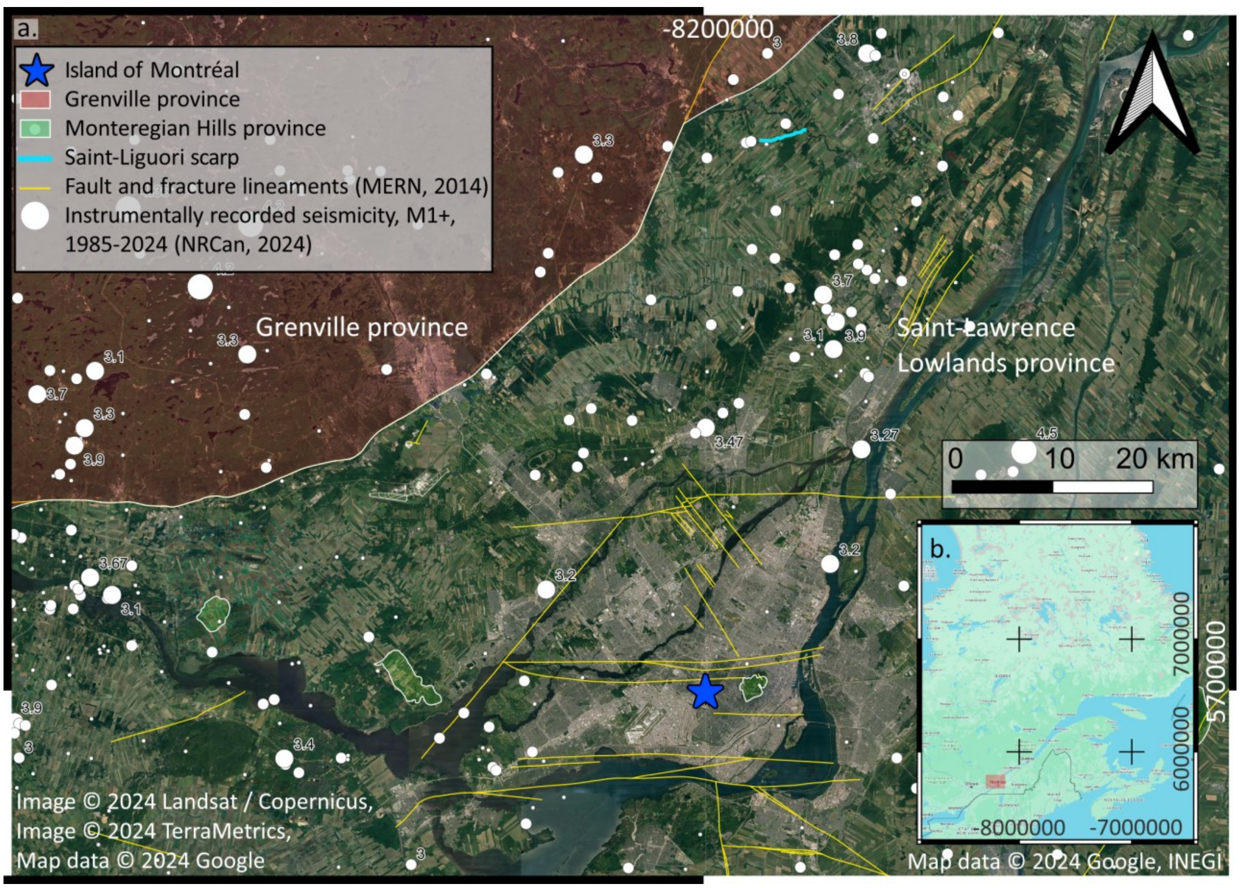

Figure 3.1 Map of the Saint-Liguori scarp (light blue) and its distance from the Island of Montréal; 2022 population 2,038,000 (Ministère de l'Économie, de l'Innovation et de l'Énergie, 2022). Basemaps for main figure and inset are Google satellite and terrain images, respectively. a) A general map of fault and fracture lineaments (yellow) was created by the Ministry of Energy and Natural Resources of Quebec (MERN) based on field observations made during cartographic surveys. b) Inset shows area of (a) in Québec in red box. / Carte comprenant la position de l'escarpement de Saint-Liguori par rapport à l'île de Montréal; population de 2022 2,038,000 (Ministère de l'Économie, de l'Innovation et de l'Énergie, 2022). Les cartes de base pour la figure proviennent de Google satellite et Google terrain, respectivement. a) La carte générale des failles et fractures (jaune) a été créée par le Ministère de l'Énergie et des Ressources Naturelles (MERN) basée sur des observations faites lors de campagnes de cartographie. b) Carte montrant l'étendue de la carte (a) dans le sud du Québec

Earthquake source faults are identified in seismically active regions by scarps and offset geomorphic features, precisely located microseismicity, and observations of surface rupture (McCalpin, 2009; Zielke *et al.*, 2015; Yu *et al.*, 2016a). Until recently, topographic maps in the province of Québec were not available in sufficient resolution to delineate the subtle geomorphic features that might be formed during moderate earthquakes. In 2016, the Québec government released lidar-derived, high-resolution digital elevation models (DEMs) that cover most of the WQSZ and two major urban centers (Montréal and Québec City) (Ministère des Forêts, 2016). We manually surveyed these elevation models to identify several potential fault scarps offsetting ~8-12 ka glaciomarine sediments (Globensky, 1987; Randour *et al.*, 2020a,b; Gourdeau *et al.*, 2023).

The young post-glacial surface history of Québec, coupled with regional low strain rates, means that if any surface-rupturing fault scarps exist we expect them to form low tectonic scarps and cumulative offsets. One of the rare intracratonic analogs of Québec that has documented surface-rupturing, post-glacial fault scarps is Fennoscandia, where paleoseismic records have been studied in detail (Smith *et al.*, 2014; Sutinen *et al.*, 2014; Mikko *et al.*, 2015; Palmu *et al.*, 2015). In glaciated environments, caution is required when studying scarps that could be associated with earthquakes. Erosion and enhancement of joints and fractures by ice plucking could form scarps during deglaciation that are not associated with seismicity, and other seismic features could have been eroded away by glacial advance and retreat. If surface processes outpace displacement, scarps don't develop strong geomorphic expressions. The spatiotemporal patterns of intraplate earthquakes are also poorly understood (Stein, 2007). For example, it is unknown whether individual faults have regular recurrence intervals or whether seismicity is chaotically distributed across a wide region of faults (Stein, 2007; Atkinson, 2007). Moreover, glaciotectonic features in tills can confound tectonic fracture identification (e.g. Pisarska-Jamroży *et al.*, 2019). The development of conceptual frameworks for patterns of intraplate seismicity requires more data to understand how these seismic zones differ from active plate boundary environments.

In spite of these challenges, paleoseismic investigations in Fennoscandia have successfully recovered seismic history on low-strain rate faults in a similar setting (e.g. Mörner *et al.*, 2000; Markovaara-Koivisto *et al.*, 2020). We assert that due to predictions of post-ice sheet flexure associated with lithospheric rebound (e.g. Lambeck *et al.*, 2017; Godbout *et al.*, 2023), similar field data is potentially recoverable in southern Québec. The main objective of this study was to demonstrate this feasibility by excavating the first paleoseismic trench in eastern Canada on a potential surface-rupturing fault scarp. Due to a lack of previous paleoseismic trenching in Québec, it took some time to develop an understanding of legal hurdles and professional cooperation necessary to pursue this research, so we document our experience here to aid future investigators working in Québec and eastern Canada. Our site specific health and safety plan (in French) is provided in the supplementary material for reference.

As part of a broader regional inventory (Gourdeau *et al.*, 2023), we identified a possible fault scarp ~45 km NE of Montréal near the village of Saint-Liguori (Fig. 3.1), which we named the "Saint Liguori scarp". Given the proximity of this scarp to the city of Montréal, it was a priority target for further investigation. Here we report the geomorphic expression of the scarp in the context of the post-glacial evolution in the St. Lawrence Valley. We present three geophysical methods (ground penetrating radar, H/V ambient seismic noise, and seismic refraction tomography) used onsite to demonstrate a subsurface bedrock scarp, and document a preliminary test pit demonstrating deformed post-glacial sediments in the proposed fault. We finally demonstrate how the results of each investigation was consistent with a recently active fault scarp until we dug a paleoseismic trench, which revealed no deformation. Our outcome demonstrates for the first time that paleoseismic trenching is possible and desirable in Québec. Trenches can provide valuable information on the glacial to post-glacial deposits that are critical for interpreting surface deformation evidence, especially in challenging and deglaciated environments. Moreover, trenching is crucial for identifying false-positives that were solely identified from geomorphic indicators.

3.2 Background

Approximately 90% of the bedrock of Québec is made of the Precambrian rocks of the Canadian shield, a cratonic setting (Hocq, 2014). The St. Lawrence river sits on the St. Lawrence platform of Cambrian-Ordovician age, preserved in the St. Lawrence aulacogen between the Grenville Orogenic belts to the north and northwest (Fig. 3.1a), and the Appalachian Mountains to the south and southwest (Tremblay *et al.*, 2013). The elevated seismicity in the St. Lawrence region has been attributed to numerous causes, including lithospheric thinning and inherited crustal faults from Paleozoic orogenesis, Mesozoic rifting (Rimando & Peace, 2021), and Cretaceous hot spot activity (Ma & Eaton, 2007), on which a recent stress perturbation caused by post-glacial rebound is superimposed (Henton *et al.*, 2006; Sella *et al.*, 2007; Goudarzi, 2016). Rimando & Peace (2021) suggested that faults with NW strikes had the highest slip tendencies (inferred from recent earthquake focal mechanisms) across eastern Canada.

The St. Lawrence valley lies in a Paleozoic aulacogen which formed during the opening of the Iapetus (proto-Atlantic) ocean (Kumarapeli & Saull, 1966), and whose bounding faults have been reactivated several times, including during the Cretaceous (Tremblay *et al.*, 2013). More recent reactivation of some scarps is possible, but not proven (e.g. Pinet *et al.*, 2020) (Fig. 3.1). The bounding normal faults (white trace in Fig. 3.1 a) have cumulative throws of 2-3 km and parallel faults interpreted from seismic reflection profiles in the St. Lawrence Estuary have throws of hundreds of meters (Tremblay *et al.*, 2013).

3.2.1 Glacial history of Québec

The Laurentide Ice Sheet (LIS) covered southern Québec ~21 ka ago during the Last Glacial Maximum (LGM) (Hocq, 2014; Dyke *et al.*, 2002; Sella *et al.*, 2007; Occhietti *et al.*, 2011). This ice sheet was up to 4 km thick in central Québec, and the weight of the ice has been shown to have significantly depressed the crust in Canada (Walcott, 1972; Simon *et al.*, 2016). Ice sheet retreat left behind depositional and erosional geomorphic features such as moraines, drumlins, eskers, erratics, glacial striations, and bedrock fractures (Bennett & Glasser, 2011; Occhietti *et al.*, 2011). Isostatic rebound is still ongoing in southern Québec at a rate of ~3-5 mm/yr (Tarayoun *et al.*, 2018).

This recent deglaciation strongly impacted the geomorphology of Québec and modified or erased evidence of scarps or offsets predating the marine incursion at ~13.1–12.8 ka (Cronin *et al.*, 2008; Occhietti *et al.*, 2011). Due to glaciation and post-glacial marine and lacustrine deposition, the land surface of southern Québec has been almost completely resurfaced or covered with thin Pleistocene-Holocene sediments (Occhietti *et al.*, 2011). The maximum marine inundation is at a present-day elevation of about 230 m, and Pleistocene deposits can reach thicknesses >100 m (e.g. near Lac St-Pierre, Lamothe, 1993). Near St-Liguori, the deposits are thin (< 5 m) due to the presence of bedrock highs in the area. Any surface scarps developed by faulting during the early glacial recession may have been eroded at this time.

Consequently, the production of earthquake-related offsets in the province, if any, must have developed since the late Pleistocene, suggesting that any scarps found in the region must have developed very recently. In a low strain rate environment, this short time period for developing evidence of fault activity suggests that any fault-related features are expected to be small in amplitude (Oliver *et al.*, 1970; Mazzotti, 2007; Tarayoun *et al.*, 2018).

3.2.2 Seismic history of greater Montréal area

There is reason to believe that Montréal faces a hazard of an ~M6 or greater earthquake due to a historical estimated M5.8-6 event which struck the then very small settlement in 1732 (Leblanc, 1981; Rosset *et al.*, 2021; Thompson Jobe *et al.*, 2022). The paleoseismic record of southern Québec is somewhat sparse, but the identification of subaqueous debris flows, landslides, and liquefaction features in lacustrine and marine sediments have led previous workers to suggest that 28-160 surface-rupturing earthquakes might have occurred in eastern Canada since the recession of the ice sheets (Fenton *et al.*, 2006; Brooks & Adams, 2020). In addition to the 1732 earthquake in Montréal, other historical earthquakes big enough to have caused surface ruptures include the 1663 M7 Charlevoix earthquake and the 1935 M6.2 Temiskaming earthquake (Leblanc, 1981; Lamontagne, 2002; Ebel, 2011). A cluster of seismicity has also been identified by (Chien & Liu, 2023) in the area of Joliette, about 60 km north-east of Montréal.

3.3 Geomorphic expression of the Saint-Liguori Scarp

Lidar-derived products, (DTM, slope) made available by the Ministère des Forêts et des Parcs since 2016, were used in QGIS and ArcGIS and converted to hillshade images to evaluate the location of potential fault scarps. We commonly used an illumination angle of 315°N at an altitude of 45° with a Z factor of 2, but theseparameters were sometimes changed to maximize visibility, contrast, and brightness.

Using these lidar-derived datasets, we applied a set of criteria for scarp identification adapted from methods used in Fennoscandia (Sutinen *et al.*, 2014; Smith *et al.*, 2014; Palmu *et al.*, 2015; Mikko *et al.*, 2015). Fault scarps and earthquake sources in Fennoscandia have been identified remotely by the observation of offset of drainage networks (either displacement of previously established channels or channel deflections recording apparent accommodation of baseline changes associated with fault throw), along-strike continuity and low sinuosity in low-relief landscapes, and soft-sediment deformation features and/or mass movement observation in the field (Smith *et al.*, 2014; Palmu *et al.*, 2015). Suspected fault scarps in Fennoscandia, as in other tectonically active regions, have also been confirmed or disproved in the field using paleoseismic trenches (Akçiz *et al.*, 2014; Smith *et al.*, 2014; Mikko *et al.*, 2015; Kozacı *et al.*, 2021). The regional scarp and possible fault dataset and detailed adaptation of scarp classification methods for use in eastern Canada and the northeastern USA (presented by Gourdeau *et al.*, 2023) and the key points relevant to the Saint-Liguori scarp are summarized here.

The Saint-Liguori scarp is situated in a low-relief, semi-agricultural area approximately

50 km north of the city center of Montréal (Fig. 3.1a). Land use in the area is dominated by small-scale grain and vegetable farming and maple syrup production. We mapped glacial features, whose apparent displacement or change in appearance across the scarp helped establish the scarp as a potential fault trace (see fig. 3.2). North-south trending ridges ±1 meter tall are the signature of ice flow, although they have not been associated with any particular advance (Fig. 3.2a). These ridges are expressed as bedrock grooves south of the scarp and as drumlins in a few places north of the scarp (Fig. 3.2b). Areas of bedrock exposure or very thin soil cover south of the scarp are unfavorable for farming and the presence of the scarp makes the terrain hard to plow. As a consequence, the scarp often delineates the end of the croplands and the beginning of the forest cultivated for maple production. We suggest that the distribution of agricultural land use was selected by early farmers for the flat areas underlain by deeper sediment, and subsequent activity likely removed any local relief along the scarp where possible.

The Saint-Liguori scarp, more than any other observed lineament observed within a 100 km-area around the city of Montréal, met the criteria for a feature of interest (Gourdeau *et al.*, 2023). The scarp is expressed as a nearly continuous, >5 km-long, ENE-trending topographic scarp, displaying a constant height of 2-3.5 meters, with bedrock exposure consistently appearing on the south side (Fig. 3.2d, e, 3.4). Quaternary sedimentary deposits are discontinuous across the scarp (see Fig. 3.2a). Detailed mapping of Quaternary deposits has not been completed in the region, due to poor exposure and land use effects which ambiguate primary landforms. The scarp is higher (2-3 m) in the forest and lower (0.5-1 m) in the plowed fields (Fig. 3.3). Several shallow channels make sharp local bends at the scarp. The scarp is best preserved where the bedrock is exposed at the surface on the south side (Fig. 3.2b). The middle section of the scarp displays more complexity, as a km-long discontinuous stepover appears with a secondary strand 100-200 m south of the main strand (Fig. 3.2b). The topographic scarp tapers in height to its endpoints, which disappear into agricultural fields (black arrows in Fig. 3.2a). Where the scarp crosses the flood-plains of the

Ouareau River, it is locally affected by fluvial terrace modification (Fig. 3.2f).

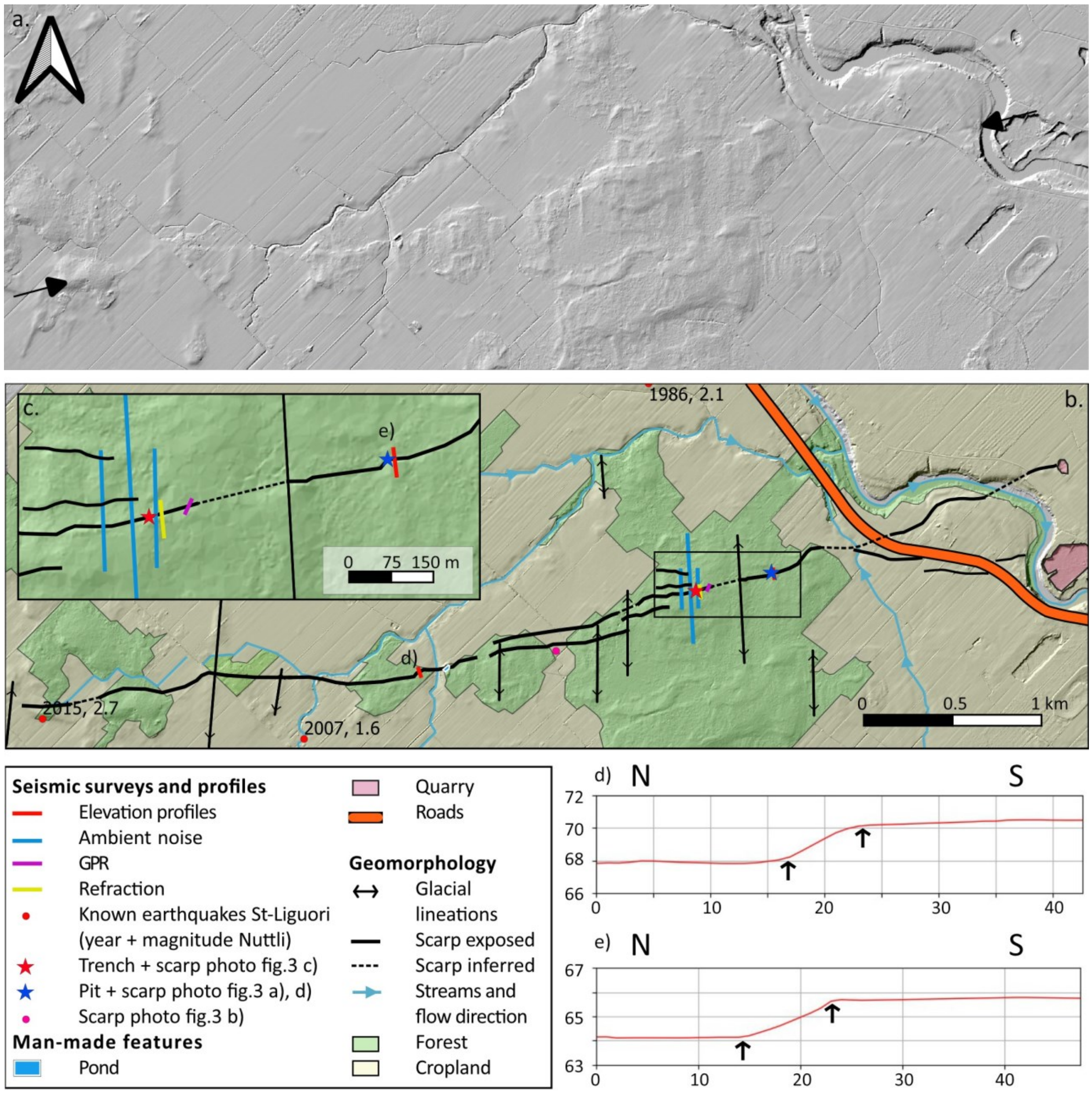

Figure 3.2 a) Lidar-derived hillshade of the Saint-Liguori scarp (light orientation is 315°,altitude of 45°, Z factor of 2. The scarp is located between the two black arrows. The original hummocky glacial geomorphology is very visible in the forested areas where the landscape hasn't been smoothed by cropland. b) Geomorphic map of the study area indicating scarp location, land cover type, and geophysical sampling locations. c) map inset of the trench area showing the location of the three geophysical surveys, the test pit and the trench. d) and e) are elevation profiles crossing the scarp. The location of the profiles are indicated on map b) and inset c), respectively. The black arrows are pointing at the location of the scarp. / Carte ombrée dérivée d'imagerie lidar de l'escarpement de Saint-Liguori (orientation de la lumière 315°,altitude de 45°, facteur Z de 2). L'escarpement se situe entre les flèches noires. La géomorphologie irrégulière originale est visible dans la forêt, là où le territoire n'a pas été aplani par l'agriculture. b) Carte géomorphique de la zone d'étude comprenant la position de l'escarpement, le type de végétation et le positionement des levés géophysiques. c) carte agrandie de la zone où la tranchée a été réalisée comprenant le positionement des 3 levés géophysiques et de l'excavation contrôle. d) et e) représentent des profils topographiques prélevés perpendiculairement à l'escarpement. La position des profils est indiquée sur la carte b) et c), respectivement. Les flèches noires indiquent la position de l'escarpement.

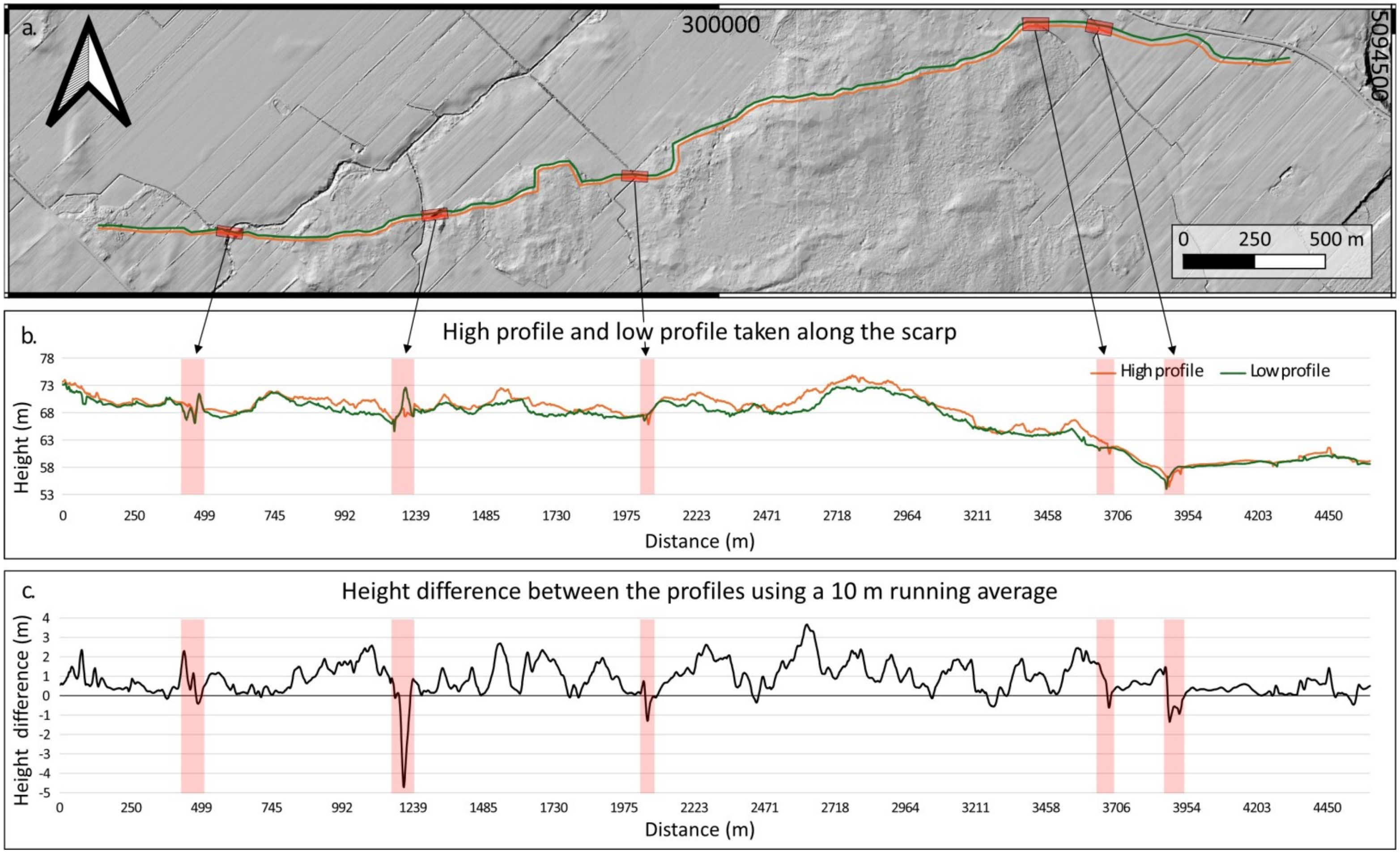

Figure 3.3 Elevation profile measured along the Saint-Liguori scarp. a) Represents the lidar imagery with the position of 2 parallel profiles, one taken at the scarp maximum height (orange), and one taken along the scarp's minimum height (green). b) Represents the elevation data retrieved from both the scarp minimum (green) and maximum elevation profiles (orange). c) Represents the height difference between both profiles, oscillating between 1 and 2 m. Plot c) has been made using a 10 m running average to reduce noise. The red polygons depict segments containing negative elevation differences, which are all associated to the presence of channels made for agriculture. The height data was retrieved from the lidar derived products available through the Ministère des Forêts, Faune et Parcs (Ministère des Forêts, 2016). / Profils d'élévation mesurés le long de l'escarpement de Saint-Liguori. a) Représente l'imagerie lidar avec la position des deux profils d'élévation prélevés en parallèle, l'un représentant la hauteur maximum de l'escarpement (orange) et l'autre la hauteur minimum (vert). b) Représente les données d'élévation prélevées le long des deux profils. c) Représente la différence de hauteur existant entre les 2 profils, oscillant entre 1 et 2 m. Le graphique c) a été réalisé en utilisant une moyenne glissante prélevée sur 10 mètres pour réduire les oscillations. Les polygones rouges représentent des segments d'élévation négative dans la différence de hauteur, segments tous associés à la présence de chenaux pour l'agriculture. Les données d'élévation ont été recueillies grâce aux produits dérivés de lidar émis par le Ministère des Forêts, Faune et Parcs (Ministère des Forêts, 2016).

3.4 Field investigations

We walked approximately 90% of the length of the identified scarp with the permission of 14 private landowners (see Acknowledgements). A ~1 m-deep, test pit was excavated on the northern side of the scarp to examine shallow sediments.

The forested areas crossed by the scarp (pale green, hummocky terrane; Fig. 3.2b) have rough topography associated with the bedrock glacial lineaments on the south side of the scarp (Fig. 3.2a, b). The forests are young (≤100 years) and are managed for maple production. Glacial erratic boulders of plutonic and gneissic rock are scattered on the land surface on both sides of the scarp, and many were observed partially buried where unconsolidated sediments are sufficiently thick.

The bedrock exposed along the scarp is a thin-bedded calcareous pebbly quartz sandstone (Fig. 3.4d). Finer layers of dolomitic to calcareous laminiated silt-sandstone are more deeply weathered. The erosion of these layers gives a step-like appearance to the bedrock scarp face (Fig. 3.4d). The 10-30 cm coarse pebbly sand layers are massive or crossbedded. These layers are made of 80% coarse, rounded, spherical, and well-sorted grains of quartz and feldspar with 5% <0.5 cm bioclasts and white-grey calcite cement.

3.4.1 Test pit

We excavated a ~90 cm-deep test pit to investigate the unconsolidated sediments on the north side of the scarp (Figs. 3.4a). The east wall was cleaned and photographed for construction of a 3D photomosaic using Agisoft Metashape (Fig. 3.5, Table 3.1). The soil present at the surface is a homogeneous, organic-rich, sediment-poor dark brown soil 30-35 cm thick, containing abundant roots of 0.5 cm to 4 cm in diameter. Approximately 60% of the soil is made of coarse to medium, moderately well-sorted quartz sand with trace micas. The soil also contains <3% 2-15 cm subangular gravel. Below the active soil layer is dense, light to medium brown compacted sandy loam. The uppermost ~25 cm is massive, clayey, and contains roots. This layer fines gradationally downsection and is predominantly made of

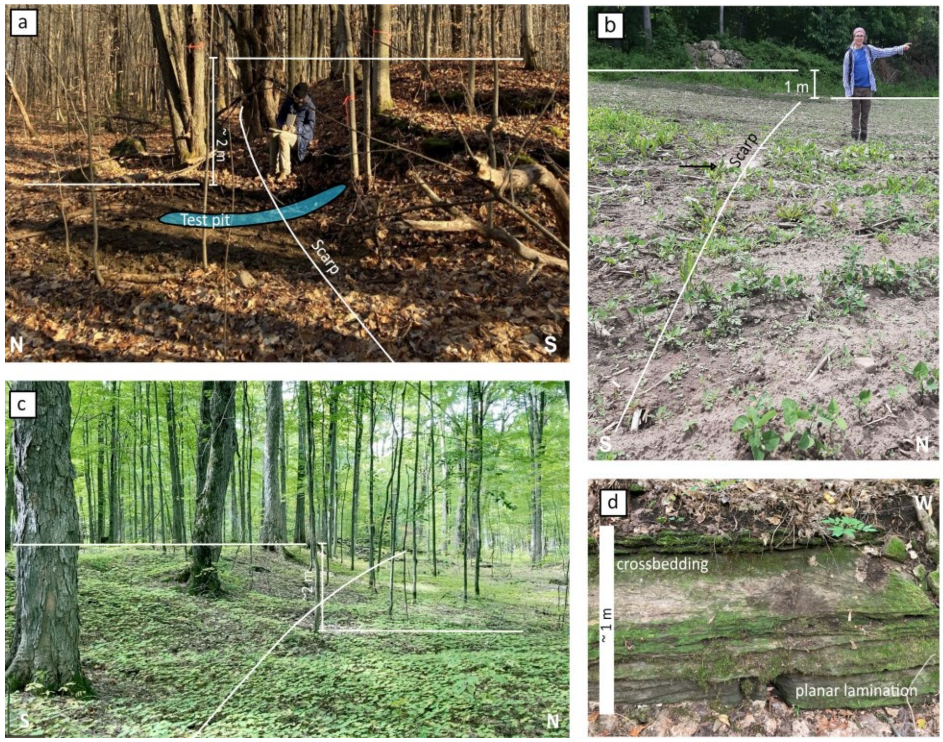

Figure 3.4 Expression of the scarp in the field. Base of scarp is marked with white lines in a), b), and c). Thin white lines marking approximate local relief. a) Expression of the scarp in the forest, where the test pit was excavated (blue polygon shows extent of pit footprint; see blue star fig. 3.2 for location). The height is large (2 m), the scarp is sharp, and the bedrock is exposed on the upper surface. b) Expression of the scarp in cropland, in the southern branch of the suspected stepover near the center of the mapped scarp length (see pink dot fig. 3.2 for location). The scarp is subtle, but ~1 m of relief is still visible. The bedrock is exposed, compromising vegetable growth. c) View looking west along the scarp at the location of the paleoseismic trench, showing continuity and consistency of scarp height (see red star fig. 3.2 for location). d) Exposed bedrock on the scarp near (a). Planar laminated dolostones at the base are overlain by crossbedded calcite-cemented pebbly quartz sandstone. The top of the scarp displays ~30 cm soil development (covered with leaves)./ Apparence de l'escarpement sur le terrain. La base de l'escarpement est définie par des lignes blanches en a), b) et c). Les autres lignes blanches et fines indiquent la position approximative du relief de l'escarpement. a) Apparence de l'escarpement dans la forêt, là où l'excavation contrôle a été effectuée (le polygone bleu indique l'étendue de l'excavation à la surface) (voir étoile bleue fig. 3.2 pour connaître le positionnement). La hauteur est importante (2 m), l'escarpement est net et le socle rocheux est exposé en surface. b) Apparence de l'escarpement dans les champs cultivés, sur l'embranchement Sud du possible stepover près du centre de l'escarpement (voir point rose fig. 3.2 pour connaître le positionnement). L'escarpement y est plus subtil, mais ~1 m de relief est tout de même visible. Le socle rocheux est exposé dans le champs, rendant la culture de légumes impossible. c) Vue de l'escarpement en direction Ouest, près de la tranchée paléosismique (voir étoile rouge fig. 3.2 pour connaître le positionnement). La constance et la continuité dans le relief de l'escarpement y sont bien visibles. d) Socle rocheux exposé près de la photo (a). Des dolomies planaires et laminées à la base sont surmontées de grès cimentés par de la calcite et comportent des lits croisés. Le haut de l'escarpement est surmonté par ~30 cm de sol (couvert de feuilles).

silt and clay with 40% medium-coarse sand. Rare cobbles and gravel were observed in the horizon, which also contains small oxidized spots surrounded by iron oxide cement (possible filled burrows). The deepest burrows were observed at 55 cm below the ground surface and have a maximum length of 10 cm.

This horizon is underlain by ~5-10 cm layers of tan sand with blue-gray lenses. Orange iron oxide cements are abundant in the sand layers. The lenses are ~1-3 cm thick and give way to more continuous layers at about 70 cm below the ground surface. The layers dip moderately north on the north wall of the pit and steepen to the south as they approach the steep bedrock contact (Fig. 3.5). Due to the alignment of some coarser sand laminae with the grey clay layers, we tentatively identified the layering as primary. The primary layering is accentuated by concentrations of authigenic iron oxide along parallel but irregular layers. The layers steepen toward the bedrock contact. Bedrock on the south wall of the pit was similar to that observed at the surface, and bedrock was not encountered north of the scarp.

Soil description of the test pit			
Depth (cm)	Label	Description	Color
Surface (0-4)	O	Uneven surface covered in maple leaves and organic material	
4-35	A	Organic-rich, many roots. Contact irregular, possibly due to tree uprooting and tilling. Contains sub-angular gravel.	Gray-brown
35-42	B	35-42 B Reduction in roots, increase in sand. Noticeably more yellow color.	Yellow-brown
42-56	C_1	Sandy parent material (40% medium-coarse sand, 60% silt and clays), fining gradationally downwards. Rare cobbles. Oxidized layers, possibly reflecting water flow paths.	Tan
56-107	C_2	Tan sand with blue-gray lenses. Abundant orange iron oxide layers.	Tan sand, blue-gray clay-rich layers

Table 3.1 Description of soil units in the test pit

3.4.2 Ground Penetrating Radar

The Ground Penetrating Radar (GPR) survey was run on the 8th of February 2022, at ambient temperatures of -2°C, while the soil was completely frozen. The GPR used was a

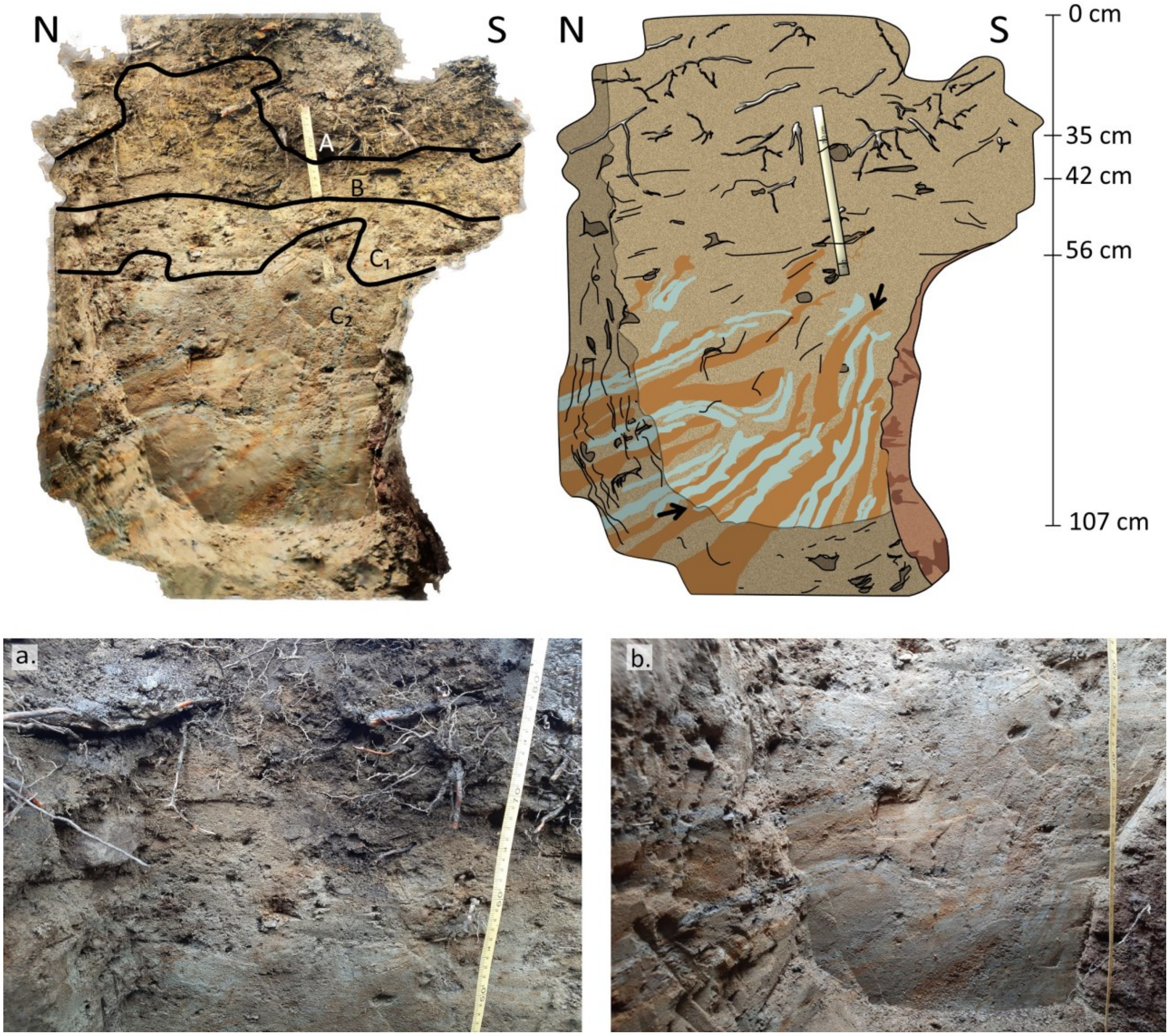

Figure 3.5 a) Eastern wall of the test pit from Agisoft Metashape model. Tape measure for scale. b) Sketch of (a), emphasizing key features. The bedrock is in reddish-brown on the southern wall of the pit. At the bottom (~56-107 cm below ground surface), blue and orange clay beds display steepening toward the bedrock interface (black arrows). This is overlain by homogeneous sandy loam 35-56 cm). The surface is organic and root-rich soil (0-35 cm). Scale in yellow. The labels A, B, C1, and C2 represent the soil horizons presented in table 3.1 c) Close-up of the upper organic-rich soil horizon. d) Close-up of the basal clay beds observed at the bottom of the pit./ Mur est de l'excavation contrôle obtenu grâce à un modèle Agisoft Metashape. Ruban à mesurer pour l'échelle. b) Croquis de (a) soulignant les éléments clés de l'exacavation. Le socle rocheux est rougeâtre le long du mur Sud. Le bas de la colonne (56-107 cm) comportent des lits d'argile bleus et oranges courbés, pointés entre les deux flèches noires. Les lits sont de plus en plus verticaux près du socle rocheux. Cette partie est surmontée par 35 à 56 cm de limon sableux homogène. La partie de 0-35 cm est riche en racines et en matière organique. L'échelle est identifiée en jaune. c) Agrandissement de la partie riche en matière organique du haut de la colonne. d) Agrandissement des lits argileux observés au bas de l'excavation.

PulseEKKO PRO model 1100 with 100 Mhz antennas. The time window was set at 200 ns, the temporal sampling interval at 0.8 ns, the antenna separation at 1 m, and the step size at

0.25 m. Figure 3.6 is interpreted using radar velocity in the subsurface at 0.165 m/ns, an appropriate velocity for ice. The parameters were set to reach as deep as possible despite the expected loss in resolution. A single 30 m-long line was run from NNE to SSW (purple line on Fig. 3.6b). We ran a non-perpendicular transect due to heavy vegetation and deep snow surrounding the area (purple line on Fig. 3.2b). The raw GPR scan (Fig. 3.6a) shows the presence of significant dipping reflectors at ~0-10 m, aligned with with the surface expression of the scarp.

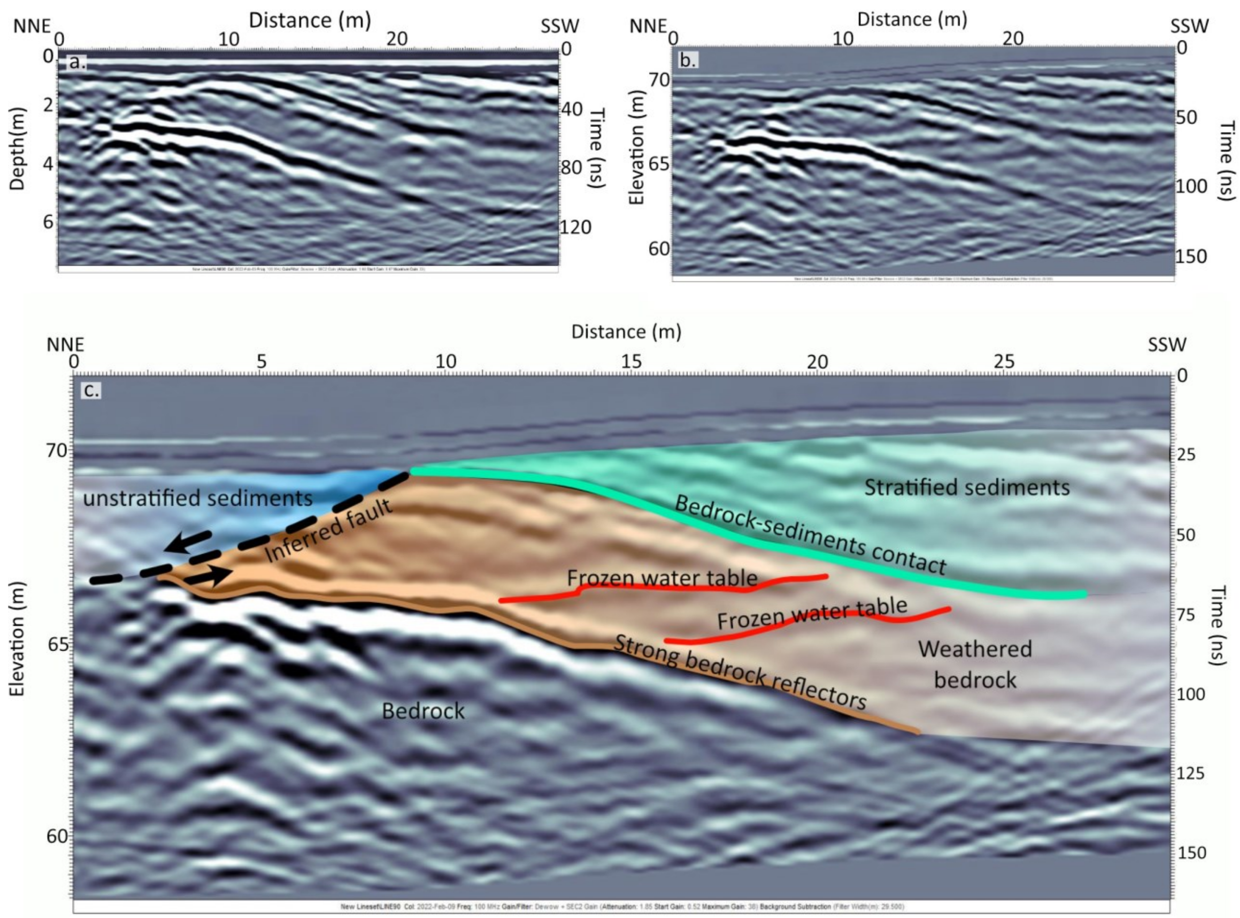

Figure 3.6 a) The raw data obtained from the GPR survey using EKKO project V5, b) GPR survey after processing, with topography considered, using EKKO project V5. Vertical axis is depth assuming uniform velocity of ice. c) Interpretation of the processed GPR survey. Calculated depths(m) are assuming a velocity of ice (v = 165 m/ns). / a) Données brutes des levés GPR obtenues à l'aide de EKKO project V5. b) Levé GPR après avoir traité les données à l'aide de EKKO project V5. L'axe des ordonnées représente la profondeur selon la vitesse dans la glace. c) Interprétation des données GPR traitées. Les profondeurs calculées utilisent la vitesse de la glace (v = 165[m/ns]).

The raw data obtained in the field was visualized and processed using the free program

Reflex 2D-quick and EKKO project V5. The data was processed by doing a static correction (repositioning the Y-axis to zero), a background removal (removing the average trace to remove surface wave and constant horizontal reflections), applying a standard SEC gain to amplify late reflections, and applying a topographic correction to correct the surface elevation profile using the GPS data. The rest of the parameters were kept at default. The color contrast was maintained to default.

Assuming the frozen soil approximates the radar velocity of ice (Fig.3.6), the reflector corresponding to the surface scarp dips gently (20°NNE) NNE down to a depth of ~2.5-3 m and is overlain by a zone of more chaotic reflectors gently dipping in both the NNE and the SSW direction (blue). We interpreted these chaotic reflectors as poorly stratified or disrupted sediments. These chaotic reflectors could be related to mixed grain sizes in the matrix, changes in soil composition, and/or disorganised and randomly oriented clasts. The bedrock is buried ~3 m at the NNE end of the line, at the junction of the strong bedrock reflectors contact (orange line, gently sloping down SSW) and the inferred fault (see Fig. 3.6). These most prominent bedrock reflections (orange line) are visible at ~5 m depth, with some deeper reflections visible at up to 10 m, and were interpreted to represent bedding planes in the bedrock. Above the bedrock, a weathered, saturated transition zone is interpreted (orange). The red and almost horizontal reflectors in the zone are interpreted to be related to the progressive freezing of the water table due to their nearly horizontal shape and presence only in the weathered and not consolidated bedrock zone. The reflectors overlying the interpreted bedrock-sediment contact (green line) follow the shallow dip of the bedrock-sediments contact (Fig. 3.6c). They were interpreted to represent unconsolidated stratified sediments, which are visible at the surface. The bedrock-sediment contact is the shallowest at 10 m along the line, concurrent with the surface expression of the scarp.

3.4.3 Ambient noise recordings

To estimate the depth to bedrock over a wider area, a campaign of ambient noise recording was carried out at 21 sites on Oct. 27th, 2022. The sites were selected along three lines perpendicular to the scarp, close to the GPR survey line. Ambient noise was recorded for 20 minutes on each site using Tromino© sensors setup in a flat zone. The records were analyzed using the Horizontal-to-Vertical Spectral Ratio (HVSR) method to estimate the fundamental resonance frequency (f_0) on site (refer to Molnar *et al.*, 2018, for more details). The data were analyzed with the Geopsy software (Wathelet *et al.*, 2020) and following the standard procedure described in the SESAME project (Acerra *et al.*, 2004). The map in Figure 3.7 locates the investigated sites grouped by predominant frequency of the peak amplitude f_0 as estimated in the HVSR spectrum. The entirety of the spectra for the 21 sites can be found in the supplementary materials.

The survey results indicate the presence of a thicker layer of sediments north of the scarp where the values of f_0 are lowest (around 10-12 Hz) and very shallow bedrock south of the scarp (with higher values of f_0), consistent with the GPR results. The value of f_0 is related to the layer thickness (H) and average shear-wave velocity (Vs) such that f_0 = Vs/4H (Roesset, 1970), assuming a homogeneous soft surface layer with a Vs of 200 m/s (as suggested by Rosset *et al.*, 2015). The thickest sediments (~4 m to bedrock) appear at sites B5, B6, B7, and C2, a couple of meters north of the scarp. Frequencies at sites B1 and B2 further north suggest similar thicknesses while the sites A1, B3, B4, and C1 suggest very shallow bedrock. The uncertainty associated with the depth estimate is significant, but this does not detract from the distribution of frequency values over the area, which indicates a relatively thicker layer of unconsoildated sediment north of the scarp.

3.4.4 Seismic refraction survey

A seismic refraction survey was run perpendicular to the scarp in the same location as the ambient noise survey (Fig. 3.2). Twenty-four geophones were spaced at a 2 m intervals

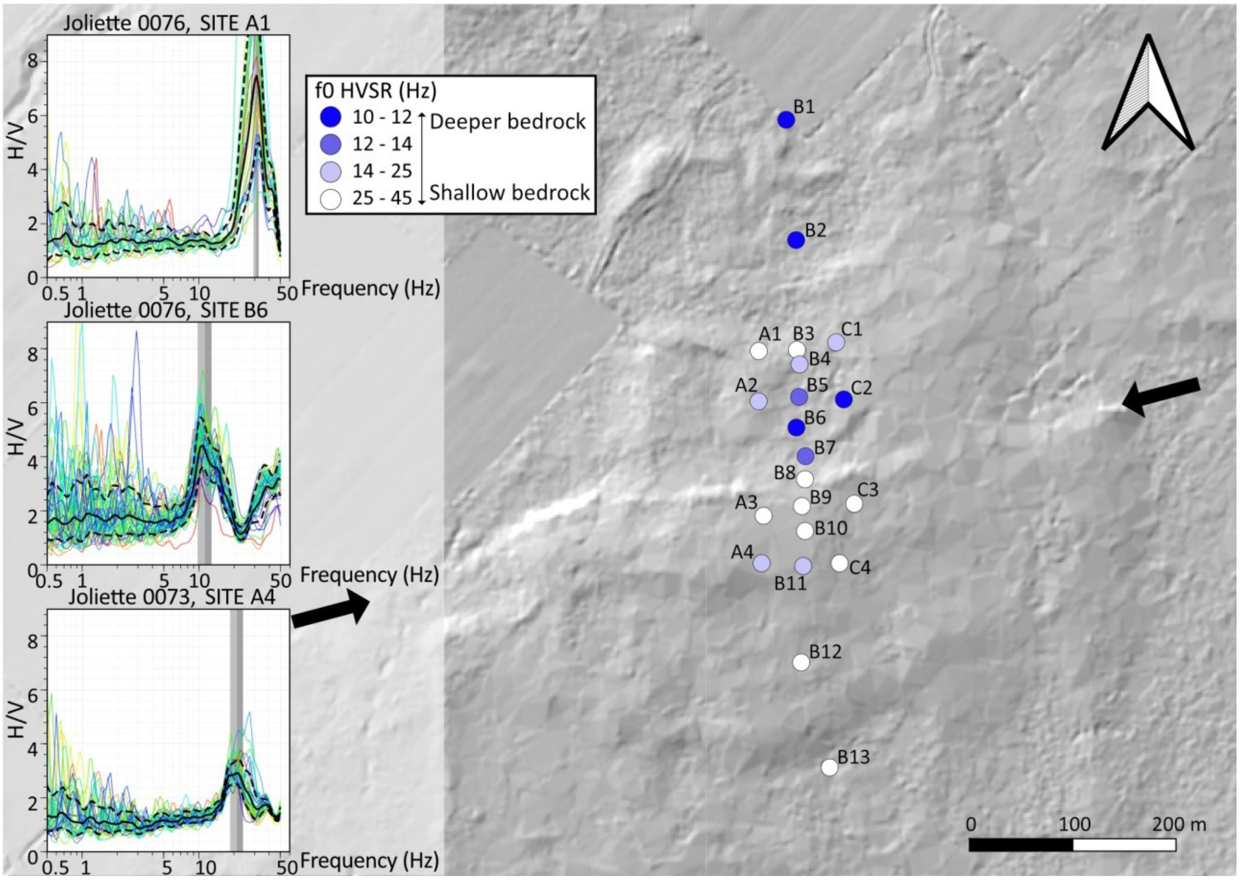

Figure 3.7 Ambient noise recording locations superimposed on lidar DEM (see fig. 3.2 for location). The scarp appears between the black arrows. Three ambient noise profiles (A, B, and C) were collected perpendicular to the scarp. The point's colors indicate the predominant frequency sampled at each site, which is roughly correlated to the bedrock depth at these locations. Three ambient noise HVSR spectra are presented on the left side of the plot for reference. The spectra for the 21 sites can be found in the supplementary materials./ Localisation des enregistrements de bruit sismique et carte lidar ombrée (voir fig. 3.2 pour positionnement). Les deux flèches noires localisent l'escarpement. Les enregistrements de bruit sismique sont localisés selon trois profils (A, B et C) perpendiculaire à l'escarpement. La couleur des ronds indique la fréquence prédominante f0 calculée pour chaque site, qui est inversement proportionnelle à la profondeur du socle rocheux. Trois exemples de spectres HVSR de bruit sismique sont présentés du côté gauche de la figure. Les spectres HVSR obtenus pour les 21 sites sont accessibles dans les documents complémentaires.

along the survey line and three source shots were hammered per array location (at -2 m, 23 m, 48 m respectively). Each geophone was moved 2 m northward to shift the array after each set of three shots, resulting in a total effective survey length of 64 m. The data was filtered between 100 and 300 Hz and grouped into common shot gathers. First arrivals were picked manually using Refrapy (Guedes *et al.*, 2022). The picked travel times were inverted for Vp to derive a 2D model using pygimli (Rücker *et al.*, 2017). The 2D model included the local elevation profile along the seismic line. The starting model for inversion extended to 16 m depth, and the initial velocity structure was a linear gradient from 300 m/s at the top of the model to 3000 m/s at the bottom. The model used an unstructured triangular mesh designed to provide the highest spatial resolution in areas with the most data coverage. The final velocity model is the result of iterative inversion, stopping when the change in the data objective function between iterations is less than 0.1%. The inversion is constrained to keep all velocities between a minimum of 100 m/s and a maximum of 4500 m/s. Figure 3.8 shows the final Vp model for the region where the data provide constraints.

The resolution of the model was assessed using superimposed checkerboard velocity anomalies (Zelt, 1998). The data can resolve velocity structure in a smooth sense but, due to sparse ray coverage, the nominal resolution limit for the model is ~8 m, meaning that velocity anomalies with a smaller length scale than 8 m may not be faithfully resolved in most of the model space. Thus, the refraction survey is broadly consistent with the results of the other geophysical investigations, but does not add any additional constraints on the subsurface structure.

3.5 Saint-Liguori trench

The geophysical and test pit observations presented above seemed to be consistent with the hypothesis that the Saint-Liguori scarp could be a post-glacial fault scarp, motivating us to excavate a paleoseismic trench at Cabane à Papio near the village of Saint-Liguori in summer 2023 (Fig. 3.1, 3.9). The trench site was chosen in consultation with the landowner, where the highest part of the scarp was accessible by four-wheeler tracks and the population of large producing maple trees was least dense. Québec law (s. 3.15.3.1(1),(2),and (3) of the Code de sécurité pour les travaux de construction) requires oversight by a professional engineer for excavations greater than 1.2 meters deep (Gouvernement du Québec, 1979). Under the law, generic excavations must be fully shored prior to allowing people working within walls >1.2 m high except in cases of certification by a professionally accredited engineer. An initial

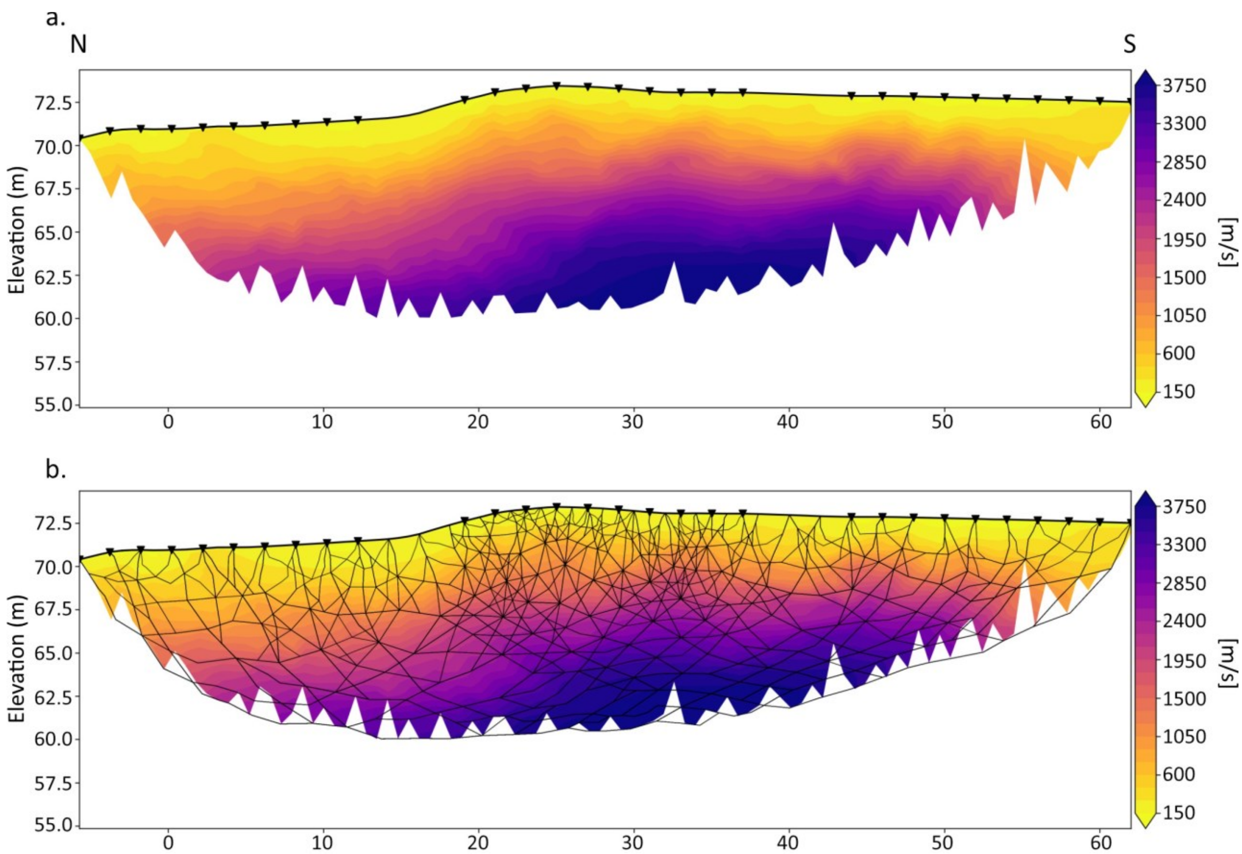

Figure 3.8 a) Processed and smoothed refraction survey results. b) Refraction velocity model with ray coverage./. a) Profil de sismique réfraction après lissage b) Profil incluant la couverture des rais sismiques

consultation with an engineering company resulted in a shoring design that could be slid along the trench wall to reveal 20 cm-square windows of the soil. We rejected this plan as untenable because it would not allow for cleaning and photographing the walls. We also contacted several government agencies and found that those with a geological mapping mandate had no experience with trenching and those overseeing roadworks had no experience with soil logging at the level of detail required for a paleoseismic trench investigation. No agency was able to offer advice or support on how to legally excavate. For several months it appeared there was no legal path forward to excavating a paleoseismic trench for logging at the site.

The breakthrough occurred through the introduction of a geotechnical engineer who had gained previous experience in paleoseismic studies (Claudine Nackers, P.Eng., M.A.Sc.). She designed a site-specific safety and excavation plan to allow trench wall cleaning and observation

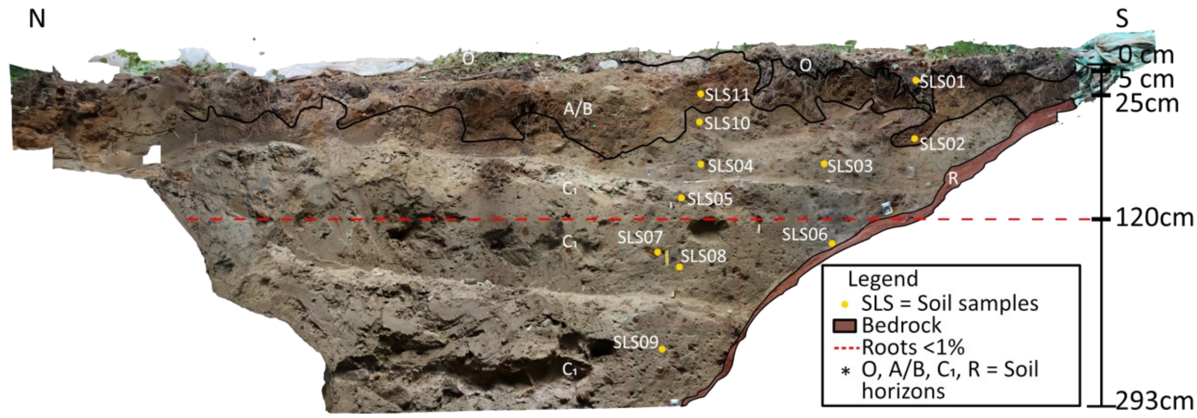

Figure 3.9 Agisoft orthophoto of the eastern wall of the trench. The soil sample locations are shown with yellow dots. The horizon names and positions are also included in the orthophoto. The sharp contacts bounding horizons O and A, marked with black dashed lines. / Orthophoto du mur est de la tranchée obtenue à l'aide d'Agisoft. Les échantillons de sol prélevés sur le mur sont identifiés en jaune. Le nom des horizons et leur postion sont aussi inclus dans l'orthophoto. Les horizons O et A, qui sont délimités par des limites nettes, sont identifiés à l'aide de lignes noires.

with contingencies depending on stability conditions encountered in the subsurface. This plan is compliant with requirements under Québec law, and engineering oversight during the excavation ensured that all conditions encountered were safe. Isra Excavation, a local company, worked closely with the engineer to ensure compliance with safety mandates and to plan adaptations after an intense rainstorm arrived while the trench was open. The benching geometry was agreed upon between the engineer and the excavator operator as the excavation continued. The site safety plan (in French) is available in the supplementary material.

The trench was opened on 13 July 2023 and reached a depth of 3.15 m (of which only 2.93 m was logged for safety reasons) by 9.12 m long and 4.2 m wide at the surface, with four benches on each long side. The south wall of the trench was bounded by the bedrock scarp, which was cleared of soil to the top of the topographic scarp. Slabs of detached bedrock up to 1 meter wide were removed from the trench by the excavator, but no similar slabs were observed as clasts in the sediment. The dense diamict matrix (described below) was slightly moist and exhibited high cohesion, resulting in favorable conditions for wall cleaning and photography. The north wall of the trench was not cleaned. The east and west walls were benched (Fig. 3.9) at intervals of 0.75-1.2 m to a width of 0.5 m meters, with benches sloping gently toward the south. The east wall was cleaned for photography and logging. The west wall was partially cleaned in the area adjacent to the bedrock scarp. The 3D model is available in the supplementary materials.

3.5.1 Bedrock description

The bedrock below the ground surface was shaped by bedding plane ledges forming a stepped wall. The bedrock comprises interbedded crystalline carbonate, calcite-cemented cross-bedded quartz grits, and reddish fissile siltstone which was not previously identified at the surface scarp. Crystalline carbonate beds (dolostone with some calcite clasts and cement) are golden brown on smooth weathered surfaces and medium gray on fresh surfaces. Lacy siliceous cements decorate wavy – likely algal – laminated beds to about 0.6-1.2 m thick. Benches on the exposed bedrock scarp are topped by thinner (30-40 cm) crossbedded quartz sandstone (0.5-2 mm) beds, with high grain sphericity and rounding. The sand is calcite cemented, resulting in a friable weathered zone extending ~5 cm below the soil interface. Thin (2-5 cm) shale interbeds occur above quartz sandstone beds and sometimes between thicker crystalline carbonate beds. The shales are massive to laminated, dark grey, plastic, and fissile where weathered. Parting surfaces are altered to brick red within a few cm of soil interface.

The bottom of the trench was reached at a subhorizontal bedding plane surface of crystalline carbonate at 293 cm below the ground surface. A deeper bench was reached on the northeast side of the trench, but due to stability concerns related to storm water ponding, we did not log that area below 293 cm. We estimate that the depth reached ~315 cm. Bedding plane slabs of bedrock detached during excavation, aided by joints oriented ~058/90, parallel to the scarp. The steps in the outcrop are formed by the upper surface of carbonate bedding planes, and the base of the ledges corresponds to the erosion of the thin reddish siltstones. This description is consistent with the Beekmantown Group, possibly the Beauharnois Formation (Hersi *et al.*, 2003), as indicated on the regional bedrock geologic map (Ministère des Ressources naturelles et des Forêts, 2021).

3.5.2 Sediment description

The diamict depositionally overlies the stepped bedrock surface (Figure 3.9). The contact was observed from the base of the organic-rich soil horizon down to the base of the pit, which was terminated at a wide bench in the bedrock 3 m below ground surface (Table 3.2; Figure 3.9).

The excavator removed 30-50 cm of organic-rich, dark brown to chestnut brown soils with abundant (10%) roots 0.5-4 cm in diameter. The soil transitions to unconsolidated but densely compacted matrix-supported diamict. The transition between the upper soils and the diamict appears at a depth of ~25 cm. The contact is sharp, but undulating. Living roots were observed down to 1.2 m below ground surface (<1% roots), penetrating the diamict. A couple of roots reached a depth of 1.5 m, only appearing in highly weathered clasts. The diamict matrix is massive and lacks visible bedding planes, lamination, or grading. Only very subtle changes in grain size, color, and composition were observed from the base of the soil to the bottom of the trench (~2 m). The matrix is pale brown (olive brown 2.5Y 4/2 and 4/3 to olive gray 5Y 4/2), and comprises ~10% clay, 70% silt, and 20% sand.

We observed irregular elongated bodies of nearly 100% brown homogeneous clay in the upper ~0.5-0.75 m of the trench wall. These comprise <1% of the diamict. They are locally branching and irregularly taper and are found in both horizontal and steep orientations, with the horizontal ones up to a few cm in diameter and steep ones more likely to be millimetric in diameter. These appear to follow root traces, and we interpret these as the weathering products of the diamict due to reactions with organic acid from the roots.

3.5.3 Clast description

In the diamict, the clast size is heterogeneous, varying from <1-20 cm, with rare clasts reaching 30 cm. The clasts had no grain-to-grain contacts and no preferred orientation

Depth (cm)	Soil Horizon	Description	Color
Surface		Uneven surface covered in maple leaves and organic detritus	Variable
0-5, variable	O	Humic. Very abundant roots (15%), cohesive, organic-rich material.	Very dark brown (7.5YR 2.5/1)
5-25, variable	A/B	Sparse fine to medium sand. Lithic sub-angular sand with yellowish quartz. Roots ~10%. Rare gravel <5%. Contains pebbles and cobbles (similar to the rest of the column). Friable, high porosity. Upper and basal contacts highly convoluted, likely due to tree felling and agricultural disturbance.	Dark yellowish brown (10YR 3/6)
25-293	C_1	Diamict. Near the upper 0.5 m there are wiggly sharp-walled tabular clay bodies, brick brown in color. Most of the thicker (up to 2 cm) clay bodies are sub-horizontal and fine roots emerge from them. Steeper clay bodies ones are more braided, thin (3 mm), and wavy. Matrix is silt to fine sand with 20% medium to coarse sand. <2-5% gravel and around 1% cobbles. <1% boulders. – Subtle transition at ~120 cm: Abrupt loss of pervasive roots (5% to <1%) and clay bodies. Roots below this level are concentrated in weathered clasts. Subtle color change. Roots are completely absent in the diamict below ~150cm.	Olive brown (2.5Y 4/3) At ~120 cm: subtle color change to Olive brown (2.5Y 4/2) and olive gray (5Y 4/2)
293 – ~315	C_2	Diamict. Not visible in the photomosaic due to reduced photo coverage at base of pit. Matrix slightly coarser than above (~ 5-10% increase in the fine to medium sand). Gravel % appears to decrease (around 2%), but overall size increased (2-4 mm predominant). Cobbles <1%.	Olive brown (2.5Y 4/3)
> 293-315 (TD)	R	Bedrock dolostone. depositional contact with diamict to surface at southern pit edge	

Table 3.2 Description of unconsolidated sediments and soils observed in the Saint-Liguori scarp trench.

and were distributed homogeneously in the diamict. They were usually angular and highly weathered. The different clast types observed are summarized in Table 3.3. We noted three colors of deeply weathered, friable, oxidized clasts (orange, dark brown, and black) that have similar grain textures, suggesting the protolith microstructure was common to all three.

The deeply weathered condition of the clasts across a range of compositions is consistent with the older glacial diamicts known from southern Québec. If correlative, this diamict may be as Illinoian (130-191 ka) (Shilts, 1992).

3.6 Discussion

Based on the geomorphic features of the scarp and the subsurface continuity implied by the geophysical investigations, we interpreted the Saint-Liguori feature as a likely candidate for a recent fault scarp. The bends in drainages flowing southward toward the scarp face (Fig. 3.2) were identified as possible deflected channels. In retrospect, the deflection does not necessarily represent channel displacement or scarp development, and we cannot be sure how much anthropogenic modification of the channels has taken place. The test pit also strongly suggested that the scarp could have been fault-related. The displacement of Holocene sediments inferred from the geomorphology, combined with the observation of curvature of layers we had interpreted as sedimentary layering against the scarp surface were perceived as drag folds indicating evidence of faulting (Grasemann *et al.*, 2005; Smith *et al.*, 2014; Mikko *et al.*, 2015; Palmu *et al.*, 2015). The data subsequently obtained in the field during the three geophysical surveys consistently indicated a steep buried bedrock scarp, consistent with a fault offset. These observations, made with multiple techniques, increased our confidence in having found a north side-down normal fault 50 km NNE of Montréal and potentially near enough to the city to represent the source fault for 1732 ~M5.8 earthquake.

Trenching in July 2023 confirmed the existence of a steep and ~horizontally bedded buried bedrock scarp at least ~3 m deep, but it was found to be depositionally overlain by an old and

Label	Approximate relative clast proportion	Size (cm)	Color	Description
Orange clasts	35%	[0.5-15]	Pale orange	Silt-sized grains, mineralogy uncertain. Homogeneous, & very friable.
Dark brown clasts	33%	[0.5-30]	Dark brown-red	Silt-sized grains with some clay, no zoning, homogeneous. Friable to the point of complete loss of cohesion, angular. Less than 1% gray lithics <0.1 cm.
Quartzite clasts	15%	[1-5]	Bright white	Sugary and friable, angular clasts, almost purely made of quartz. Wide variety of intraclast grain sizes (0.1 cm-1 cm) but homogeneously distributed. Larger grain fraction are sub-angular and represent 10% of the matrix, while tiny grains (<0.5cm, 90% of the matrix) are rounded. Sometimes present with thin, cohesive dark gray weathered cortices.
Granite clasts	8%	[0.5-7]	Pink	Granite containing coarse 50% k-feldspar, 20% coarse plagioclase, 20% coarse Quartz, and 10% micas of 0.1-0.5 cm. The clasts are sub-angular, hard, and weakly weathered.
Gray greenstone clasts	5%	[1-15]	Gray	Fine-grained, hard, sub-angular pebbles and cobbles. Silicified greenstone. Rough weathered surface with thin cortex.
Black clasts	2%	up to 20	Black	Powdery, highly weathered, and angular clasts. Mineralogy uncertain. May be a darker version of the dark-brown clasts.
Other metamorphic rocks	2%	[0.5-7]	Black and white	Mica-dominated (mica concentration >90%, 0.1-0.3 cm) granites are observed in the matrix. Some gneissic tonalites have also been found in the matrix. Pieces of meta-quartz veins are also observed.

Table 3.3 Diamict clast descriptions from trench wall.

completely undeformed diamict. The lack of bedding in the diamict corresponds to the chaotic unit overlaying the bedrock interpreted from the GPR profile, and the observed bedding also approximately matches the interpretations made on the GPR (Fig. 3.6). The diamict displays evidence of intense post-depositional weathering without physical deformation, as evidenced by the preservation of sharp clast boundaries for lithoclasts that are completely friable and weathered beyond identification. If any post-depositional deformation had affected the diamict, we would expect to see disruption of the boundaries, deformation, and disaggregation of these clasts, but they were observed completely intact. The massive matrix of the diamict is homogeneous mixed fine sand-silt with no detectable deformation bands, fractures, fissures, rotated/oriented clasts, or other features typically associated with faulting or shearing in unconsolidated to weakly consolidated sediments (Table 3.2; c.f. Bray *et al.*, 1994; Oettle & Bray, 2013; Balsamo *et al.*, 2014). Delicate diagenetic/weathering features were observed intact, including the wavy-tabular and tubular clay bodies associated with roots. The roots that formed the clay bodies are older than the modern root systems, so the fact that we do not observe offset or contortion of these features adds to the evidence that the diamict has not experienced deformation. The variable clast lithology is consistent with glacially transported coarse clasts primarily derived from the Grenville belt (granite and quartzite). The deeply weathered orange, brown, and black clasts are of unknown affinity, but based on the color, the protolith may be mafic or ultramafic. Due to the lack of clast alignment and matrix shear fabric and absence of faceted clasts, lack of sorted or laminated beds, the origin of this diamict remains uncertain but the variety and size distribution of lithoclasts, and high matrix fraction, could suggest basal deposition by lodgment or melt-out, melt-out, or debris flow origins in a pro- to subglacial setting.

This study highlights the importance of trenching to accurately identify fault scarps for paleoseismic studies. Although the geophysics results were suggestive, no conclusions could be drawn until the absence of deformation of the sediments was directly observed (c.f. Akçiz *et al.*, 2014). Trenches have been used to assess the seismic origin of scarps and assess the timing of fault activity, notably in related recently deglaciated and intraplate landscapes, and have proved their worth (Mörner *et al.*, 2000; Markovaara-Koivisto *et al.*, 2020; Figueiredo *et al.*, 2022). Even in active plate boundary settings, with strong geomorphic expression of fast-slipping faults with recent ruptures, not every paleoseismic trench is successful (Akçiz *et al.*, 2014).

Although we did not discover a recently active fault, this project still has an important value, since it represents the first paleoseismic trench attempted in Québec. One of the strong outcomes of this project was the creation of a network of engineers, geologists, and governmental agencies that are now familiar with the field of paleoseismology and the protocols associated with paleoseismic work. Together, the techniques used in this paper and the trench establish a set of guidelines that will simplify the study of other scarps in Québec and stimulate the emergence of paleoseismic studies. As suggested by Brooks & Adams (2020), the availability of new landscape data such as lidar-derived elevation models should facilitate the discovery of new candidates of glacially-induced or younger faults in eastern Canada. Without these discoveries, it is not possible to constrain source-specific seismic hazard scenarios, in particular for eastern Canada's major cities (Rosset *et al.*, 2021, 2023).

3.7 Conclusion

A wide range of techniques have been used to assess the nature of the Saint-Liguori scarp. The lidar-derived data product, the test pit, and the three geophysical surveys all revealed details consistent with disrupted sediments or offset bedrock that led to a consistent conclusion: this scarp was likely to be a fault scarp. However, opening a paleoseismic trench in July 2023 revealed the absence of syn- or post-glacial deformation in a very old diamict buried against the bedrock scarp, completely disproving our earlier interpretation. The scarp is not a surface-rupturing post-glacial fault scarp. This unexpected finding highlights the importance of paleoseismic trenches for identifying active faults. Challenging environments, such as the heavily vegetated and recently deglaciated landscape of southern Québec make fault identification challenging, particularly in light of the low regional strain rate. This paper documents an important breakthrough in the field of intracratonic paleoseismology in eastern Canada, since it represents the first paleoseismic trench attempted in the province of Québec. This project facilitated the development the creation of a network of geoscientists and engineers who are now aware of and interested in intraplate trenching and paleoseismology. This network will be crucial in the upcoming years, since governmental policies and laws in Québec do not account for the logistical demands of paleoseismology, creating a barrier to fault mapping and the development of a prehistoric seismic record for the region.

Data and code availability

Data associated with this project will be publicly available at Borealis.ca. The data files include: Complete Agisoft Metashape model of the trench wall, including component photo set and a 3D model of the trench (https://doi.org/10.5683/SP3/7OZT0V), a complete Agisoft Metashape model of the test pit, including component photo set (https://doi.org/10.5683/SP3/CJYTXW), the site-specific safety plan (in French; https://doi.org/10.5683/SP3/AQJKYT), a photo gallery of the expression of the scarp in the field (https://doi.org/10.5683/SP3/6PJ8E8) the complete ambient noise spectra collected at 21 sites (https://doi.org/10.5683/SP3/MFSRWQ), seismic reflection profile and datset (https://doi.org/10.5683/SP3/GTPCZ1), and the GPR dataset (https://doi.org/10.5683/SP3/FPDSOE).

CHAPTER 4

Trench planning and logistics

The realization of the paleoseismic trench in St. Liguori brought important logistical challenges. First, the location of the scarp led to additional constraints because of the presence of harvested maple trees. We thus had to build a trusting relationship with the landowners to convince them to allow us to dig on their property. The final trench site was decided in consultation with Mario Richer, the owner of the property, at a site adjacent to a 4-wheel drive track that would allow access for a backhoe with a minimum of damage. M. Richer also expressed concerns about the risk of damage to maple trees whose roots were impacted by excavation. We needed to insure against future damage to the maple farm if the harm to the trees was not immediately realized. To do so, a contract was written by the legal counsel of McGill, to guarantee financial compensation in case of tree damage for a duration of 3 years after the trench closure. Legal preparation and safeguarding of the value of the trees made the landowners more comfortable with the trench planning. Trust relationships were also built with all the private properties and landowners visited in the course of walking out the scarp, which we kept updated on the advances of the project by occasional email and phone calls before every visit.

The excavation of the trench was also complicated by legal restrictions for excavation safety in Québec. Since the St. Liguori trench was the first paleoseismic trench attempted in the province, the provincial laws addressing construction safety practices were not well-adapted to the scientific needs. The project fell under the construction industry guidelines and jurisdiction, holding us from digging deeper than 1.2 m without a professional soil stability assessment, which could be based on drill investigations (Gouvernement du Québec, 1979). These industrial practices, in place for the construction industry, were not realistic for our objectives. We first had a discussion with the CNESST (Commission des normes, de l'équité, de la santé et de la sécurité du travail), who didn't have the authority to allow exceptions. We then contacted the Ministry of Resources of Québec and the Ministry of Transport of Québec and gave them presentations regarding our project to see if they could facilitate our work. Although they were interested in the scientific outcomes of the project, they had no way to help us. Finally, since there was no way out of the law, we decided to find a geotechnical engineer who would recognize the project's value upstream, understand the logistical constraints associated with the project, and collaborate with us to create a safe and realistic procedure adapted to our scientific objectives. However, we did acquire seismic velocity information from a series of surveys (Chapter 3). When combined with well-log data acqured from Ministère de l'Environnement (2024) we were able to develop a reasonably constrained estimation of sediment properties that supported the trench safety plan.

Most excavations in Québec are shored with plywood or steel plates to prevent any possibility of cave-in. This construction is inappropriate for paleoseismic trenches where detailed cleaning and observation of the complete walls is essential. After trying several contacts, we finally found a geotechnical engineer who was able to create an optimized safety plan for our trench (available on Borealis, link in Chapter 3), which included hand augering to test soil compaction before trenching, the construction of benches to reduce the height of individual wall segments, a safety plan for evacuation, and her presence on site to evaluate the sediment as it was exposed, plus constant updates on the conditions of the trench throughout the project. This scenario met the CNESST requirements since the endorsement of the project by an engineer represented legal protection concerning the law. I included the safety plan as an appendix to Chapter 3 as a resource in support of future paleoseismic research in Québec. If more paleoseismic trenches had to be built in Québec in the future, the law would probably need to be adapted to facilitate our work, or engineers will need to develop a more common understanding of how to excavate paleoseismic trenches within the legal constraints. The law could be inspired by the safe methods already approved in other regions around the world, such as the United States or in British Columbia.

CHAPTER 5

Conclusion

This thesis represents a very promising and essential step for the field of paleoseismology in Québec and in deglaciated intracratonic landscapes, which will hopefully eventually help to better assess seismic hazard in the WQSZ. Currently, there are no realistic earthquake scenarios including observation-based location, orientation, and length of source faults used to estimate seismic shaking probabilities in Québec. There is no data to constrain characteristic earthquake magnitude or timing of past events. Nevertheless, the WQSZ is a region of high earthquake risk that is poorly understood and should be closely studied. The recent release of publicly available LiDAR imagery represents the perfect opportunity to study surface-rupturing paleo-earthquakes and refine our understanding of the earthquake record and distribution. Field assessment, such as the seismic surveys and paleoseismic trench realized at Saint-Liguori scarp, even if non-conclusive, pave the way for future surveys and highlight the importance of combining remote sensing and field assessment when identifying potential surface-rupturing fault scarps. Hopefully, the potential scarp map realized in specific areas of southern Québec and our suggested methodology will encourage public and/or private agencies to complete the mapping and investigate the highly-ranking candidates in the field to improve our understanding of post-glacial seismicity. In addition to the immediate need for these investigations for seismic hazard models, these results could potentially be useful in other intracratonic settings and extrapolated to other deglaciated and highly vegetated landscapes.

Bibliography

Acerra, C., Aguacil, G., Anastasiadis, A., Atakan, K., Azzara, R., Bard, P.-Y., Basili, R., Bertrand, E., Bettig, B., Blarel, F., *et al.* (2004). Guidelines for the implementation of the H/V spectral ratio technique on ambient vibrations measurements, processing and interpretation. *European Commission–EVG1-CT-2000-00026 SESAME*.

Adams, J. (1989). Postglacial faulting in eastern Canada: nature, origin and seismic hazard implications. *Tectonophysics*, *163* (3), 323–331. Paleoseismity and neotectonics.

Adams, J. (1996). Paleoseismology in Canada: A dozen years of progress. *Journal of Geophysical Research*, *101* (B3), 6193–6207.

Adams, J. & Basham, P. (1991). The seismicity and seismotectonics of eastern Canada. In *Neotectonics of North America*, Geological Society of America. 261–267. URL https://doi.org/10.1130/DNAG-CSMS-NEO.261.

Adams, J., Wetmiller, R. J., Hasegawa, H. S., & Drysdale, J. (1991). The first surface faulting from a historical intraplate earthquake in North America. *Nature*, *352*, 617–619.

Akçiz, S. O., Ludwig, L. G., Zielke, O., & Arrowsmith, J. R. (2014). Three-dimensional investigation of a 5 m deflected swale along the san andreas fault in the carrizo plain. *Bulletin of the Seismological Society of America*, *104* (6), 2799–2808.

Anderson, J. G., Wesnousky, S. G., & Stirling, M. W. (1996). Earthquake size as a function of fault slip rate. *Bulletin of the Seismological Society of America*, *86* (3), 683–690.

Atkinson, G. M. (2007). Challenges in seismic hazard analysis for continental interiors. In S. Stein & S. Mazzotti (Eds.), *Continental Intraplate Earthquakes: Science, Hazard, and Policy Issues: Geological Society of America Special Paper 425*, The Geological Society of America. 329–344.

Balsamo, F., Aldega, L., De Paola, N., Faoro, I., & Storti, F. (2014). The signature and mechanics of earthquake ruptures along shallow creeping faults in poorly lithified sediments. *Geology*, *42* (5), 435–438.

Bégin, C. & Filion, L. (2010). Age of landslides along the grande rivière de la baleine estuary, eastern coast of hudson bay, québec (canada). *Tree Rings and Natural Hazards: A State-of-Art*, 107–120.

Bélec, G. (2016). *Seismic assessment of unreinforced masonry buildings in Canada*. Ph.D. thesis, Université d'Ottawa/University of Ottawa.

Bennett, M. M. & Glasser, N. F. (2011). *Glacial geology: ice sheets and landforms*. John Wiley & Sons.

Bent, A. L. (1996). An improved source mechanism for the 1935 Timiskaming, Quebec earthquake from regional waveforms. *Pure and Applied Geophysics*, *146*, 5–20.

Bent, A. L., Lamontagne, M., Adams, J., Woodgold, C. R., Halchuk, S., Drysdale, J., Wetmiller, R. J., Ma, S., & Dastous, J.-B. (2002). The Kipawa, Quebec "Millennium" earthquake. *Seismological Research Letters*, *73* (2), 285–297.

Berglund, M. & Dahlström, N. (2015). Post-glacial fault scarps in jämtland, central sweden. *Gff*, *137* (4), 339–343.

Bray, J. D., Seed, R. B., Ciuff, L. S., & Seed, H. B. (1994). Earthquake fault rupture propagation through soil. *Journal of Geotechnical Engineering*, *120* (3), 543–561.

Brooks, G. R. (2013). A massive sensitive clay landslide, quyon valley, southwestern quebec, canada, and evidence for a paleoearthquake triggering mechanism. *Quaternary Research*, *80* (3), 425–434.

Brooks, G. R. (2014). Prehistoric sensitive clay landslides and paleoseismicity in the ottawa valley, canada. *Landslides in sensitive clays: From geosciences to risk management*, 119–131.

Brooks, G. R. (2018). Deglacial record of palaeoearthquakes interpreted from mass transport deposits at three lakes near rouyn-noranda, north-western quebec, canada. *Sedimentology*, *65* (7), 2439–2467.

Brooks, G. R. (2020). Evidence of a strong paleoearthquake in ~9.1 ka cal BP interpreted from mass transport deposits, western Quebec–northeastern Ontario, Canada. *Quaternary Science Reviews*, *234*, 106250.

Brooks, G. R. & Adams, J. (2020). A review of evidence of glacially-induced faulting and seismic shaking in eastern canada. *Quaternary Science Reviews*, *228*, 106070.

Brooks, G. R. & Perret, D. (2023). A long-term context for the 1663 charlevoix ce earthquake interpreted from the postglacial landslide record in the gouffre valley, quebec, canada. *Quaternary Science Reviews*, *309*, 108096.

Brooks, G. R. & Pugin, A. J.-M. (2020). Assessment of a seismo-neotectonic origin for the New Liskeard–Thornloe scarp, Timiskaming graben, northeastern Ontario. *Canadian Journal of Earth Sciences*, *57* (2), 267–274.

Brouard, E., Roy, M., Dubé-Loubert, H., Lamarche, O., & Hébert, S. (2020). Carte des dépôts de surface de la province de Québec : rapport sur les méthodes et les données. Tech. Rep. MB 2020-10, Ministère de l'Énergie et des Ressources Naturelles. Scale = 1:2,500,000.

Brown, D., Ryan, P. D., Zagorevski, A., & van Staal, C. (2011). The record of ordovician arc–arc and arc–continent collisions in the canadian appalachians during the closure of iapetus. *Arc-continent collision*, 341–371.

Bucknam, R. & Anderson, R. (1979). Estimation of fault-scarp ages from a scarp-height–slope-angle relationship. *Geology*, *7* (1), 11–14.

Bungum, H. & Eldholm, O. (2022). The conundrums of the postglacial tectonic response of the fennoscandian and canadian shields. *Earth-Science Reviews*, 104146.

Calais, E., Camelbeeck, T., Stein, S., Liu, M., & Craig, T. (2016). A new paradigm for large earthquakes in stable continental plate interiors. *Geophysical Research Letters*, *43* (20), 10–621.

Canada, N. R. (2023). National risk profile a national emergency preparedness and awareness tool. Tech. rep., Government of Canada.

Candela, T., Rosset, P., & Chouinard, L. (2021). A quantitative approach to assess seismic vulnerability of touristic accommodations: Case study in Montreal, Canada. *GeoHazards*, *2* (2), 137–152.

Chien, J. & Liu, Y. (2023). Application of a novel workflow to enhance seismicity catalog and compute earthquake source parameters in the western québec seismic zone. In *American Geophysical Union Fall Meeting; presentation S21E-0339, San Francisco, USA*. URL https://agu.confex.com/agu/fm23/meetingapp.cgi/Paper/1387806.

Clark, C. D., Knight, J. K., & Gray, J. T. (2000). Geomorphological reconstruction of the labrador sector of the laurentide ice sheet. *Quaternary Science Reviews*, *19* (13), 1343–1366.

Clark, P. U., Shakun, J. D., Baker, P. A., Bartlein, P. J., Brewer, S., Brook, E., Carlson, A. E., Cheng, H., Kaufman, D. S., Liu, Z., *et al.* (2012). Global climate evolution during the last deglaciation. *Proceedings of the National Academy of Sciences*, *109* (19), E1134–E1142.

Collettini, C., Chiaraluce, L., Pucci, S., Barchi, M. R., & Cocco, M. (2005). Looking at fault reactivation matching structural geology and seismological data. *Journal of Structural Geology*, *27* (5), 937–942.

Comeau, F.-A., Raymond, J., Malo, M., Dezayes, C., & Carreau, M. (2017). Geothermal potential of northern québec: a regional assessment. *Geothermal Resources Council Transactions*, *41*, 1076–1094.

Convertito, V., Emolo, A., & Zollo, A. (2006). Seismic-hazard assessment for a characteristic earthquake scenario: An integrated probabilistic–deterministic method. *Bulletin of the Seismological Society of America*, *96* (2), 377–391.

Craig, T., Calais, E., Fleitout, L., Bollinger, L., & Scotti, O. (2016). Evidence for the release of long-term tectonic strain stored in continental interiors through intraplate earthquakes. *Geophysical Research Letters*, *43* (13), 6826–6836.

Cramer, C. H. (2001). The New Madrid seismic zone: capturing variability in seismic hazard analyses. *Seismological Research Letters*, *72* (6), 664–672.

Cronin, T. M., Manley, P. L., Brachfeld, S., Manley, T., Willard, D., Guilbault, J.-P., Rayburn, J. A., Thunell, R., & Berke, M. (2008). Impacts of post-glacial lake drainage events and revised chronology of the champlain sea episode 13–9 ka. *Palaeogeography, Palaeoclimatology, Palaeoecology*, *262* (1-2), 46–60.

Dawers, N. H. & Anders, M. H. (1995). Displacement-length scaling and fault linkage. *Journal of Structural Geology*, *17* (5), 607–614.

de l'Énergie et des Ressources naturelles, M. (2021). Géobase du réseau hydrographique du québec (grhq) - service wms. Tech. rep., Données Québec. https://www.donneesquebec.ca/recherche/dataset/grhq/resource/f933b563-52a0-4c21-af08-f22687f566bf.

des Ressources naturelles et des forêts, M. (2024). DonnÉes vectorielles et services web - sigÉom téléchargement par thème. Tech. rep., Gouvernement du Québec. https://sigeom.mines.gouv.qc.ca/signet/classes/I1102_indexAccueil?l=f#.

Doig, R. (1990). 2300 yr history of seismicity from silting events, in Lake Tadoussac, Charlevoix, Quebec. *Geology*, *18* (9), 820–823.

Doig, R. (1998). 3000-year paleoseismological record from the region of the 1988 saguenay, quebec, earthquake. *Bulletin of the Seismological Society of America*, *88* (5), 1198–1203.

Doughty, M., Eyles, N., & Daurio, L. (2010). Earthquake-triggered slumps (1935 timiskaming m6. 2) in lake kipawa, western quebec seismic zone, canada. *Sedimentary Geology*, *228* (3-4), 113–118.

Doughty, M., Eyles, N., Eyles, C., Wallace, K., & Boyce, J. (2014). Lake sediments as natural seismographs: Earthquake-related deformations (seismites) in central Canadian lakes. *Sedimentary Geology*, *313* , 45–67.

Dyke, A., Andrews, J., Clark, P., England, J., Miller, G., Shaw, J., & Veillette, J. (2002). The laurentide and innuitian ice sheets during the last glacial maximum. *Quaternary Science Reviews*, *21* (1-3), 9–31.

Dyke, A., Vincent, J., Andrews, J., Dredge, L., & Cowan, W. (1989). The Laurentide Ice Sheet and an introduction to the Quaternary geology of the Canadian Shield. In R. J. Fulton (Ed.), *Quaternary Geology of Canada and Greenland*, Geological Survey of Canada, vol. 1. 178–189.

Dyke, A. S. (2004). An outline of north american deglaciation with emphasis on central and northern canada. *Developments in quaternary sciences*, *2* , 373–424.

Earthquakes Canada (2020). 2020 National Building Code of Canada seismic hazard maps. Tech. Rep. Article 1.1.3.1 of Division B, Government of Canada. Retrieved October 2023 from https://earthquakescanada.nrcan.gc.ca/hazard-alea/zoning-zonage/NBCC2020maps-en.php.

Ebel, J. E. (2011). A new analysis of the magnitude of the february 1663 earthquake at charlevoix, quebec. *Bulletin of the Seismological Society of America*, *101* (3), 1024–1038.

Esri, Maxar, Geographics, E., FSA, U., USGS, Aerogrid, IGN, IGP, & the GIS User Community (2021). World imagery. Tech. rep., Esri. Https://www.arcgis.com/home/item.html?id=10df2279f9684e4a9f6a7f08febac2a9 (accessed December 2021).

Estay, N. P., Yáñez, G., Carretier, S., Lira, E., & Maringue, J. (2016). Seismic hazard in low slip rate crustal faults, estimating the characteristic event and the most hazardous zone: study case san ramón fault, in southern andes. *Natural Hazards and Earth System Sciences*, *16* (12), 2511–2528.

Fenton, C. (1994). Postglacial faulting in eastern canada: an annotated bibliography. Tech. rep., Geological Survey of Canada, Open File 2774.

Fenton, C. (1999). Glacio-isostatic (postglacial) faulting: Criteria for recognition. *Identifying Faults and Determining Their Origins, US Nuclear Regulatory Commission, NUREG/CR-5503, Appendix A, pp. A-51–A-99*.

Fenton, C. H., Adams, J., & Halchuk, S. (2006). Seismic hazards assessment for radioactive waste disposal sites in regions of low seismic activity. *Geotechnical & Geological Engineering*, *24*, 579–592.

Figueiredo, P., Hill, J., Merschat, A., Scheip, C., Stewart, K., Owen, L., Wooten, R., Carter, M., Szymanski, E., Horton, S., *et al.* (2022). The mw 5.1, 9 august 2020, sparta earthquake, north carolina: The first documented seismic surface rupture in the eastern united states. *GSA Today*, *32* (3-4).

Filion, L. (1987). Holocene development of parabolic dunes in the central St. Lawrence Lowland, Québec. *Quaternary Research*, *28* (2), 196–209.

Filion, L., Quinty, F., & Bégin, C. (1991). A chronology of landslide activity in the valley of rivière du gouffre, charlevoix, quebec. *Canadian Journal of Earth Sciences*, *28* (2), 250–256.

Firth, C. R. & Stewart, I. S. (2000). Postglacial tectonics of the scottish glacio-isostatic uplift centre. *Quaternary Science Reviews*, *19* (14-15), 1469–1493.

Fulton, R. J. & Prest, V. K. (1987). Introduction: The laurentide ice sheet and its significance. *Géographie physique et Quaternaire*, *41* (2), 181–186.

Ghofrani, H., Atkinson, G. M., Chouinard, L., Rosset, P., & Tiampo, K. F. (2015). Scenario shakemaps for Montreal. *Canadian Journal of Civil Engineering*, *42* (7), 463–476.

Giona Bucci, M. & Schoenbohm, L. M. (2022). Tectono-geomorphic analysis in low relief, low tectonic activity areas: case study of the temiskaming region in the western quebec seismic zone (wqsz), eastern canada. *Remote Sensing*, *14* (15), 3587.

Globensky, Y. (1987). Géologie des basses-terres du Saint-Laurent. Tech. Rep. MM 85-02, Les publications du Ministère de l'Énergie et des Ressources Naturelles Québec.

Godbout, P.-M., Brouard, E., & Roy, M. (2023). 1-km resolution rebound surfaces and paleotopography of glaciated North America since the Last Glacial Maximum. *Scientific Data*, *10* (1), 735.

Goudarzi, M. A. (2016). *GPS inferred velocity and strain rate fields in eastern Canada*. Ph.D. thesis, Université Laval.

Gourdeau, A. (2021). *Where is the fault that caused the 1732 Montréal earthquake?*. Bs thesis, unpublished, McGill University.

Gourdeau, A., Prush, V., Rowe, C., Nackers, C., Mark, H., Morris, I., Rosset, P., Lamothe, M., Chouinard, L., & Tarling, M. (submitted). Investigation of suspected Holocene fault scarp near Montréal, Québec: The first paleoseismic trench in eastern Canada. *Seismica*.

Gourdeau, A., Prush, V., Rowe, C. D., Wang, K., Laly, M., Rosset, P., Chouinard, L., Lamothe, M., Nackers, I. M. C., & Mark, H. (2023). An Ongoing Search for Active Faults in the Western Quebec Seismic Zone, Eastern Canada. In *American Geophysical Union Fall Meeting; presentation T11D-0188, San Francisco, USA*. URL https://agu.confex.com/agu/fm23/meetingapp.cgi/Paper/1365245.

Gouvernement du Québec (1979). Code de sécurité pour les travaux de construction en date du 1er juillet 2023, loi sur la santé et la sécurité du travail, chapitre s-2.1, a. 223, section iii : Chantiers de construction (3.15.3.). URL https://www.legisquebec.gouv.qc.ca/fr/document/lc/S-2.1?langCont=en#se:223. Accessed 2023-07-01 from https://www.legisquebec.gouv.qc.ca/fr/document/lc/S-2.1?langCont=en#se:223.

Graham, J. (2005). *Naming the Laurentians: A History of Place Names 'up North'*. Les Editions Main Street Inc.

Grasemann, B., Martel, S., & Passchier, C. (2005). Reverse and normal drag along a fault. *Journal of Structural Geology*, *27* (6), 999–1010.

Guedes, V. J. C. B., Maciel, S. T. R., & Rocha, M. P. (2022). Refrapy: A python program for seismic refraction data analysis. *Computers & Geosciences*, *159*, 105020.

Halchuk, S., Allen, T., Adams, J., & Onur, T. (2019). Contribution of the Leech River Valley-Devil's Mountain Fault System to Seismic Hazard in Victoria, BC. In *Proceedings of the 12th Canadian Conference on Earthquake Engineering, Quebec City, QC, Canada*. 17–20.

Halchuk, S. C., Allen, T. I., Adams, J., & Rogers, G. C. (2014). Fifth generation seismic hazard model input files as proposed to produce values for the 2015 national building code of Canada, Open File Report 7576. Tech. rep., Geological Survey of Canada.

Hampel, A., Hetzel, R., Maniatis, G., & Karow, T. (2009). Three-dimensional numerical modeling of slip rate variations on normal and thrust fault arrays during ice cap growth and melting. *Journal of Geophysical Research: Solid Earth*, *114* (B8).

Hanson, K., Kelson, K., Angell, M., & Lettis, W. (1999). Identifying faults and determining their origins. *United States Nuclear Regulatory Commission (NRC), NUREG/CR-5503, variously paginated*.

Harrichhausen, N., Morell, K. D., Regalla, C., Bennett, S. E., Leonard, L. J., Lynch, E. M., & Nissen, E. (2021). Paleoseismic trenching reveals Late Quaternary kinematics of the Leech River fault: Implications for forearc strain accumulation in northern Cascadia. *Bulletin of the Seismological Society of America*, *111* (2), 1110–1138.

Heidbach, O., Rajabi, M., Cui, X., Fuchs, K., Müller, B., Reinecker, J., Reiter, K., Tingay, M., Wenzel, F., Xie, F., *et al.* (2018). The world stress map database release 2016: Crustal stress pattern across scales. *Tectonophysics*, *744*, 484–498.

Henton, J. A., Craymer, M. R., Ferland, R., Dragert, H., Mazzotti, S., & Forbes, D. L. (2006). Crustal motion and deformation monitoring of the Canadian landmass. *Geomatica*, *60* (2), 173–191.

Hersi, O. S., Lavoie, D., & Nowlan, G. (2003). Reappraisal of the Beekmantown Group sedimentology and stratigraphy, Montréal area, southwestern Quebec: implications for understanding the depositional evolution of the Lower–Middle Ordovician Laurentian passive margin of eastern Canada. *Canadian Journal of Earth Sciences*, *40* (2), 149–176.

Hobbs, T. E., Journeay, J. M., Rao, A. S., Kolaj, M., Martins, L., LeSueur, P., Simionato, M., Silva, V., Pagani, M., Johnson, K., Rotheram, D., & Chow, W. (2023). A national risk model for Canada: methodology and scientific basis. *Earthquake Spectra*, *39* (3), 1410–1434.

Hocq, M. (2014). Géologie du Québec: Introduction. Tech. Rep. MM 94-01, Les publications du Ministère de l'Énergie et des Ressources Naturelles Québec.

Hocq, M., Caty, J.-L., Charbonnneau, J.-M., & Simard, A. (1994). *Géologie générale*. Les publications du Québec. URL https://gq.mines.gouv.qc.ca/documents/EXAMINE/MM9401/MM9401.pdf.

Johnson, M. D., Fredin, O., Ojala, A. E., & Peterson, G. (2015). Unraveling scandinavian geomorphology: the lidar revolution.

Jones, R., Whitehouse, P., Bentley, M., Small, D., & Dalton, A. (2019). Impact of glacial isostatic adjustment on cosmogenic surface-exposure dating. *Quaternary Science Reviews*, *212* , 206–212.

Kanamori, H. (2003). Earthquake prediction: An overview. *International Geophysics*, *81* , 1205–1216.

Kim, Y.-S. & Sanderson, D. J. (2005). The relationship between displacement and length of faults: a review. *Earth-Science Reviews*, *68* (3-4), 317–334.

Kolaj, M., Adams, J., & Halchuk, S. (2020a). Seismic hazard in southeastern canada: uncertainty and controls on seismic hazard in a region of low-to-moderate seismicity. In *17th World Conference on Earthquake Engineering*.

Kolaj, M., Adams, J., & Halchuk, S. (2020b). The 6th generation seismic hazard model of Canada. In *17th World Conference on Earthquake Engineering*. 1–12.

Kolaj, M., Halchuk, S. C., & Adams, J. (2023). Sixth Generation seismic hazard model of Canada: final input files used to generate the 2020 National Building Code of Canada seismic hazard values. Version 1.0. Open file report no. 8924, Geological Survey of Canada. URL https://doi.org/10.4095/331387.

Kozacı, Ö., Madugo, C. M., Bachhuber, J. L., Hitchcock, C. S., Kottke, A. R., Higgins, K., Wade, A., & Rittenour, T. (2021). Rapid postearthquake field reconnaissance, paleoseismic trenching, and gis-based fault slip variability measurements along the mw 6.4 and mw 7.1 ridgecrest earthquake sequence, southern california. *Bulletin of the Seismological Society of America*, *111* (5), 2334–2357.

Kumarapeli, P. & Saull, V. A. (1966). The st. lawrence valley system: a north american equivalent of the east african rift valley system. *Canadian Journal of Earth Sciences*, *3* (5), 639–658.

Lajeunesse, P., Sinkunas, B., Morissette, A., Normandeau, A., Joyal, G., St-Onge, G., & Locat, J. (2017). Large-scale seismically-induced mass-movements in a former glacial lake basin: Lake témiscouata, northeastern appalachians (eastern canada). *Marine Geology*, *384* , 120–130.

Laly, M. J. L. (2021). *Finding Postglacial Faults in the Charlevoix Seismic Zone Using Lidar-Derived Bare-Earth Imagery*. Bs thesis, unpublished, McGill University.

Lamarche, L., Bondue, V., Lemelin, M.-J., Lamothe, M., & Roy, A. (2007). Deciphering the Holocene evolution of the St. Lawrence River drainage system using luminescence and radiocarbon dating. *Quaternary Geochronology*, *2* (1-4), 155–161.

Lambeck, K., Purcell, A., & Zhao, S. (2017). The north american late wisconsin ice sheet and mantle viscosity from glacial rebound analyses. *Quaternary Science Reviews*, *158* , 172–210.

Lambert, C., Gervais, F., & Moukhsil, A. (2018). Reconstruire l'architecture de l'ouest de la Province de Grenville, Québec: Résultats préliminaires de la cartographie géologique le long de la route 117. Tech. Rep. MB 2019-05, Ministère de l'Énergie et des Ressources Naturelles.

Lamontagne, M. (2002). An overview of some significant eastern canadian earthquakes and their impacts on the geological environment, buildings and the public. *Natural hazards*, *26* , 55–68.

Lamontagne, M. & Bent, A. L. (2021). Earthquakes in the eastern Canadian Arctic: past occurrences, present hazard, and future risk. *Seismological Society of America*, *92* (5), 2824–2837.

Lamontagne, M. & Flynn, B. (2016). Perception of earthquake hazard and risk in the province of Quebec and the need to raise earthquake awareness in this intraplate region. *Seismological Research Letters*, *87* (6), 1426–1432.

Lamontagne, M., Halchuk, S., Cassidy, J., & Rogers, G. (2008). Significant Canadian earthquakes of the period 1600–2006. *Seismological Research Letters*, *79* (2), 211–223.

Lamontagne, M., Halchuk, S., Cassidy, J. F., & Rogers, G. C. (2018). Significant Canadian Earthquakes 1600-2017. Open file report 8285, Geological Survey of Canada. URL publications.gc.ca/pub?id=9.880099&sl=0.

Lamontagne, M., Keating, P., & Toutin, T. (2000). Complex faulting confounds earthquake research in the charlevoix seismic zone, québec. *Eos, Transactions American Geophysical Union*, *81* (26), 289–293.

Lamothe, M. (1993). Géologie des formations quaternaires de la région du lac saint-pierre. Tech. rep., Rapport Statutaire Intragaz, Min Ress Nat Québec.

Lang, G. & ten Brink, U. S. (2022). Quantifying permanent uplift due to lithosphere-hotspot interaction. *Tectonics*, *41* (12), e2022TC007448.

Lebedev, S., Grannell, J., Arroucau, P., Bonadio, R., Agostinetti, N. P., & Bean, C. J. (2023). Seismicity of ireland, and why it is so low: How the thickness of the lithosphere controls intraplate seismicity. *Geophysical Journal International*, *235* (1), 431–447.

Leblanc, G. (1981). A closer look at the september 16, 1732, montreal earthquake. *Canadian Journal of Earth Sciences*, *18* (3), 539–550.

Leboeuf, A., Fradette, M.-S., & Pomerleau, I. (2021). *User's Guide: Products Derived from LiDAR Data - 2nd edition*. Ministère de l'Énergie et des Ressources naturelles.

Lemieux, Y., Tremblay, A., & Lavoie, D. (2003). Structural analysis of supracrustal faults in the Charlevoix area, Quebec: relation to impact cratering and the St-Laurent fault system. *Canadian Journal of Earth Sciences*, *40* (2), 221–235.

Leonard, M. (2014). Self-consistent earthquake fault-scaling relations: Update and extension to stable continental strike-slip faults. *Bulletin of the Seismological Society of America*, *104* (6), 2953–2965.

Li, Q., Liu, M., & Stein, S. (2009). Spatiotemporal complexity of continental intraplate seismicity: Insights from geodynamic modeling and implications for seismic hazard estimation. *Bulletin of the Seismological Society of America*, *99* (1), 52–60.

Lindblom, E., Lund, B., Tryggvason, A., Uski, M., Bödvarsson, R., Juhlin, C., & Roberts, R. (2015). Microearthquakes illuminate the deep structure of the endglacial pärvie fault, northern sweden. *Geophysical Journal International*, *201* (3), 1704–1716.

Lowe, D. (2024). Aulacogens of the neoproterozoic to ordovician laurentian iapetan margin. *Earth-Science Reviews*, 104829.

Lukk, A. & Sidorin, A. Y. (2019). On the problem of accounting for paleoearthquakes when evaluating the seismic hazard of fennoscandia. *Izvestiya, Atmospheric and Oceanic Physics*, *55*, 1699–1714.

Lund Snee, J. & Zoback, M. (2020). State of stress in areas of induced seismicity across north america. In *AGU Fall Meeting Abstracts*. vol. 2020, MR019–0001.

Ma, S. & Eaton, D. W. (2007). Western quebec seismic zone (canada): Clustered, midcrustal seismicity along a mesozoic hot spot track. *Journal of Geophysical Research: Solid Earth*, *112* (B6).

Markovaara-Koivisto, M., Ojala, A. E., Mattila, J., Kukkonen, I., Aro, I., Pullinen, A., Hänninen, P., Middleton, M., Sutinen, A., Majaniemi, J., *et al.* (2020). Geomorphological evidence of paleoseismicity: surficial and underground structures of pasmajärvi postglacial fault. *Earth Surface Processes and Landforms*, *45* (12), 3011–3024.

Mattila, J., Ojala, A., Ruskeeniemi, T., Palmu, J.-P., Aaltonen, I., Käpyaho, A., Lindberg, A., & Sutinen, R. (2019). Evidence of multiple slip events on postglacial faults in northern fennoscandia. *Quaternary Science Reviews*, *215*, 242–252.

Mazzotti, S. (2007). Geodynamic models for earthquake studies in intraplate North America. In S. Stein & S. Mazzotti (Eds.), *Continental Intraplate Earthquakes: Science, Hazard, and Policy Issues*, The Geological Society of America, vol. 425 of *Geological Society of America Special Papers*. 17–33.

Mazzotti, S. & Gueydan, F. (2018). Control of tectonic inheritance on continental intraplate strain rate and seismicity. *Tectonophysics*, *746*, 602–610.

Mazzotti, S. & Townend, J. (2010). State of stress in central and eastern north american seismic zones. *Lithosphere*, *2* (2), 76–83.

McCalpin, J. (Ed.) (2009). *Paleoseismology, 2nd Edition*. San Diego Academic Press, Elsevier Inc.

Mérindol, M., St-Onge, G., Sultan, N., Lajeunesse, P., & Garziglia, S. (2022). Earthquake-triggered submarine landslides in the st. lawrence estuary (québec, canada) during the last two millennia and the record of the major 1663 ce m$\geq$7 event. *Quaternary Science Reviews*, *291*, 107640.

Mikko, H., Smith, C. A., Lund, B., Ask, M. V., & Munier, R. (2015). LiDAR-derived inventory of post-glacial fault scarps in Sweden. *GFF*, *137* (4), 334–338.

Ministère de l'Économie, de l'Innovation et de l'Énergie (2022). Démographie, population. Https://www.economie.gouv.qc.ca/pages-regionales/montreal/portrait-regional/demographie, retrieved 17 July 2023.

Ministère de l'Environnement, F. e. P., Lutte contre les changements climatiques (2024). Système d'information hydrogéologique (sih). Tech. rep., Données Québec. URL https://www.donneesquebec.ca/recherche/dataset/eau-souterraines-sih-index.

Ministère des Forêts, Q. P. D. Q., Faune et Parcs (2016). LiDAR - Modèles Numériques (terrain, canopée, pente). https://www.donneesquebec.ca/recherche/fr/dataset/produits-derives-de-base-du-lidar.

Ministère des Ressources naturelles et des Forêts (2021). système d'information géominière, Carte interactive. Tech. rep., Gouvernement du Québec. Quebec Geomining Information System retrieved on January 22 2024 from https://sigeom.mines.gouv.qc.ca/signet/classes/I1108_afchCarteIntr.

Molnar, S., Cassidy, J., Castellaro, S., Cornou, C., Crow, H., Hunter, J., Matsushima, S., Sánchez-Sesma, F., & Yong, A. (2018). Application of microtremor horizontal-to-vertical spectral ratio (MHVSR) analysis for site characterization: State of the art. *Surveys in Geophysics*, *39*, 613–631.

Morell, K., Regalla, C., Amos, C., Bennett, S., Leonard, L., Graham, A., Reedy, T., Levson, V., & Telka, A. (2018). Holocene surface rupture history of an active forearc fault redefines seismic hazard in southwestern british columbia, canada. *Geophysical Research Letters*, *45* (21), 11–605.

Morell, K. D., Styron, R., Stirling, M., Griffin, J., Archuleta, R., & Onur, T. (2020). Seismic hazard analyses from geologic and geomorphic data: Current and future challenges. *Tectonics*, *39* (10), e2018TC005365.

Mörner, N.-A. (2004). Active faults and paleoseismicity in fennoscandia, especially sweden. primary structures and secondary effects. *Tectonophysics*, *380* (3-4), 139–157.

Mörner, N.-A., Tröften, P. E., Sjöberg, R., Grant, D., Dawson, S., Bronge, C., Kvamsdal, O., & Sidén, A. (2000). Deglacial paleoseismicity in sweden: the 9663 bp iggesund event. *Quaternary Science Reviews*, *19* (14-15), 1461–1468.

Muir Wood, R. (1993). A review of the seismotectonics of Sweden. Report conducted for swedish nuclear fuel and waste management co. skb-tr–93-13, EQE International Ltd.

Muir-Wood, R. (2000). Deglaciation seismotectonics: a principal influence on intraplate seismogenesis at high latitudes. *Quaternary Science Reviews*, *19* (14-15), 1399–1411.

Munier, R., Adams, J., Brandes, C., Brooks, G., Dehls, J., Einarsson, P., Gibbons, S. J., Ásta Rut Hjartardóttir, Hogaas, F., Johansen, T. A., Kvaerna, T., Mattila, J., Mikko, H., Müller, K., Nikolaeva, S. B., Ojala, A., Olesen, O., Olsen, L., Palmu, J.-P., Ruskeeniemi, T., Ruud, B. O., Sandersen, P. B. E., Shvarev, S. V., Smith, C. A., Steffen, H., Steffen, R., Sutinen, R., & Tassis, G. (2020). International database of Glacially Induced Faults. URL https://doi.org/10.1594/PANGAEA.922705.

Nollet, M.-J., Chaallal, O., & Lefebvre, K. (2005). Seismic vulnerability study of historical buildings in Old Montreal: Overview and perspectives. *WIT Transactions on The Built Environment*, *83* .

Novoa, N. (2013). Evaluation of potential post-glacial faults using bare-earth lidar topographic data near ridley island, british columbia. Tech. rep., University of Washington. Capstone reports of the Masters in Earth & Space Sciences - Applied Geosciences.

Occhietti, S., ChartierH, M., Hillaire-Marcel, C., Cournoyer, M., Cumbaa, S. L., & Harington, R. (2001). Paléoenvironnements de la mer de champlain dans la région de québec, entre 11 300 et 9750 bp: le site de saint-nicolas. *Géographie physique et Quaternaire*, *55* (1), 23–46.

Occhietti, S., Parent, M., Lajeunesse, P., Robert, F., & Govare, É. (2011). Late Pleistocene–early Holocene decay of the Laurentide ice sheet in Québec–Labrador. In *Developments in quaternary sciences*, Elsevier, vol. 15. 601–630.

Oettle, N. K. & Bray, J. D. (2013). Fault rupture propagation through previously ruptured soil. *Journal of Geotechnical and Geoenvironmental Engineering*, *139* (10), 1637–1647.

Öhrling, C., Peterson, G., & Mikko, H. (2018). Detailed geomorphological analysis of lidar derived elevation data, forsmark. Tech. rep., SKB R-18-10. Svensk Kärnbränslehantering AB.

Ojala, A. E., Mattila, J., Markovaara-Koivisto, M., Ruskeeniemi, T., Palmu, J.-P., & Sutinen, R. (2019). Distribution and morphology of landslides in northern finland: An analysis of postglacial seismic activity. *Geomorphology*, *326* , 190–201.

Olesen, O., Blikra, L. H., Braathen, A., Dehls, J. F., Olsen, L., Rise, L., Roberts, D., Riis, F., Faleide, J. I., & Anda, E. (2004). Neotectonic deformation in norway and its implications: a review. *Norwegian Journal of Geology/Norsk Geologisk Forening*, *84* (1).

Oliver, J., Johnson, T., & Dorman, J. (1970). Postglacial faulting and seismicity in new york and quebec. *Canadian Journal of Earth Sciences*, *7* (2), 579–590.

Osinski, G. R., Grieve, R. A., Ferriere, L., Losiak, A., Pickersgill, A. E., Cavosie, A. J., Hibbard, S. M., Hill, P. J., Bermudez, J. J., Marion, C. L., *et al.* (2022). Impact earth: A review of the terrestrial impact record. *Earth-Science Reviews*, *232* , 104112.

Ouellet, M. (1997). Lake sediments and holocene seismic hazard assessment within the st. lawrence valley, québec. *Geological Society of America Bulletin*, *109* (6), 631–642.

Pagani, M., Monelli, D., Weatherill, G., Danciu, L., Crowley, H., Silva, V., Henshaw, P., Butler, L., Nastasi, M., Panzeri, L., *et al.* (2014). OpenQuake engine: An open hazard (and risk) software for the global earthquake model. *Seismological Research Letters*, *85* (3), 692–702.

Palmu, J.-P., Ojala, A. E., Ruskeeniemi, T., Sutinen, R., & Mattila, J. (2015). LiDAR DEM detection and classification of postglacial faults and seismically-induced landforms in Finland: a paleoseismic database. *Gff* , *137* (4), 344–352.

Pavlides, S. & Caputo, R. (2004). Magnitude versus faults' surface parameters: quantitative relationships from the aegean region. *Tectonophysics*, *380* (3-4), 159–188.

Peltier, W. R. (2004). Global glacial isostasy and the surface of the ice-age earth: the ice-5g (vm2) model and grace. *Annu. Rev. Earth Planet. Sci.*, *32* , 111–149.

Persaud, M. & Pfiffner, O.-A. (2004). Active deformation in the eastern swiss alps: post-glacial faults, seismicity and surface uplift. *Tectonophysics*, *385* (1-4), 59–84.

Pinet, N., Lamontagne, M., Duchesne, M. J., & Brake, V. I. (2020). Hunting for Quaternary faults in eastern Canada: A critical appraisal of two potential candidates. *Seismological Research Letters*, *92* (2A), 1102–1111. URL https://doi.org/10.1785/0220200322.

Pisarska-Jamroży, M., Belzyt, S., Bitinas, A., Jusienė, A., & Woronko, B. (2019). Seismic shocks, periglacial conditions and glaciotectonics as causes of the deformation of a Pleistocene meandering river succession in central Lithuania. *Baltica*, *32* (1), 63–77.

Poncet, R., Campbell, C., Dias, F., Locat, J., & Mosher, D. (2010). A study of the tsunami effects of two landslides in the St. Lawrence estuary. In *Submarine Mass Movements and Their Consequences*, Springer, vol. 28 of *Advances in Natural and Technological Hazards Research*. 755–764.

Quinn, P. E. (2009). *Large landslides in sensitive clay in eastern Canada and the associated hazard and risk to linear infrastructure*. Ph.d thesis, Queen's University.

Randour, I., Daigneault, R.-A., Lamothe, M., Roy, M., & Robitaille, A. (2020a). Cartographie des formations superficielles de la région des Laurentides-Lanaudière, phase 2. *Gouvernement du Québec, Canada*.

Randour, I., Daigneault, R.-A., Lamothe, M., Roy, M., & Robitaille, A. (2020b). Région des Laurentides. Tech. Rep. MB202008PLAN006, Ministère des Ressources naturelles et des Forêts. URL https://gq.mines.gouv.qc.ca/documents/EXAMINE/MB202008/MB202008PLAN001.pdf.

Rimando, J. M. & Peace, A. L. (2021). Reactivation potential of intraplate faults in the western quebec seismic zone, eastern canada. *Earth and Space Science*, *8* (8), e2021EA001825.

Rimando, J. M., Peace, A. L., Goda, K., Sirous, N., Rosset, P., & Chouinard, L. (2023). Coseismic Coulomb stress changes on intraplate faults in the western Quebec seismic zone following three major earthquakes in the past century. *Canadian Journal of Earth Sciences*, *60* (12), 1674–1687.

Rimando, R. E. (1994). *Tectonic framework and relative ages of structures within the Ottawa-Bonnechere graben.*. University of Ottawa (Canada).

Robert, B., Domeier, M., & Jakob, J. (2021). On the origins of the iapetus ocean. *Earth-Science Reviews*, *221* , 103791.

Robin, C., Craymer, M., Ferland, R., James, T., Lapelle, E., Piraszewski, M., & Zhao, Y. (2020). *NAD83v70VG: a new national crustal velocity model for Canada*. Natural Resources Canada= Ressources naturelles Canada.

Rocher, M., Tremblay, A., Lavoie, D., & Campeau, A. (2003). Brittle fault evolution of the Montreal area (St Lawrence Lowlands, Canada): rift-related structural inheritance and tectonism approached by palaeostress analysis. *Geological Magazine*, *140* (2), 157–172.

Roesset, J. (1970). Fundamentals of soil amplification. In R. Hansen (Ed.), *Seismic Design for Nuclear Power Plants*, M.I.T. Press. 183–244.

Rondenay, S., Bostock, M. G., Hearn, T. M., White, D. J., & Ellis, R. M. (2000). Lithospheric assembly and modification of the SE Canadian Shield: Abitibi-Grenville teleseismic experiment. *Journal of Geophysical Research: Solid Earth*, *105* (B6), 13735–13754.

Rosset, P., Bour-Belvaux, M., , & Chouinard, L. (2015). Estimation and comparison of Vs30; microzonation maps for montreal using multiple sources of information. *Bulletin of Earthquake Engineering*, *13* (8), 2225–2239.

Rosset, P. & Chouinard, L. (2009). Characterization of site effects in Montreal, Canada. *Natural hazards*, *48* , 295–308.

Rosset, P., Chouinard, L., & Nollet, M.-J. (2021). Consequences on residential buildings in greater Montreal for a repeat of the 1732 M5.8 Montreal earthquake. In *Canadian Society of Civil Engineering Annual Conference*. Springer, 667–679.

Rosset, P., Long, X., & Chouinard, L. (2023). Influence of the 2020 Seismic Hazard Update on Residential Losses in Greater Montreal, Canada. *GeoHazards*, *4* (4), 406–420.

Rücker, C., Günther, T., & Wagner, F. M. (2017). pygimli: An open-source library for modelling and inversion in geophysics. *Computers & Geosciences*, *109* , 106–123.

Sare, R., Hilley, G. E., & DeLong, S. B. (2019). Regional-scale detection of fault scarps and other tectonic landforms: Examples from northern california. *Journal of Geophysical Research: Solid Earth*, *124* (1), 1016–1035.

Sasseville, C., Clauer, N., & Tremblay, A. (2012). Timing of fault reactivation in the upper crust of the St. Lawrence rift system, Canada, by K–Ar dating of illite-rich fault rocks. *Canadian Journal of Earth Sciences*, *49* (5), 637–652.

Schwartz, D. P. & Coppersmith, J. (1984). Fault behavior and characteristic earthquakes: examples from Wasatch and San Andreas faults. *Journal of Geophysical Research*, *89* , 5681–5698.

Scott, C., Adam, R., Arrowsmith, R., Madugo, C., Powell, J., Ford, J., Gray, B., Koehler, R., Thompson, S., Sarmiento, A., *et al.* (2023). Evaluating how well active fault mapping predicts earthquake surface-rupture locations. *Geosphere*, *19* (4), 1128–1156.

Sella, G. F., Stein, S., Dixon, T. H., Craymer, M., James, T. S., Mazzotti, S., & Dokka, R. K. (2007). Observation of glacial isostatic adjustment in "stable" north america with gps. *Geophysical Research Letters*, *34* (2).

Shilts, W. & Clague, J. J. (1992). Documentation of earthquake-induced disturbance of lake sediments using subbottom acoustic profiling. *Canadian Journal of Earth Sciences*, *29* (5), 1018–1042.

Shilts, W. W. (1992). Sangamonian and early Wisconsinan events in the St. Lawrence Lowland and Appalachians of southern Quebec, Canada. *The last interglacial-glacial transition in North America*, *270*, 171.

Shilts, W. W., Aylsworth, J. M., Kaszycki, C. A., & Klassen, R. A. (1987). Canadian shield. In *Geomorphic Systems of North America*, Geological Society of America Boulder, Colorado, vol. 2. 119–161.

Simon, K., James, T., Henton, J., & Dyke, A. (2016). A glacial isostatic adjustment model for the central and northern laurentide ice sheet based on relative sea level and gps measurements. *Geophysical Journal International*, *205* (3), 1618–1636.

Smith, C. A., Sundh, M., & Mikko, H. (2014). Surficial geology indicates early Holocene faulting and seismicity, central Sweden. *International Journal of Earth Sciences*, *103*, 1711–1724.

Soto-Cordero, L., Meltzer, A., & Stachnik, J. (2018). Crustal structure, intraplate seismicity, and seismic hazard in the mid-Atlantic United States. *Seismological Research Letters*, *89* (1), 241–252.

St-Onge, G., Mulder, T., Piper, D. J., Hillaire-Marcel, C., & Stoner, J. S. (2004). Earthquake and flood-induced turbidites in the Saguenay Fjord (Québec): a Holocene paleoseismicity record. *Quaternary Science Reviews*, *23* (3-4), 283–294.

Steffen, H., Olesen, O., & Sutinen, R. (2021). *Glacially-triggered faulting*. Cambridge University Press.

Steffen, R., Steffen, H., Wu, P., & Eaton, D. W. (2014a). Stress and fault parameters affecting fault slip magnitude and activation time during a glacial cycle. *Tectonics*, *33* (7), 1461–1476.

Steffen, R., Wu, P., Steffen, H., & Eaton, D. W. (2014b). On the implementation of faults in finite-element glacial isostatic adjustment models. *Computers & Geosciences*, *62*, 150–159.

Stein, S. (2007). Approaches to continental intraplate earthquake issues. In S. Stein & S. Mazzotti (Eds.), *Continental Intraplate Earthquakes: Science, Hazard, and Policy Issues*, Geological Society of America Special Paper 425. 1–16.

Stein, S., Friedrich, A., & Newman, A. (2005). Dependence of possible characteristic earthquakes on spatial sampling: illustration for the Wasatch seismic zone, Utah. *Seismological Research Letters*, *76*, 432–436.

Stein, S., Liu, M., Camelbeeck, T., Merino, M., Landgraf, A., Hintersberger, E., & Kübler, S. (2017). Challenges in assessing seismic hazard in intraplate Europe. *Geological Society, London, Special Publications*, *432* (1), 13–28.

Stewart, I. S., Sauber, J., & Rose, J. (2000). Glacio-seismotectonics: ice sheets, crustal deformation and seismicity. *Quaternary Science Reviews*, *19* (14-15), 1367–1389.

Stokes, C., Margold, M., Clark, C., & Tarasov, L. (2016). Ice stream activity scaled to ice sheet volume during laurentide ice sheet deglaciation. *Nature*, *530* (7590), 322–326.

Stroeven, A. P., Hättestrand, C., Kleman, J., Heyman, J., Fabel, D., Fredin, O., Goodfellow, B. W., Harbor, J. M., Jansen, J. D., Olsen, L., *et al.* (2016). Deglaciation of fennoscandia. *Quaternary Science Reviews*, *147*, 91–121.

Sutinen, R., Hyvönen, E., Middleton, M., & Ruskeeniemi, T. (2014). Airborne lidar detection of postglacial faults and pulju moraine in palojärvi, finnish lapland. *Global and Planetary Change*, *115*, 24–32.

Swafford, L. & Stein, S. (2007). Limitations of the short earthquake record for seismicity and seismic hazard studies. In S. Stein & S. Mazzotti (Eds.), *Continental Intraplate Earthquakes: Science, Hazard, and Policy Issues*, Geological Society of America Special Paper 425. 45–58.

Talwani, P. (1989). Characteristic features of intraplate earthquakes and the models proposed to explain them. In S. Gregersen & P. W. Basham (Eds.), *Earthquakes at North-Atlantic passive margins: Neotectonics and postglacial rebound*, Kluwer Academic Publishers. 563–579.

Tapponnier, P., Ryerson, F. J., Van der Woerd, J., Mériaux, A.-S., & Lasserre, C. (2001). Long-term slip rates and characteristic slip: keys to active fault behaviour and earthquake hazard. *Comptes Rendus de l'Académie des Sciences-Series IIA-Earth and Planetary Science*, *333* (9), 483–494.

Tarayoun, A., Mazzotti, S., Craymer, M., & Henton, J. (2018). Structural inheritance control on intraplate present-day deformation: Gps strain rate variations in the saint lawrence valley, eastern canada. *Journal of Geophysical Research: Solid Earth*, *123* (8), 7004–7020.

Tarayoun, A., Mazzotti, S., & Gueydan, F. (2019). Quantitative impact of structural inheritance on present-day deformation and seismicity concentration in intraplate deformation zones. *Earth and Planetary Science Letters*, *518*, 160–171.

Thompson Jobe, J., Hatem, A., Gold, R., DuRoss, C., Reitman, N., Briggs, R., & Collett, C. (2022). Earthquake geology inputs for the National Seismic Hazard Model (NSHM) 2023 (central and eastern United States), version 1.0. Tech. rep., U.S. Geological Survey data release, https://doi.org/10.5066/P94HLE5G.

Tremblay, A. & Lemieux, Y. (2001). Supracrustal faults of the St. Lawrence rift system between Cap-Tourmente and Baie-Saint-Paul, Québec. Current research 2001-d15, Geological Survey of Canada Current Research.

Tremblay, A., Long, B., & Massé, M. (2003). Supracrustal faults of the St. Lawrence rift system, Québec: kinematics and geometry as revealed by field mapping and marine seismic reflection data. *Tectonophysics*, *369* (3-4), 231–252.

Tremblay, A., Roden-Tice, M. K., Brandt, J. A., & Megan, T. W. (2013). Mesozoic fault reactivation along the st. lawrence rift system, eastern canada: Thermochronologic evidence from apatite fission-track dating. *Bulletin*, *125* (5-6), 794–810.

Trottier, A.-P., Lajeunesse, P., Normandeau, A., & Gagnon-Poiré, A. (2019). Deglacial and postglacial paleoseismological archives in mass movement deposits of lakes of south-central québec. *Canadian Journal of Earth Sciences*, *56* (1), 60–76.

Trugman, D. T. & Ben-Zion, Y. (2023). Coherent spatial variations in the productivity of earthquake sequences in California and Nevada. *The Seismic Record*, *3* (4), 322–331.

Tuttle, M. & Seeber, L. (1991). Historic and prehistoric earthquake-induced liquefaction in Newbury, Massachusetts. *Geology*, *19* (6), 594–597.

Tuttle, M. P. & Atkinson, G. M. (2010). Localization of large earthquakes in the Charlevoix seismic zone, Quebec, Canada, during the past 10,000 years. *Seismological Research Letters*, *81* (1), 140–147.

Vallage, A. & Bollinger, L. (2020). Testing fault models in intraplate settings: a potential for challenging the seismic hazard assessment inputs and hypothesis? *Pure and Applied Geophysics*, *177* (5), 1879–1889.

van der Meij, W. M., Meijles, E. W., Marcos, D., Harkema, T. T., Candel, J. H., & Maas, G. J. (2022). Comparing geomorphological maps made manually and by deep learning. *Earth Surface Processes and Landforms*, *47* (4), 1089–1107.

Villemaire, M., Darbyshire, F., & Bastow, I. (2012). P-wave tomography of eastern north america: Evidence for mantle evolution from archean to phanerozoic, and modification during subsequent hot spot tectonism. *Journal of Geophysical Research: Solid Earth*, *117* (B12).

Walcott, R. (1972). Late quaternary vertical movements in eastern north america: Quantitative evidence of glacio-isostatic rebound. *Reviews of Geophysics*, *10* (4), 849–884.

Wallace, R. E. (1977). Profiles and ages of young fault scarps, north-central Nevada. *Geological Society of America Bulletin*, *88* (9), 1267–1281.

Wang, K. (2022). *Post Glacial Faults in Western Quebec Seismic Zone*. Bs thesis, unpublished, McGill University.

Wang, Z. (2007). Seismic hazard and risk assessment in the intraplate environment: The New Madrid Seismic Zone of the central United States. In S. Stein & S. Mazzotti (Eds.), *Continental Intraplate Earthquakes: Science, Hazard, and Policy Issues*, Geological Society of America Special Paper 425. 363–374.

Wathelet, M., Chatelain, J.-L., Cornou, C., Giulio, G. D., Guillier, B., Ohrnberger, M., & Savvaidis, A. (2020). Geopsy: A user-friendly open-source tool set for ambient vibration processing. *Seismological Research Letters*, *91* (3), 1878–1889.

Weber, J., Stein, S., & Engeln, J. (1998). Estimation of intraplate strain accumulation in the New Madrid seismic zone from repeat GPS surveys. *Tectonics*, *17* (2), 250–266.

Wells, D. L. & Coppersmith, K. J. (1994). New empirical relationships among magnitude, rupture length, rupture width, rupture area, and surface displacement. *Bulletin of the seismological Society of America*, *84* (4), 974–1002.

Wesnousky, S. G. (1994). The Gutenberg-Richter or characteristic earthquake distribution, which is it? *Bulletin of the Seismological Society of America*, *84* (6), 1940–1959.

Wesnousky, S. G. (2006). Predicting the endpoints of earthquake ruptures. *Nature*, *444* (7117), 358–360.

Willeit, M., Ganopolski, A., Calov, R., & Brovkin, V. (2019). Mid-pleistocene transition in glacial cycles explained by declining co2 and regolith removal. *Science Advances*, *5* (4), eaav7337.

Williams, R. T., Goodwin, L. B., Sharp, W. D., & Mozley, P. S. (2017). Reading a 400,000-year record of earthquake frequency for an intraplate fault. *Proceedings of the National Academy of Sciences*, *114* (19), 4893–4898.

Wu, P. & Johnston, P. (2000). Can deglaciation trigger earthquakes in n. america? *Geophysical Research Letters*, *27* (9), 1323–1326.

Wu, P., Johnston, P., & Lambeck, K. (1999). Postglacial rebound and fault instability in fennoscandia. *Geophysical Journal International*, *139* (3), 657–670.

Youngs, R. R. & Coppersmith, K. J. (1985). Implications of fault slip rates and earthquake recurrence models to probabilistic seismic hazard estimates. *Bulletin of the Seismological society of America*, *75* (4), 939–964.

Yu, H., Liu, Y., Harrington, R. M., & Lamontagne, M. (2016a). Seismicity along st. lawrence paleorift faults overprinted by a meteorite impact structure in charlevoix, québec, eastern canada. *Bulletin of the Seismological Society of America*, *106* (6), 2663–2673.

Yu, K., Chouinard, L. E., & Rosset, P. (2016b). Seismic vulnerability assessment for Montreal. *Georisk: Assessment and Management of Risk for Engineered Systems and Geohazards*, *10* (2), 164–178.

Zelt, C. A. (1998). Lateral velocity resolution from three-dimensional seismic refraction data. *Geophysical Journal International*, *135* (3), 1101–1112.

Zielke, O., Klinger, Y., & Arrowsmith, J. R. (2015). Fault slip and earthquake recurrence along strike-slip faults—contributions of high-resolution geomorphic data. *Tectonophysics*, *638* , 43–62.